Applications of Point-Contact Spectroscopy

A.M. Duif

Applications of Point-Contact Spectroscopy

Applications of Point-Contact Spectroscopy

Proefschrift

ter verkrijging van de graad van
doctor in de wiskunde en natuurwetenschappen
aan de Katholieke Universiteit te Nijmegen,
op gezag van de Rector Magnificus Prof. Dr. B.M.F. van Iersel
volgens besluit van het College van Decanen
in het openbaar te verdedigen
op maandag 7 december 1987
des namiddags te 3.30 uur

door
Andreas Maria Duif
geboren te Venlo

1987

Druk: Krips Repro, Meppel

Promotor : Prof. Dr. P. Wyder

Co-referent : Dr. A.G.M. Jansen

Erg veel mensen hebben een stempel gedrukt op de totstandkoming van dit proefschrift. Daarvoor wil ik hen allen op deze plaats heel hartelijk danken. In het bijzonder dank aan alle mensen van de afdeling Exp. Nat. 4 in Nijmegen en van het M.P.I. in Grenoble, die vaak wat extra kleur aan het (wetenschappelijke) leven gaven. Met name ook dank aan Oleg, Sasha en vooral Louis, die een grote wetenschappelijke bijdrage hebben geleverd aan de inhoud van dit boekje. De laatste in het bijzonder ook dank voor het schrappen van de ergste onzin die anders de verdere bladzijden van dit proefschrift zou hebben ontsierd. Tevens wil ik allen bedanken die het voor mij mogelijk hebben gemaakt een paar jaar in Grenoble te werken.
Ten slotte dank ik het thuisfront voor hun belangstelling en medeleven tijdens de afgelopen jaren.

Many people have put their stamp upon the realization of this thesis. At this place I want to thank them cordially for that. Especially I want to thank all the people of Exp. Nat. 4 in Nijmegen and at the M.P.I. in Grenoble, who often gave some extra colour to (scientific) life. I want to mention expressly Oleg, Sasha and certainly Louis for their large scientific contribution to this booklet. The latter I am grateful for striking out all the nonsense which would have disfigured the rest of this thesis. Also I would like to thank all the people who made it possible for me to spend a few years in Grenoble.
In conclusion I want to thank the home front for their interest and sympathy during the past years.

Part of this work has been supported by the Stichting voor Fundamenteel Onderzoek der Materie (F.O.M.), with financial support from the Nederlandse Organisatie voor Zuiver Wetenschappelijk Onderzoek (Z.W.O.).

" Fue en esa ocasión cuando Aureliano le oyó decir:
- Si no temes a Dios, témele a los metales. "

José Arcadio Buendía en
Cien años de soledad,
Gabriel García Márquez

" Het was bij die gelegenheid dat Aureliano hem hoorde zeggen:
' Wie God niet vreest, hij vreze de metalen. ' "

José Arcadio Buendía in
Honderd jaar eenzaamheid,
Gabriel García Márquez.

TABLE OF CONTENTS

CHAPTER 1

GENERAL INTRODUCTION

Metal physics is one of the oldest branches of solid state physics which has its roots in the beginning of this century. Names like Drude, Sommerfeld and Bloch may sound familiar to everybody and appear in almost all textbooks on solid state physics on one of the first pages. A "simple" model of metallic conduction as the one by Drude is still very popular in modern metal physics.

One can say that it all started with this Drude theory for metals. Since this, solid state physics has known a large number of topics. Superconductivity, already discovered in 1911, fascinated both experimental and theoretical physicists. The "conventional" superconductivity got its theoretical foundations around 1960 with the BCS theory for superconductivity and the Ginzburg-Landau and the Abrikosov-Gor'kov theory for superconductors in magnetic fields. Most properties of superconductors are well understood with these theories. Nowadays the new high-T_c superconductors bring new activity and excitement in this field.

In the sixties tunneling was develloped as an important technique in solid state physics. Experiments were performed on a great variety of materials. Results and applications of tunneling since that time are the measurements of the superconducting energy gap, Josephson effect, SQUIDS, devices with a negative differential resistance, applied as oscillating devices, nowadays even at roomtemperatures, the study of non-equilibrium effects in superconductors etc.

Another subject in metal physics which attracted the attention of metal physicists is the study of systems consisting of non-magnetic metals with magnetic impurities dissolved in them. Already in the early thirties the first experiments were performed, but the main activity on this subject took place after Ruderman, Kittel, Kasuya and Yosida came with their theory for the inter-impurity interaction and Kondo for the single-impurity problem. Spin glasses became interest in the seventies because of the observed transition at a distinct temperature, most clearly observed in susceptibility experiments.

In 1975 intermetallic compounds were discovered, exhibiting a huge specific heat at low temperatures, due to the existence of heavy electrons or quasiparticles at the Fermi level. In a number of these systems superconductivity was discovered and antiferromagnetic order in some others. These heavy fermion systems nowadays receive much attention in metal physics.

The development of the Scanning Tunneling Microscope, leading to the 1986 Nobel Prize in physics, gave rise to a renewed interest in tunneling during the past few years. This development of the STM was a big step in surface science and made it possible to study clean surfaces on atomic scale.

The subject of this thesis touches a number of the mentioned topics in solid state physics. It deals about the applications of the point-contact technique, a technique which is related with tunneling, but which is essentially different. In point contacts between two metals, a real, conducting bridge is

made between the two metals. Such a contact is characterized by the quotient of the electron mean free path ℓ of the metal and the contact radius a. When this quotient ℓ/a is large compared with unity, the electrons which pass the contact, will be accelerated over the mean free path and will thus gain an energy eV where V is the applied voltage over the contact. A subsequent inelastic scattering can now be probed by measuring the voltage-dependent resistance change of the contact.

This method of obtaining information about the energy-dependence of the scattering of conduction electrons was discovered by Yanson in 1974 who examined the I-V characteristics of shorted MIM tunnel junctions. The method was developed further by Jansen who used a sharply etched whisker and pressed it on a flat surface, which made it possible to study a large number of materials. The newest technique of pressing together two sharp edges of two bulk pieces gives even the possibility to study single crystal contacts.

During the past few years the point-contact method has been used for the study of several types of interactions of the conduction electrons. Mainly the electron-phonon interaction has been studied thoroughly, but also the interaction of the conduction electrons with magnons, paramagnetic impurities and crystal-field levels. This thesis deals with the exploitation of the point-contact method. It is organized as follows. Chapter 2 gives a review of the most important developments of point-contact spectroscopy during the last few years. After a short summary of the theory on point contacts a number of interesting experiments is discussed, performed during the last few years, illustrating the important criteria of point-contact experiments. In chapter 3 experiments are described on AuMn and CuMn Kondo and spin glass systems and a model is presented which is compared with the experimental data. Chapter 4 deals with point-contact experiments in bismuth. With these experiments superconducting clusters are observed at the surface with a diameter of roughly 100 nm. In the next two chapters point-contact experiments are described on the heavy-fermion system UPt_3. In chapter 5 the measured differential resistance as a function of applied bias voltage over the contact is analyzed using a heating model and a resemblance is found with the temperature-dependent differential resistance at zero bias. Chapter 6 reports on high-frequency rectification experiments in UPt_3 point contacts. The results of these experiments can be explained with a heating model. In the last chapter the phonon spectrum is analyzed which is emitted by a point contact between a Au whisker and a thin Au film, evaporated on the surface of a Si crystal. In this Si crystal the phonons are detected with phonon-induced conductivity due to the ionization of B^+ impurity levels in the Si.

CHAPTER 2

POINT-CONTACT SPECTROSCOPY (REVIEW)

2.1. Introduction.

Point-contact spectroscopy nowadays has become a well-established technique in the study of the interaction mechanisms of the electrons with all kinds of elementary excitations in metals. Small constrictions between two metals show deviations from Ohm's law. The nonlinearity is a measure for the inelastic scattering of the conduction electrons, where the applied voltage defines the energy scale for the interaction process. Those nonlinearities in the current-voltage characteristics were discovered by Yanson who examined the I-V characteristics of shorted MIM-tunnel junctions (Yanson, 1974). In the second derivative d^2V/dI^2 of the voltage V with respect to the current I, he found structures which turned out to coincide with the Eliashberg function α^2F for the electron-phonon interaction. This Yanson-experiment set going a whole series of experiments in which mainly the electron-phonon interaction was studied in all kinds of materials. But also other scattering mechanisms of the electrons were observed in point-contact experiments, like e.g. electron-magnetic impurity interaction and electron-magnon interaction.

Although point-contact experiments with superconductors show interesting features, we will restrict ourselves to point-contact experiments on normal (N-N) contacts. In this article we will not give a detailed description of the complete point-contact theory but only give the main results. For a complete theory on point contacts in the ballistic regime we want to refer to Kulik et al. (1977) and Jansen et al. (1980). For a theory on point contacts in the dirty limit we refer to Kulik and Yanson (1978). We will also not give a complete survey on all possible materials which are studied during the last years. For reviews on this see Yanson (1983) and Yanson and Shklyarevskii (1986). Here we will discuss the possibilities of the technique and a number of new interesting experiments which are performed during the last few years.

In the first part of this review the spectroscopic side of the point-contact technique stands central. Here the aim is to obtain an energy-resolved determination of the inverse scattering time $1/\tau$ of the electrons with elementary excitations in the metal. The important criterea in a point-contact experiment will be explained and illustrated with typical examples of spectroscopic applications, which also show the limitations of this technique. The understanding of point-contact spectroscopy has initiated experiments dealing with aspects other than just spectroscopy, exploiting the small dimension of the contact. A considerable number of experiments of this kind are performed during the last few years, for instance those dealing with the thermal conductivity, with the quenching of phonon drag in the thermopower of point contacts, with thermo-electric effects, those on double point contacts, and on point contacts in magnetic fields.

2.2. Characterization of a point contact.

There are three methods of fabricating a point contact between two metals. The first point contacts existed of a short circuit in a MIM tunnel junction. The method was extended by the so-called pressure-type contacts in which a sharp whisker is pressed on a flat surface. With this technique it was easier to control the diameter of the contact which is an important parameter in the experiments. The spear-anvil contacts made the point-contact technique accessible for the study of a large number of materials. The newest method is just pressing together two sharp edges of two bulk pieces. Besides the advantage of the pressure-type contacts, now even single crystal contacts could be made.

The two typical lengths for the characterization of the contact problem are the electron mean free path ℓ and the radius a of the constriction. Actually the mean free path involves an elastic mean free path ℓ_e and an inelastic one, $\ell_i(\epsilon)$. The inelastic mean free path depends on the electron energy ϵ=eV with respect to the Fermi level. Comparing these typical lengths with each other, three regimes are possible.

The first regime is the ballistic regime in which the electron mean free path ℓ is much larger than the contact dimension a. In this regime an applied voltage will accelerate the electrons within a mean free path length. Thus the electrons then will pass through the contact ballistically, gaining an energy eV where V is the applied voltage over the contact. The problem can be treated analogously to the problem of the flow of a dilute gas through a hole (Knudsen, 1934). Sharvin realized the peculiar transport of current through such a ballistic contact and calculated the resistance (Sharvin, 1965). He found a resistance $R_S = 4\rho\ell/3\pi a^2$ where ρ is the resistivity of the material under study. The expression for the Sharvin resistance R_S is independent of the electron mean free path.

The opposite case of this ballistic regime is the dirty, thermal or Maxwell regime, where the mean free path of the electrons is much smaller than the contact radius a. For this regime the Poisson equation can be solved using the proper boundary conditions, leading to a resistance $R_M = \rho/2a$, already calculated by Maxwell (1904). In contrast with the ballistic regime, where the electrons loose their energy on a rather large distance from the constriction, in this regime they loose their energy in the contact area itself. Therefore this Joule heating leads to an increase of temperature at the center of the contact. When one is not in one of these two limits, one could easily expect some interpolation of the two limiting resistances (Wexler, 1966):

$$R = \frac{4\rho\ell}{3\pi a^2} + \Gamma(K)\,\frac{\rho}{2a} = \frac{4\rho\ell}{3\pi a^2}\left[\,1 + \frac{3\pi}{8}\,\Gamma(K)\,\frac{a}{\ell}\,\right]. \qquad (2.1)$$

Here $K=\ell/a$ is the Knudsen number and $\Gamma(K)$ is a slowly varying function of order of unity.

The third possible regime is the so-called diffusive regime. This is the regime where the elastic mean free path ℓ_e of the electrons is small compared with the contact dimension but where the diffusion length $\Lambda=(\ell_i\ell_e)^{1/2}$ for inelastic scattering is still bigger than the contact dimension. In this case still no heating occurs in the contact area.

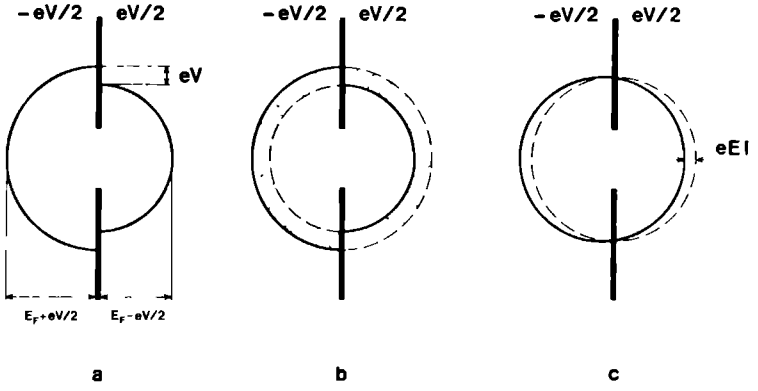

Fig. 2.1. Distribution of the electronic energy at the center of the contact for an applied voltage V over a point contact in the ballistic (a), diffusive (b) and thermal regime (c).

Figure 2.1 shows the difference in the electron distribution functions at the center of the contact for the three regimes. In part (a) the deformed Fermi spheres are depicted for the ballistic regime. Since there is ballistic flow of electrons from both sides of the contact, the Fermi sphere consists of two half-spheres with a difference in radius equal to the applied energy eV. The picture for the diffuse regime (fig. 2.1b) differs from the "ballistic picture" because the elastic scattering redistributes the electrons isotropically over the Fermi sphere, but still in an energy shell with a width given by the applied voltage (dotted area). Since there is still a bigger number of electrons in the left half-sphere than in the right one, there is a net flow of electrons from the right to the left. Figure 2.1c just shows the shifted Fermi-sphere which is valid for a point contact in the thermal regime, as is normal for the uniform transport of electrons in a conductor. Because of strong inelastic scattering the shift in energy space will be smaller than the applied voltage. In the next paragraph we will show how these three different microcontact regimes manifest themselves in the experiments and how the observed nonli-

nearities can be explained theoretically.

2.3. Nonlinearities observed with point contacts.

2.3.1 Ballistic regime

In the ballistic point-contact regime, direct energy-resolved information is obtained about the inelastic scattering of the electrons in the contact region. Figure 2.2 shows a pronounced example of the information obtained with point contacts. This figure shows the current-voltage characteristic and its derivatives of a Cu-Cu point contact in the ballistic regime, measured at liquid helium temperatures. The dashed curve in figure 2.2c represents the phonon density of states F(ϵ) obtained with neutron scattering experiments.

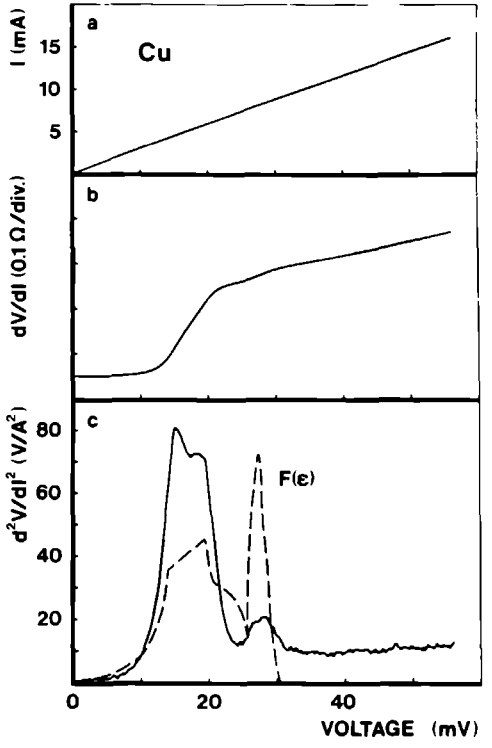

Fig. 2.2. Measured current-voltage characteristic (a), differential resistance dV/dI (b) and second derivative d^2V/dI^2 (c) for a Cu-Cu point contact with resistance R_0=3.3 Ω at temperature 1.5 K. The dashed curve in part c represents the phonon density of states $F(\epsilon)$ obtained from neutron-scattering experiments.

There is a clear resemblance between this curve and the measured second derivative d^2V/dI^2. For an interpretation of this result it is necessary to solve the Bolzmann equation for the point-contact problem. This can be done iteratively. The zeroth order solution describes the ballistic injection of electrons without any scattering and yields the expression for the Sharvin resistance. The first order solution describes the inelastic scattering of the injected electrons, back through the orifice. This first order correction $I^{(1)}$ to the total current leads to a correction of the order of $a/\ell(\epsilon)$ in the resistance, analogously to the second term in equation (2.1). This correction $I^{(1)}$ to the total current is given by

$$I^{(1)} = - \frac{2\pi e}{\hbar} \Omega_{eff} N(0) \int_0^{eV} d\epsilon \int_0^{\epsilon} d\epsilon' S(\epsilon-\epsilon') . \qquad (2.2)$$

Here N(0) is the density of states at the Fermi level, Ω_{eff} is a kind of effective volume in which the inelastic scattering of electrons which contribute to $I^{(1)}$, takes place and $S(\epsilon)$ is the spectral function for the concerned interaction. This spectral function $S(\epsilon)$ consists of an integration over all initial and final electron states $|\mathbf{k}\rangle$ and $|\mathbf{k}'\rangle$, of the scattering matrix elements $|g_{\mathbf{k}\mathbf{k}'}|$, and an efficiency function $\eta(\mathbf{k},\mathbf{k}')$:

$$S(\epsilon) = \frac{N(0)}{32\pi^2} \int \frac{d^2\mathbf{k}}{k^2} \int \frac{d^2\mathbf{k}'}{k'^2} |g_{\mathbf{k}\mathbf{k}'}| \, \eta(\mathbf{k},\mathbf{k}') \, \delta(\epsilon-\epsilon_{\mathbf{k}}+\epsilon_{\mathbf{k}'}) . \qquad (2.3)$$

The efficiency function $\eta(\mathbf{k},\mathbf{k}')$ is the normalized common volume of two cylinders through the boundary of the orifice, one parallel to $\mathbf{k}$ of the incoming electron and the other parallel to $\mathbf{k}'$ of the inelastic scattered electron. Retaining only the angular dependence in the scattering event, the efficiency can be written as $\eta(\theta)=(1-\theta/\mathrm{tg}\theta)/2$ (van Gelder, 1980), analogously to the function $(1-\cos\theta)$ in the electrical transport problem. The effective volume in the ballistic regime is given by $\Omega_{eff}=8a^3/3$. The expression for the differential conductivity dI/dV is now given by

$$\frac{dI}{dV} = \frac{1}{R_S} - \frac{2}{3} e^2 a^3 N(0) \frac{1}{\tau(eV)} . \qquad (2.4)$$

This inverse scattering time $1/\tau(eV)$ of an electron with energy eV above the Fermi level is related to the spectral function $S(\epsilon)$ via

$$\frac{1}{\tau}(eV) = \frac{2\pi}{\hbar} \int_0^{eV} S(\epsilon)\, d\epsilon \,. \tag{2.5}$$

The second derivative d^2I/dV^2 of the current with respect to the voltage is directly proportional to the spectral function $S(\epsilon)$ since

$$\frac{d^2I}{dV^2} = - \frac{2\pi e^3}{\hbar} \Omega_{eff}\, N(0)\, S(eV) \,, \tag{2.6}$$

and thus a direct measurement of the spectral function S(eV) is possible. For the case of electron-phonon interaction as in figure 2.2, the spectral function $S(\epsilon)$ is the well-known Eliashberg function $\alpha^2F(\epsilon)$ with as a slight modification the efficiency function $\eta(\mathbf{k},\mathbf{k}')$ as mentioned above. This method of obtaining phonon spectra has been used extensively during the last years. For many (normal) metals it was the first method to give the detailed energy-dependence of the electron-phonon interaction function $\alpha^2F(\epsilon)$. For a complete review on the investigation of the electron-phonon interaction by means of point contacts, we refer to Yanson (1983).

In measurements on the point contact electron-phonon interaction function $\alpha^2F_p(\epsilon)$, often a considerable background is found (Jansen et al., 1980). One expects the function α^2F_p to be zero above the Debye energy which due to equation (2.6) should lead to $d^2I/dV^2=0$ for these energies. That this does not happen is generally understood to be due to the presence of nonequilibrium phonons in the system. This leads to an additional scattering of the electrons with these nonequilibrium phonons and therefore to a background signal which is not included in theory. The background signal is a smooth signal which is zero at zero energy, increases smoothly at the phonon energies and saturates above the maximum phonon energy. This background signal B(eV) is best described by the integral $B(eV) = \kappa \int_0^{eV} \alpha^2F_p(\epsilon)/\epsilon \, d\epsilon$, where κ is some constant. Thus the measured signal is commonly believed to be

$$\frac{d^2I}{dV^2} = \text{const} \left[\alpha^2F_p(eV) + \kappa \int_0^{eV} \frac{\alpha^2F_p(\epsilon)}{\epsilon}\, d\epsilon \right] . \tag{2.7}$$

This assumption gives us the possibility to correct for the background and to determine the point contact electron-phonon interaction function $\alpha^2F_p(\epsilon)$.

2.3.2 Diffusive regime

In the diffusive point-contact regime it is still possible to obtain direct energy-resolved information about the inelastic scattering of the electrons as in the ballistic regime. Figure 2.3 shows very nicely the transition from a point contact in the ballistic regime to a point contact in the diffusive regime

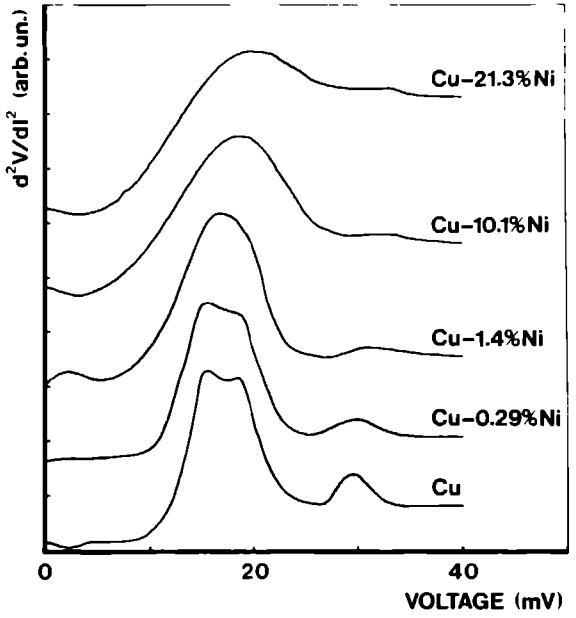

Fig. 2.3. Measured point-contact spectra d^2V/dI^2 for point contacts consisting of pure Cu and some CuNi alloys, showing the transition from the ballistic to the diffusive regime. By increasing the Ni concentration the Knudsen ratio ℓ_e/a goes from 29 to 0.07. The spectra were measured at T=4.2 K. [after Lysykh et al., 1980]

(Lysykh et al., 1980). The lowest curve represents the phonon spectrum of a pure Cu-Cu point contact. Adding Ni to the sample (other curves) reduces

the elastic mean free path of the electrons in the material under study and brings the point contacts into the diffusive regime. Most striking features of these curves b-e is the reduction of the signal, the broadening of the spectra and a shift of the phonon peaks to higher energies. For a theoretical understanding we still can use equations (2.2-2.6). The spectral function $S(\epsilon)$ however, now contains an other efficiency function $\eta(\mathbf{k},\mathbf{k}')$, where the demands on momentum conservation are less stringent because of the elastic scattering (Kulik and Yanson, 1978). This explains a different shape of the measured spectral function in this diffusive regime compared with the one measured in the ballistic regime. The reduction of the signal can be explained with the effective volume Ω_{eff}. In the diffusive regime this effective volume is given by $\Omega_{eff}=\pi a^2 \ell_e/4$, where ℓ_e is the elastic mean free path. The efficiency volumes are sketched schematically in figure 2.4. Figure 2.4a shows the effective volume for a point contact in the ballistic regime except from a prefactor. If an inelastic scattering process takes place outside this volume the chance of the electron to flow back through the orifice becomes very small because of the small solid angle $\Omega(\mathbf{r})$ under which the orifice is seen from that point. Therefore inelastic scattering processes outside this volume hardly contribute to the backflow current $I^{(1)}$ and therefore hardly to the observed nonlinearities and the spectral function $S(\epsilon)$. The reduced effective volume for the diffusive case is depicted in figure 2.4b. As already mentioned only those electrons which pass the orifice and then are scattered back inelastically through the orifice (or those electrons who would have passed the contact without the inelastic scattering) contribute to the spectral function $S(\epsilon)$. Because of the diffusive electron transport with elastic scattering the efficiency of the backflow processes after an inelastic scattering process will be reduced by a factor a/ℓ_e and will be most effective in a volume with a distance ℓ_e from the contact.

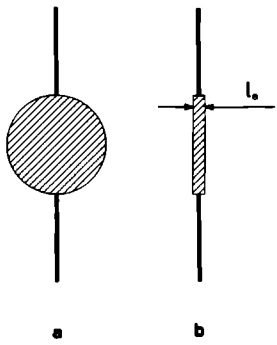

Fig. 2.4. Schematic representation of the efficiency volume Ω_{eff} of a point contact in the ballistic regime (a) and in the diffusion regime (b).

If the microcontact diameter d becomes larger than both the elastic and the inelastic mean free path of the electrons, then the microcontact is in the thermal regime. In this regime almost all the energy is dissipated in the contact area which leads to an increase in temperature at the orifice itself. It can be shown that this maximum temperature T_{max} at the center of the contact for this Maxwell regime is given by (Holm, 1967):

$$T_{max}^2 = T_{bath}^2 + V^2/4L \ , \tag{2.8}$$

where T_{bath} is the bath temperature and L is the Lorenz number. Since by approximation one can say that the center of the point contact gives the largest contribution to the Maxwell resistance $R_M=\rho/2a$, one actually measures the temperature dependent resistivity $\rho(T_{max})$ in measuring the voltage dependent point contact resistance $R_M(V)$.

Relation (2.8) can be observed in the measured d^2V/dI^2 spectrum of a Ni-Ni point contact as shown in figure 2.5. At low voltages this spectrum exhibits the phonon structure as can be seen in the expanded inset in this figure. From this we can conclude that the contact for these low voltages is in the ballistic or in the diffusive regime. At higher voltages however, a huge nonlinearity shows up which can be understood in terms of the ferromagnetic transition of Ni. At high voltages the electron mean free path

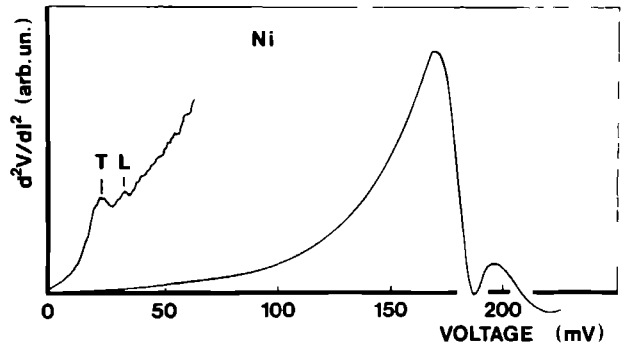

Fig. 2.5. Measured d^2V/dI^2 spectrum of a Ni-Ni point contact with resistance R_0=6.5 Ω at temperature T=1.5 K, revealing the phonon structure at low voltages (expanded curve) and the ferromagnetic transition at high voltages.

becomes so small that the contact is in the thermal regime. Using equation (2.8) we calculate the temperature of the contact at the voltage at which the transition is observed. This temperature agrees very well with the Curie temperature of Ni.

An approximation which is less rough than the proportionality $R_M(V) \propto \rho(T_{max})$ as mentioned above, is the model of spherical spreading out. In this model both the equipotential and the isothermal surfaces are assumed to be hemispheres around the contact. Using this model one can calculate the correlation between the I-V characteristic and the temperature-dependent resistivity of the metal. One then finds the relation (Verkin et al., 1980):

$$I(V) = 2Va \int_0^1 \frac{dx}{\rho\,(T_{max}\sqrt{1-x^2})}\,, \tag{2.9}$$

where T_{max} is again the temperature at the center of the contact, given by equation (2.8). This relation can be used to calculate the current-voltage characteristics of point contacts in the thermal regime, using the temperature-dependent resistivity of the studied material.

2.4. On the relation between point-contact spectroscopy and tunneling.

For measuring the function α^2F another powerful method exists using superconducting tunneling (McMillan and Rowell, 1965). With superconducting tunnel junctions the normalised density of states N(E)/N(0) in the superconductor can directly be obtained from the differential conductivity $(dI/dV)_S$ in the superconducting state divided by $(dI/dV)_N$ in the normal state. From the measured many-particle density of states McMillan and Rowell calculated α^2F using an iterative computer calculation. This method can be utilized for strong-coupling superconducting metals. It is however also possible to see the electron-phonon interaction in tunneling experiments between normal metals because of the inelastic scattering of tunneling electrons which opens extra channels for the electrons to tunnel through the barrier. Thus in tunneling experiments with normal metals the inelastic scattering of electrons leads to an increase of the total current. This is the main difference with point-contact spectroscopy, where according to equation (2.2) the inelastic scattering of electrons gives a negative contribution to the total current (backflow). As a typical example of the relation between tunneling and point-contact spectroscopy we want to mention the experiments on metals with paramagnetic impurities dissolved in them. The experimental res-

ults are shown in figure 2.6. As we will explain in the next paragraph, point-contact experiments on noble metals, e.g. Au or Cu, with paramagnetic impurities, e.g. Mn, show an anomalous structure around zero bias voltage. The observed maximum in the point-contact resistance can be explained in terms of the Kondo problem. Applying an external magnetic field, this maximum is reduced because spin-flip processes are forbidden for voltages $V<g\mu_B B/e$, leading to a structure with a double peak. The decrease of point-contact resistance when applying a magnetic field, can clearly be seen in

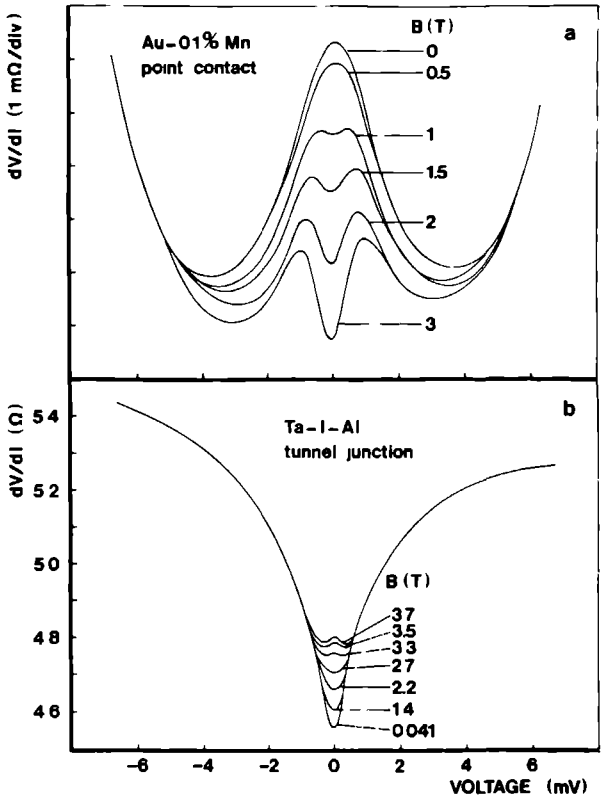

Fig. 2.6. Measured differential resistance dV/dI for a Au-0.1 at.% Mn point contact (upper curves) and for a Ta-I-Al tunnel junction (lower curves, after Shen and Rowell, 1968) at different magnetic fields, showing the opposite behaviour in voltage and magnetic field dependence, between point-contact spectroscopy and tunneling.

figure 2.6a. Figure 2.6b shows the results of measurements on a Ta-I-Al tunnel junction (Shen and Rowell, 1968). A comparison of both figures clearly shows the opposite behaviour between tunneling and point-contact spectroscopy. While in the point-contact case the differential resistance dV/dI is decreased with applying an external field, in the tunnel experiments it is increased as explained above.

2.5. Point-contact spectroscopy applied to other scattering mechanisms.

As we already mentioned in the preceding paragraphs the point-contact method has most successfully and most intensively been applied to the scattering of the electrons with phonons. However also experiments can be done on other inelastic scattering mechanisms. In this section we will discuss briefly a number of point-contact experiments, dealing with scattering mechanisms other than the electron-phonon interaction.

2.5.1 Electron-magnon scattering

The inelastic scattering of electrons with magnons is most clearly be observed in point-contact experiments by Akimenko et al. (1982). They carried out experiments on gadolinium, terbium and holmium. For these materials the total of electron-magnon and electron-phonon interaction functions was measured. The most pronounced magnon spectra they found in their experiments on gadolinium. Here the electron-magnon interaction turns out to be much stronger than the electron-phonon interaction since no structure was found at the expected phonon energies. At low energies, theory predicts the electron-magnon interaction function $S(\epsilon)$ to be proportional with the applied voltage (Kulik and Shekhter, 1980). This indeed is found in the experiments on Gd. The experiments with Tb and Gd show the electron-magnon interaction in the spectra superimposed on the electron-phonon structure.

2.5.2 Crystal field levels

In point-contact experiments on $PrNi_5$, the level energies of the Pr^{3+} ion in the crystal electric field of this $PrNi_5$ were determined directly (Akimenko et al., 1984a). The measured spectra show a number of singularities on a rather large background. Observed maxima in the d^2V/dI^2 curves were clearly identified as the Pr^{3+} transition from the ground state into the excited

states. This could be made plausible by comparing the point-contact data with the results of neutron-scattering experiments. Applying an external magnetic field shifts the transitions towards somewhat lower energies and induces an additional structure due to a transition which was forbidden in zero field.

Crystal field excitations were also found in point-contact experiments by Frankowski and Wachter (1982). In their experiments on TmSe they found a maximum in the d^2V/dI^2 characteristic at 5 mV which was ascribed to these excitations.

2.5.3 Scattering with paramagnetic impurities

The differential resistance of point contacts consisting of noble metals with very dilute paramagnetic impurities dissolved in them shows a maximum at zero bias voltage (Jansen et al.,1980, Duif et al., 1987). In these Kondo-systems the s-d exchange interaction between the conduction electrons and the local moments yields a logarithmic energy dependence of the inverse scattering time $1/\tau(eV)$. As can easily be seen from equation (2.4), the measured change in differential resistance ΔR is directly proportional to this inverse scattering time $1/\tau(eV)$

The logarithmic divergence of the energy-dependent scattering rate was measured in the voltage dependence of the point-contact resistance. When an external magnetic field B is applied, the observed zero-bias maximum splits up. This splitting is visible in figure 2.6. As already mentioned, the decrease in differential resistance and the occurrence of a double peak structure can be explained with the absence of spin-flip scattering at low enough voltages. This type of scattering costs an energy $\Delta=g\mu_B B$, which is not available at low bias voltages. At voltages $V=\pm\Delta/e$, this spin-flip scattering restarts contributing to the differential resistance, yielding a maximum in the contact resistance nearby these voltages. Using the Hamiltonian for the s-d interaction between conduction electrons and local moments, it is possible to calculate the differential resistance of the point contacts of these systems (d'Ambrumenil and White, 1982). From a comparison between measured and calculated spectra the Zeeman energy Δ can be determined as a function of field. Extrapolating this energy Δ to zero external field still leaves in many cases some non-zero value. This can be explained by the presence of internal fields which occur in the somewhat more concentrated samples (spin glasses). These internal fields arise from the indirect exchange interaction (RKKY) between the impurity spins themselves. Figure 2.7 shows how these internal fields manifest themselves in the measured point-contact spectra. Part (a) shows the measured differential resistance of three AuMn point contacts without magnetic field. In the more concentrated samples a splitting occurs

due to the internal fields which become more pronounced when the impurity concentration is increased. Part (b) gives the calculated differential resistance for these three samples. A comparison between both plots shows that the theory gives a good description of the experiment.

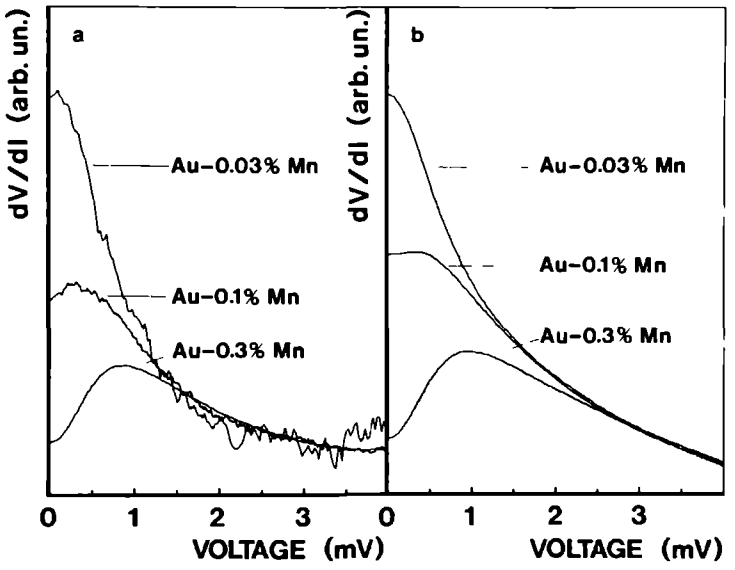

Fig. 2.7. Measured differential resistance dV/dI for three AuMn point contacts with different Mn concentrations (left curves) and calculated differential resistance for these contacts (right curves).

2.5.4 Mixed valencies and heavy fermions

In the past few years a considerable number of point-contact experiments have been performed on various valence fluctuations and heavy fermion systems. In general very large nonlinearities are found in the current-voltage characteristics, leading to rather large changes in the measured differential resistance dV/dI. In the experiments on valence-fluctuation compounds, both minima and maxima were observed in the resistance around zero bias voltage. For instance in experiments on YbCuAl and $YbCu_2Si_2$ a minimum was observed in dV/dI (Bussian et al., 1982). The temperature-dependent resistivity $\rho(T)$ of these materials also exhibits a minimum at zero temperature. In

experiments on SmB_6 and TmSe a maximum was observed in dV/dI at zero bias voltage (Frankowski and Wachter, 1982). However, here the resistivity also has a maximum at zero temperature. Some different interpretations exist of the observed phenomena. Bussian et al. (1982) explained their results with the energy-dependent interconfigurational scattering of the conduction electrons. Frankowski and Wachter (1982) explained their results on TmSe and SmB_6 with the existence of a hybridisation gap in the electron density of states in these materials. In point-contact experiments on heavy-fermion compounds a minimum is found in the differential resistance at zero bias voltage (see e.g. Kunii, 1987; Paulus and Voss, 1985; Moser et al., 1985; Moser et al., 1986). This behaviour has been explained with the narrow maximum in the electron density of states around the Fermi level of these materials (Moser et al., 1985).

Analogously to a tunneling experiment it is often stated for a point-contact experiment in heavy fermion systems that the differential conductance dI/dV is proportional to the electron density of states N(eV) at an energy eV above the Fermi level. Hence one could directly probe with a point contact the strong resonance in the density of states around the Fermi level in heavy fermion systems. However a simple analysis shows that the energy-dependent density of states does not enter the expression for the resistance of a point contact in the clean limit. To calculate the current in the ballistic limit one has to sum the electron velocity over all possible k-states. The sum over k-states results in an energy-dependent density of states, which is cancelled by the electron velocity. Via the same reasoning as for a tunneling experiment between normal metals (Harrison, 1961), the resistance of a point contact does not contain the energy-dependent density of states in its voltage dependence. For superconductors however it is possible to determine the normalized density of states of the superconductor in a tunneling experiment.

A different approach in the interpretation of the point-contact experiments on these valence fluctuation and heavy fermion systems is in terms of the heating model (section 2.3.3). It is more and more believed that for the discussed compounds a ballistic point-contact model is not applicable (see e.g. Neidyuk et al.,1985).

Measurements on UPt_3 (Lysykh et al., 1987) show that there is a strong resemblance between the voltage dependent differential point-contact resistance and the temperature dependent bulk resistivity of this heavy fermion system. However quantitatively the relative change in this temperature dependent bulk resistivity is a few times larger than the relative change in the voltage dependent differential resistance. A better quantitative agreement is found by comparing the voltage-dependent resistance at low temperatures with the temperature-dependent resistance at zero voltage. For a normal metal like Cu with point contacts in the clean limit a distinct difference is seen in these two dependences of the point contact resistance (Jansen et al.,

1987). Still quantitatively the temperature-dependent resistance can not be explained fully from the temperature-dependent resistivity in terms of the heating model ($R(T)=\rho(T)/2a$). An explanation could be a deviation of the resistivity on the local scale of the point contact compared with the bulk value. Figure 2.8 shows the comparison between the measured voltage dependence of the differential resistance of a UPt_3-UPt_3 point contact at constant bath temperature (solid line) with the measured temperature dependence of dV/dI at zero bias (dots). For the scaling between temperature and voltage, equation (2.8) has been used with experimental values for the temperature-dependent Lorenz number of UPt_3. There is a good agreement between the functional dependence of dV/dI(V) and dV/dI(T).

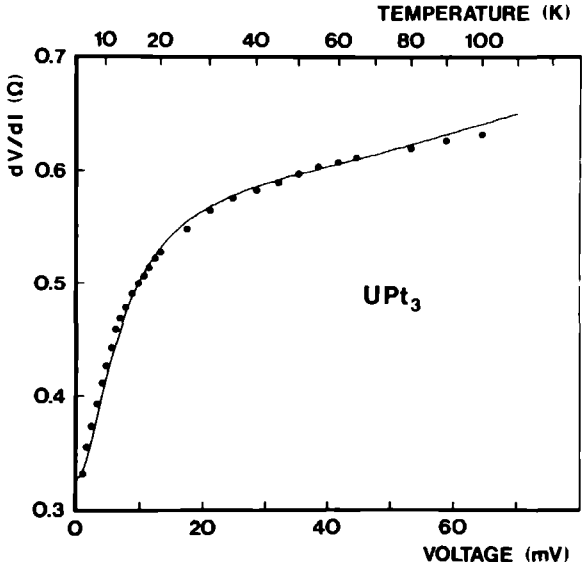

Fig. 2.8. Comparison between the voltage-dependent differential resistance dV/dI(V) of a UPt_3-UPt_3 point contact, measured at 4.2 K (solid line) with its temperature-dependent differential resistance dV/dI(T), measured at V=0 (dots). Equation (2.8) has been used for the matching between voltage and temperature scale.

2.6. Temperature effects in point contacts.

In this section we will focus on the thermal aspects of point-contact spectroscopy. It is evident that in all experiments on point contacts, temperature plays a significant role in the interpretation of the results. As we already mentioned in section 2.3.3, temperature is essential in the interpretation of the observed current-voltage characteristics of dirty contacts, where Joule heating takes place close to the center of the contact. For clean contacts the bath-temperature determines the resolution of the measured spectra. In equations (2.2-2.6), for simplicity an infinitesimal temperature ($T \rightarrow 0$) was assumed. At finite temperatures, the measured d^2I/dV^2 spectra will be smeared with a bell-shaped function with half-width 5.4 k_BT (van Gelder et al., 1980). It is clear that at helium temperatures this thermal smearing in general does not have a great influence on the spectra since the resolution then is about 1 meV while the spectra in general are much broader than this. Only at higher temperatures the effect becomes noticeable.

Recently a number of experiments have been performed in which the transport properties of point contacts were studied with an applied temperature gradient in the contact area. Concerning the heat flux through a contact it was shown that for contacts in the clean limit the quotient of the electrical and thermal resistance follows the Wiedemann-Franz law as for bulk material.

In the presence of electrical and thermal gradients, the influence of thermo-electric effect has been observed in point contacts. In a point contact the phonon drag contribution to the thermopower is quenched due to the small dimensions of the contact. The thermopower of a point contact therefore shows a distinct difference with that of bulk material.

Point contacts between different materials often show asymmetries in the current-voltage characteristics, which are not expected on basis of the in paragraph 3 discussed transport properties of a point contact. The asymmetries could be due to the Seebeck effect for the case of dirty contacts where the local heating causes intrinsic temperature gradients in the contact.

The measured temperature of the two banks forming a point contact was found to be asymmetric as a function of applied bias voltage. The voltage dependence of these asymmetries reveal phonon structures as can also be measured with normal point-contacts techniques.

2.6.1 Thermal conductivity of metallic point contacts

When a temperature gradient is applied to a point contact, then again the transport equations for phonons and electrons have to be solved using extra boundary conditions which involve the temperature at both sides of the point

contact with an applied temperature gradient. In contrast to the thermal conductivity of point contacts between nonconducting systems in the case of contacts between good conductors, the phonon contribution to the heat flow can be neglected with respect to the electric contribution. This of course does not mean that the phonon system does not play any role. The scattering of electrons with phonons will influence the current and the heatflow. This however, will be an effect of second order. In the zeroth order approximation, comparable with the ballistic injection of electrons without scattering, the heat flux Q(T) can be calculated easily. Measurements of both the thermal and the electrical resistance as a function of temperature, enable a determination of the temperature dependence of the Lorenz number L(T), assuming the Wiedemann-Franz law to be valid.

For the electronic distribution (figure 2.1a) in zeroth order approximation, i.e. the pure ballistic case without scattering, the entropy flux I_S is given by:

$$I_S^{(0)} = - \frac{m a^2}{2\pi\hbar^3} \int_0^\infty \epsilon \left[g^{T_2}(\epsilon - eV/2 - \mu_2) - g^{T_1}(\epsilon + eV/2 - \mu_1) \right] d\epsilon \,, \qquad (2.10)$$

where a quadratic dispersion law is assumed (Bogachek et al., 1985). Here the function $g(\epsilon)$ is given by $g(\epsilon) = f_0(\epsilon)\ln(f_0(\epsilon)) + f_0(-\epsilon)\ln(f_0(-\epsilon))$ in which $f_0(\epsilon)$ is the normal Fermi distribution function. μ_1 and μ_2 in equation (2.10) are the chemical potentials on both sides of the contact at temperatures T_1 and T_2 respectively. From this one can write as a simple result for the entropy flux:

$$I_S^{(0)} = - \frac{em}{\hbar^3} \frac{\pi a^2}{12} (T_1 + T_2) \cdot V^* + \frac{\pi^2 k_B^2}{3e^2} \frac{T_2 - T_1}{R_{el}} \,. \qquad (2.11)$$

Here $V^* = V + (\mu_1 - \mu_2)/e$ and R_{el} is the electrical resistance of the point contact, given by the Sharvin resistance R_S. Since the first term of this equation is much smaller than the second term, one can write for the heat flux $Q = I_S \cdot T$:

$$Q = \frac{\pi^2 k_B^2}{3e^2} \frac{T \Delta T}{R_{el}} \,. \qquad (2.12)$$

When $T_2 >> T_1$ this gives a quadratic temperature dependence of the heat flow. From equation (2.12) we now find an expression for the ratio between the electrical resistance R_{el} and the thermal resistance $R_{th} = \Delta T/Q$:

$$\frac{R_{el}}{R_{th}} = \frac{\pi^2 k_B^2}{3e^2} \cdot T = L_0 T \,, \tag{2.13}$$

where L_0 is the Lorenz number. Thus also in the case of point contacts, the Wiedemann-Franz law is valid.

Measurements of the heat flow through metallic constrictions were performed by Shklyarevskii et al. (1986b). They measured the heat flux through Au-Au point contacts at temperatures between 4.2 and 140 K. Figure 2.9 shows the measured heat flux Q as a function of point-contact resistance for

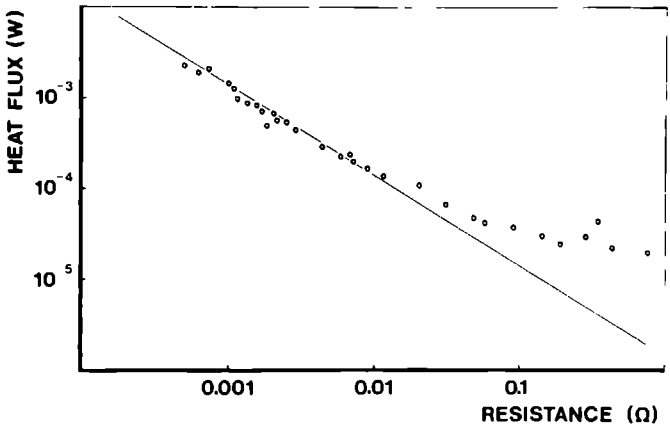

Fig. 2.9. Measured heat flux through different Au-Au point contacts as a function of contact resistance. The temperature at both sides of the contacts was T_1=4.2 K and T_2=10 K. The solid line represents the theoretical dependence, calculated with equation (2.12). [after Shklyarevskii et al., 1986b]

different contacts. The solid line in this figure is calculated with equation (2.12). A clear agreement is found between theory and experiment for contact resistances below approximately 0.01 Ω. For contacts with a larger resistance there is a strong discrepancy between theory and experiment. It can be assumed that in these cases the phonon flow through electrically non-conducting regions of the contact is large compared with the heatflow by electrons through the contact. For low contact resistances the measured heat flux indeed is quadratic in temperature up to 20-30 K, according to equation (2.12) for large ΔT=T-4.2K. At higher temperatures the exponent in this dependence is slightly smaller and for very low resistances (i.e. large contact

diameter) it even becomes linear, which is in agreement with the constant thermal conductivity for bulk metals at sufficiently high temperatures.

Equation (2.14) provides a possibility to measure the temperature dependence of the Lorenz number L. In the cited experimental work, the temperature dependence of L was determined. The behaviour which was found is similar as for bulk metal.

2.6.2 Thermoelectric effects in metallic point contacts

Recently a number of experiments are performed in which the influence is studied of the presence of a temperature gradient in the contact region on the electric properties of both metallic and semiconducting point contacts. In this section we will discuss the case of metallic contacts, in the next section on semiconducting ones. Temperature gradients in the contact region can be obtained by heating one side of the contact, but also by Joule heating by a current through the contact.

In the case of a homogeneous contact with a temperature difference $\Delta T=T_2-T_1$ across it, the electrical current for a ballistic contact is given by:

$$I^{(0)} = \frac{em a^2}{2\pi\hbar^3} \int_0^\infty \epsilon \left[f_0^{T_2}(\epsilon - ev/2 - \mu_2) - f_0^{T_1}(\epsilon + eV/2 - \mu_1) \right] d\epsilon \,, \qquad (2.14)$$

where f_0^T is the Fermi distribution at temperature T and μ_1 and μ_2 are the temperature dependent chemical potentials. Usually, i.e. when no temperature gradient is applied, this equation leads to the Sharvin resistance. With an applied temperature gradient it is possible to calculate from equation (2.14) at zero current density the diffusion term $S_{pc}^{\,e}$ in the thermopower of the point contact, which is then given by:

$$S_{pc}^{\,e} \equiv \lim_{\Delta T \to 0} \frac{\Delta\mu - eV}{e\,\Delta T}\bigg|_{I=0} = -\frac{1}{eT}\left[\frac{F_2}{F_1} - \mu_1\right]. \qquad (2.15)$$

Here $\Delta\mu=\mu_2-\mu_1$ is the difference in chemical potential and F_1 and F_2 are given by $F_n = \int \epsilon^n(\partial f_0/\partial\epsilon)\, d\epsilon$. Here a free-electron model with a spherical Fermi surface was assumed. We want to emphasize the fact that this is only the electron-diffusion term in the thermopower. In a metal the total thermopower is given by $S=S^e+S^{ph}$ where S^{ph} is the phonon-drag term in the thermopower which is due to the transport of electrons by the nonequilibrium

phonon system. The temperature dependence of the phonon-drag thermopower S^{ph} of bulk metals shows a maximum at about 0.2 θ_D where θ_D is the Debye temperature. This is because this phonon-drag component in a simple model is proportional to the lattice specific heat with a reduction factor $\alpha=\tau_{p,x}/(\tau_{p,x}+\tau_{p,e})$ for the efficiency of energy transport from the phonon system with respect to the electrons. ($\tau_{p,e}$ is the phonon-electron scattering time and $\tau_{p,x}$ the scattering time of phonons with other scatterers, e.g. phonons.) At low temperatures the phonons interact primarily with electrons and $\alpha=1$, but at high temperatures $\alpha=0$. As a result the thermopower of bulk material shows a maximum superimposed on a linear term from the diffusional contribution of the electrons. Note that for the electronic thermopower S^e of metals, the same expression is found as equation (2.15) for the point-contact case. In the point-contact case however, at low temperatures, the scattering of phonons ($\tau_{p,x}$) will be determined by the contact dimension so that α will be small and the phonon drag will be suppressed. Therefore the phonon drag term of the bulk material will be larger than that of a point contact.

Thermopowers in homogeneous metallic point contacts were measured by Shklyarevskii et al. (1986a). In their experiment, the Seebeck voltage was measured between the isothermal terminals of a chain, made of one metal, containing a point contact, over which a temperature difference $\Delta T=T-4.2K$ was applied by heating one side of the contact. The measurements were performed without any electrical current. The measured Seebeck-voltage in this case is equal to the difference between the thermal voltage over the bulk part and the point-contact part such that

$$V_{tot}(T) = V_{bulk} - V_{p.c.} = \int_{4.2}^{T} [\, S_{bulk}(T') - S_{p.c.}(T') \,]\, dT' \,. \qquad (2.16)$$

Here S_{bulk} and $S_{p.c.}$ are the bulk and the point contact thermopowers. An example is given in figure 2.10 for a Au point contact. We see that the measured thermopower resembles (even in absolute value) the bulk thermopower which is also plotted in this figure. At low temperatures there is a difference in the measured thermopower for different point contacts measured in the same set-up. Probably these effects are due to the Kondo effect, because especially the thermopower is very sensitive to small amounts of paramagnetic impurities. Because of a local distribution of paramagnetic impurities the measured thermopower changes from contact to contact with respect to the bulk thermopower. In measurements on Ag these effects were absent and the bulk thermopower was directly obtained in the point-contact arrangement. At high temperatures the measured thermopower becomes con-

stant. This constant background is not yet explained.

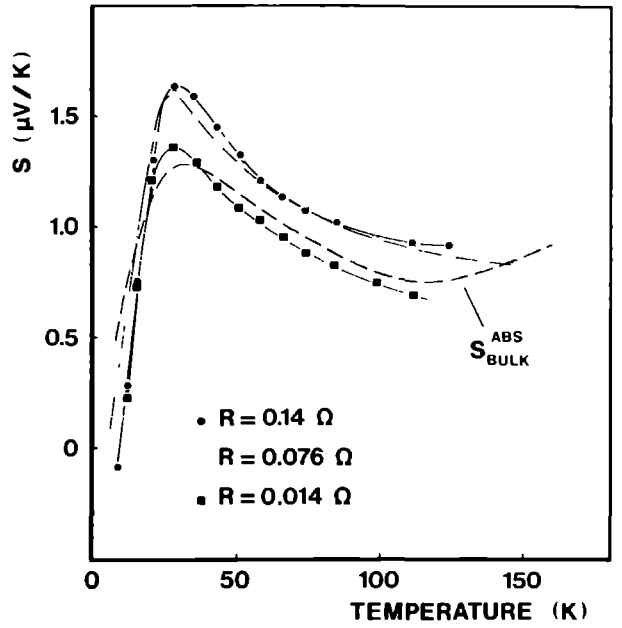

Fig. 2.10. Measured thermopower $S=S_{bulk}-S_{p.c.}$ as a function of temperature, measured over Au chains containing point contacts with indicated resistances. The dashed curve represents the absolute thermopower $S_{bulk}{}^{abs}$ for Au [after Pearson, (1961)].

An other case in which thermoelectric effects come into play is that of a current flowing through a nonhomogeneous point contact in the thermal limit. When heating occurs in the contact region, then the Seebeck effect will cause an extra voltage over the contact due to the different thermopowers of the two materials which form the contact. Besides this effect the Peltier effect will cause an extra heating or cooling of the contact, depending on the direction of the current flow. A third effect, the Thomson effect gives an extra heating in the contact area due to the presence of both a temperature gradient as an electric field. All these three effects together influence the voltage over the contact and consequently asymmetries in the current-voltage characteristics and their derivatives are observed. At low temperatures (i.e. low voltage over the dirty contact) the Seebeck effect is dominant.

These thermal voltages and asymmetries of the current-voltage charac-

teristics in nonhomogeneous point contacts were studied by Naidyuk et al. (1985). The most pronounced example of the studied phenomenon they found, was the shift in voltage at which the ferromagnetic transition shows up in Cu-Ni point contacts. As we already showed in figure 2.5 point contacts consisting of Ni show this transition around 190 mV, which corresponds in view of the heating model (eq. 2.8) with the Curie temperature of Ni. In the experiments on Cu-Ni, the same transition occurs, which however also depends a little on the sign of the applied bias. The difference ΔV between positive and negative bias is approximately 10 mV. This asymmetry can be explained with the Seebeck effect. Analogous to equation (2.16) one can easily show that the observed difference $\Delta V(V)$ must be equal to

$$\Delta V(V) = 2 \int_{T_{bath}}^{T_{max}} [\, S_A(T) - S_B(T) \,]\, dT \qquad (2.17)$$

in which T_{bath} is the bath temperature, T_{max} is the maximum temperature at the center of the contact given by equation (2.8) and $S_A(T)$ and $S_B(T)$ are the temperature dependent thermopowers of materials A and B between which the point contact is made. Calculation of this integral, using the temperature dependent thermopowers of Ni and Cu as known from literature, gives $\Delta V \simeq 22$mV which is of the same order as the measured value. This only gives a crude estimate of the voltage difference ΔV since at these high temperatures also the Peltier and Thomsom effects have to be incorporated.

Finally measurements were performed on Cu-CuFe and Cu-CuMn point contacts. Here already an asymmetry is observed for low energies ($eV \ll k_B\theta_D$) in the structure related to the Kondo effect. These contacts are believed to be in an intermediate state between diffusion and ballistic regime. From the observed asymmetry it can be concluded that even in this case a nonuniform temperature distribution is present in the contact area. It is possible that this temperature distribution has to be seen as the non-equilibrium distributions of electrons and/or phonons on both sides of the contacts.

2.6.3 Thermoelectric effects in semiconductor point contacts

Up to the present, electrical measurements on semiconductor point contacts were only performed in short-circuited MOS structures (Pepper, 1980a,b,c), showing a rich structure in the spectra due to phonons, and in In-InGaAs microchannel-contacts where an oscillatory behaviour is found

due to LO phonons (Pong-Fei Lu et al., 1985). A problem in pressure-type contacts with semiconductors is a very large contact resistance which occurs in most cases. Most probably surface states play a dominant role in this kind of experiments, leading to irreproducable results. In metal-semiconductor point contacts a Schottky barrier will be formed, then leading to large contact resistances at low voltages and large nonlinearities.

With a Cu-semiconductor-Cu chain with a constriction in the semiconductor part, Trzcinski et al. (1986) measured the thermoelectric voltage of Si

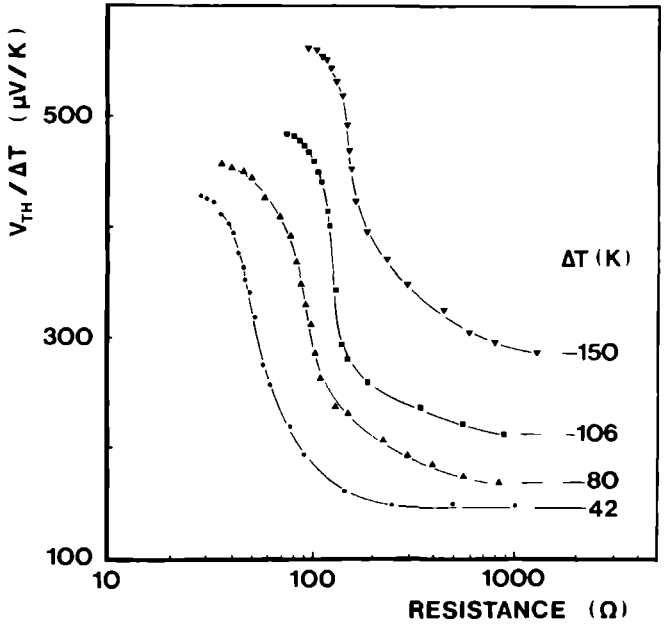

Fig. 2.11. Thermoelectric voltage V_{th}, divided by the temperature difference ΔT, measured over Cu-Si-Cu chains with a constriction in the Si, as a function of contact resistance for different applied temperature gradients ΔT over the contact as indicated in the figure. One side of the contacts was always kept on a constant temperature T_1=300 K. [after Trzcinski et al., 1986]

point contacts as a function of contact resistance. No electrical current was applied but one side of the contact was heated. Thus this experiment is the semiconductor-equivalent of the experiment by Shklyarevskii et al. (1986a) on metals, as discussed in section 2.6.2, but here the experiments were per-

formed at roomtemperature. Also here the thermopower can be thought of to exist of an electronic part and a phonon-drag part. Figure 2.11 shows the measured thermal voltage over the contacts, measured as a function of contact resistance for different applied temperature gradients. At a certain resistance, slightly dependent on the applied temperature gradient, a sharp drop of thermal voltage takes place within a narrow range of R. This sudden drop is ascribed to the quenching of phonon drag when the phonon mean free path becomes comparable with the contact dimension. The observed temperature dependence can be explained by the presence of more short-wavelength phonons at higher temperatures of which the scattering is less affected by a size reduction and therefore the effect occurs at smaller contact dimensions. A universal scaling was found, combining the effects of temperature and sample dimension.

2.6.4 Thermal phonon spectroscopy in Cu point contacts

In section 2.6.1 we already discussed the heat transport through metallic contacts due to an applied voltage and a temperature difference between the contact members. However the discussed transport is only the zeroth order approximation, comparable with the zeroth order solution in the electrical case, i.e. the ballistic injection of electrons without any scattering. In both cases no electron-phonon scattering effects can be expected to show up in the observed characteristics. In the second order solution however, these effects have to be considered. Bogachek et al. (1985) predicted a voltage dependent first order heat flux $Q^{(1)}$ from which the second derivative is given by

$$\frac{d^2Q^{(1)}}{dV^2} = -\frac{8}{3}\,\pi e^3 a^3\, A\, N(0)\, V\, \alpha^2F_p(T,eV/\hbar)\,, \qquad (2.18)$$

where A is a factor which is a measure of the regime in which the contact is. For instance in the ballistic regime this constant A is equal to unity. In the thermal regime however, it is reduced to $A = 8\ell_e/3\pi a \ll 1$. This means as we already have seen in the electric spectra, i.e. d^2V/dI^2, that the signals are considerably reduced when the contact is not (any more) in the ballistic state. In equation (2.18) N(0) is the electron density of states at the Fermi surface and the temperature dependence of the function α^2F_p has to be taken into account. We must remark that this equation (2.18) is only valid for the case that there is no temperature difference between both parts of the contact, i.e. $T_1=T_2$. For the case that the parts of the contact are not strictly kept at the same temperature, a temperature difference will occur which will also

contain structure because of the electron-phonon interaction.

Experiments on this subject were reported by Reiffers et al. (1986). They measured very accurately the temperature of both the two contact members as a function of the applied voltage. Their contacts were made between two pieces of bulk material to which thermometers were attached. In the measurements of temperature versus applied bias voltage, an asymmetry was

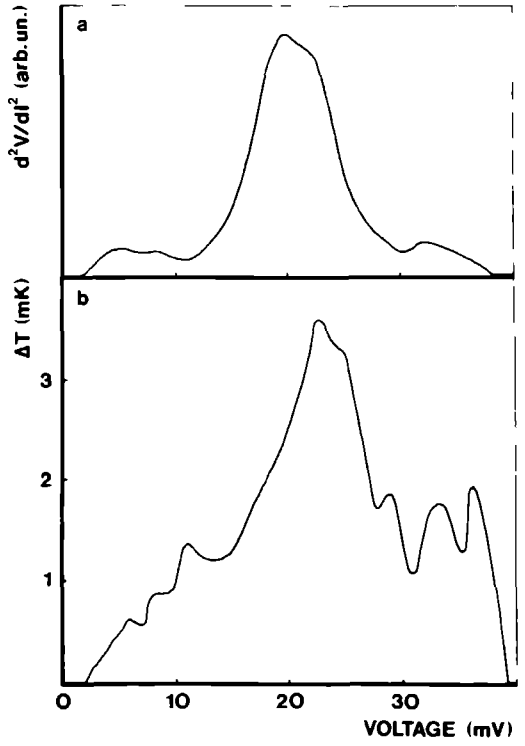

Fig. 2.12. Comparison between the measured d^2V/dI^2 spectrum as a function of bias voltage of a Cu point contact with resistance R_0=0.84 Ω at temperature T=0.72 K (a) and the measured asymmetry ΔT in temperature difference between the two contact members, between positive and negative bias for the same contact at the same bath temperature (b). [after Reiffers et al., 1986]

found with respect to V=0. In figure 2.12 their results are depicted. Part (a) gives the well known electron-phonon interaction point-contact spectrum of

copper, part (b) the measured temperature difference between positive and negative bias as was measured in these experiments. There is a striking resemblance between the measured second derivative d^2V/dI^2 and the measured temperature difference ΔT in this experiment. The occurrence of maxima at the same energies as where the phonon peaks in d^2V/dI^2 occur implies that the electron-phonon interaction does also in this experiment play an essential role in the shape of the measured asymmetry, as was more or less predicted by the theory of Bogachek et al. (1985).

Besides the broad maxima at the energies of the transversal and the longitudinal phonons additional structure with maxima and minima is found in these experiments, which occur probably due to different mechanisms of scattering. The positions of these maxima and minima are in reasonably good agreement with the position of the extrema in noise spectra of copper point contacts (Akimenko et al., 1984b).

2.7. Special experiments on and with point contacts.

We will now discuss a number of experiments which were performed recently and which are different from the traditional type of experiments in which interaction mechanisms of the conduction electrons with elementary excitations in the metal are studied.

The influence of a magnetic field for instance on bulk material is fairly well understood but a point contact shows some unexpected, interesting features when it is placed in a magnetic field. Measurements on point contacts in high magnetic fields display a quadratic magnetoresistance and superimposed on that Shubnikov-de Haas like oscillations.

Metallic point contacts can also be brought into a high-frequency electromagnetic field. Already for long time they are used as HF rectifiers, mixers and harmonic generators. The origin of the rectifying mechanism can be explained in terms of the discussed models of the non-linear current-voltage characteristics in point contacts. Also here one has to distinguish between point contacts in the ballistic and those in the thermal regime. The results of measurements in both these regimes are different. This provides a new method to distinguish between the two regimes. When the applied laser frequency is chosen large enough, photon-assisted-tunneling effects come into play.

With double point contacts a number of experiments have been performed in which the electrons were injected by the first contact and with help of a transversal magnetic field were focussed on the second contact. This set up gives the possibility to study the Fermi surface of the metal and even the energy dependence of the electron-phonon interaction for electrons in a

specific orbit on the Fermi sphere.

Noise measurements on Cu-Cu show that point contacts exhibit a $1/f$ noise spectrum. As a function of applied bias voltage the spectral density of this noise shows a quadratic dependence. However on this quadratic dependence a structure with minima and maxima is superimposed. The positions of these extrema coincide with different phonon processes in the examined material.

At last experiments are described in which the phonon spectrum generated with a point contact were examined. In the ballistic regime one expects a phonon distribution with a cut off energy equal to the applied energy eV. In an experiment in which B^+ impurities in Si were used as a phonon detector, this distribution could not be confirmed, probably due to a premature thermalisation of the phonon system.

2.7.1 Point contacts in high magnetic fields

Magnetic fields have mostly been applied in point contact experiments as a tool to change some material parameters of the metal under study. For instance magnetic fields have been used to quench superconductivity in order to enable measurements of the electron-phonon interaction for point contacts in the normal state. An other example is the influence of magnetic fields on magnetic excitations to be studied with the point-contact technique. However recently also a number of experiments have been performed in which the direct influence was studied of a magnetic field on the point-contact resistance. The most striking phenomena which occur in these experiments are the observed magnetoresistance and an oscillating magnetic field dependence of the contact resistance.

Due to the change in the electron trajectories, the "classical" magnetoresistance affects the resistivity of the material under study. Hence the Maxwell part $R_M = \rho/2a$ of the point-contact resistance changes as the bulk magneto resistivity. The superimposed oscillatory behaviour of point contacts in magnetic fields can be ascribed to the Landau-quantisation of the electron orbits.

2.7.1.1 Magnetoresistance in metallic point contacts

We will first focus on the observed classical magnetoresistance in metallic point contacts. As we already mentioned in paragraph 2, in a simple picture the point-contact resistance can be thought of to exist of a ballistic part, the Sharvin resistance, and a diffusive part, the Maxwell resistance (equation 2.1). For a clean contact the Sharvin resistance will dominate and the Maxwell resistance will hardly be noticeable. However the resistivity of the material under study can be affected considerably by applying a magnetic

field. The Maxwell resistance becomes more important, and can even give the main contribution to the observed magnetoresistance.

The resistivity of a metal is in general strongly dependent on the direction and the size of the magnetic field. We must however distinguish here compensated metals, i.e. where the number of holes and electrons is equal, and uncompensated metals. In the case of compensated metals the transversal magneto resistivity ρ_t is according to the LAK theory (Lifshitz et al., 1956) given by

$$\rho_t = (1 + \beta^2)\, \rho_0 \,. \tag{2.19}$$

Here ρ_0 is the zero-field resistivity and β is a parameter proportional to the magnetic field and in a simple picture equals to $\beta = \omega_c \tau$, with the cyclotron frequency $\omega_c = eB/m^*$, and the electron relaxation time τ. The longitudinal resistivity ρ_l is not affected by the magnetic field. In high magnetic fields, values for β of 10^3 can easily be obtained for pure materials and the resistivity will be very anisotropic in a magnetic field. As a consequence the point-contact resistance will have an important Maxwell component originating from the resistivity component perpendicular to the magnetic field. For a point contact placed on a sample of thickness d in a magnetic field perpendicular to this sample, the magneto resistance component resembles the square resistance ρ_t/d and can be written as

$$R = (1 + \beta^2)\, \frac{\rho}{2\pi d} \ln (D/4a) \,. \tag{2.20}$$

Here D is the sample diameter where the sample is assumed to be circular with the current and voltage contacts on its border, and a is the radius of the point contact. From equation (2.20) we see that we also can expect a quadratic magnetic-field dependence of the Maxwell resistance as in bulk materials. With the semiclassical theory no effect of a magnetic field is expected on the Sharvin resistance, which is independent of the electronic scattering time.

In an experiment Swartjes measured this effect on bismuth (Swartjes, 1987). He measured both the bulk and the point-contact magnetoresistance of this material. A comparison of both measurements confirmed the validity of equation (2.20) for the resistance of a point contact in a magnetic field.

In the case of uncompensated materials the magnetoresistance is usually very small. However in the Corbino geometry with a central contact on a circular sample, and the other contact on the total contour, again a quadratic magnetic field dependence is found. The origin for this magnetoresistance lies in the circular symmetry of the Corbino geometry, which hinders the

built up of a Hall voltage. Usually in uncompensated metals, the Hall voltage compensates the deflection of electrons in a magnetic field, and the magnetoresistance is small. A point contact can be regarded as a Corbino geometry and will thus exhibit a considerable magnetic field dependence. In this case a similar expression as equation (2.20) can be given for the point-contact magnetoresistance. In a point-contact experiment with Al this effect was observed (Swartjes, 1987)

2.7.1.2 Magneto-oscillations in metallic point contacts

It is commonly known that a number of physical quantities of metals show oscillations when measured as a function of magnetic field. The origin of these oscillations lies in a redistribution of the electrons when the Landau tubes cross the Fermi surface for increasing magnetic field. Well known examples of this oscillatory behaviour are the de Haas-van Alphen effect in the magnetic susceptibility and the Shubnikov-de Haas effect in the electrical resistivity. The latter manifests itself in the Maxwell resistance since this is according to equation (2.20) proportional to the resistivity.

When the typical length on which an electron is localised, becomes large compared with the contact dimension, a semiclassical calculation as is used to derive the Sharvin resistance is not applicable any more, but a quantummechanical approach is necessary. In the case of no applied magnetic field, this length is the de Broglie wavelength $\lambda=2\pi/k_F$ which will in most cases be small compared with the contact dimension. When a magnetic field is applied, this length becomes the magnetic length $\Lambda=(2\hbar/eB)^{1/2}$ which is comparable with the contact dimension for fields of the order of 5 T.

A quantummechanical approach with the Wigner formalism for the problem was used by Bogachek et al. (1985) for the case $\Lambda<<a$. They found oscillations in the point-contact resistance proportional to $z^{-3/2}$, where $z=\mu/\hbar\omega_c$ is the number of filled Landau levels below the chemical potential μ. In an other approach (Swartjes et al., 1987) the problem is considered as a diffraction problem for the case $\lambda>a$ or $\Lambda>a$. The wavefunctions of the incoming electrons will lose their directional information after passing the contact. As a consequence of this, in the derivation of the Sharvin resistance, which is a summation over all the perpendicular components of the electron velocity in k-space, i.e. $\int d^3k\ v_z$, the term $dk_z v_z$ has to be replaced by $\sum_{j'} dk_{z,j} v_{z,j'} \Delta_\gamma(j,j')$, where the summation goes over all possible plane wave directions of the outgoing electron. The function $\Delta_\gamma(j,j')$ describes the coupling between k_z and v_z and depends on the ratio γ between contact diameter and electron wavelength. A calculation using this approach yields

(Swartjes et al., 1987) for the case that no magnetic field is applied:

$$\frac{1}{R} = -\frac{e^2}{2\pi\hbar}\frac{Sk_F^2}{2\pi}\int_0^{2k_Fa} d\xi\ \eta(\xi/2k_Fa)\ \frac{d}{d\xi}((\sin\xi)/\xi)^2\ , \qquad (2.21)$$

which in the semiclassical limit $k_Fa>>1$ reduces to the Sharvin resistance R_S. In this equation S is the contact area and $\eta(\xi)$ is the overlap of the contact with itself when shifted over the vector ξ. This ξ is any vector laying in the contact area. Equation (2.21) describes the quantummechanical deviation from the Sharvin resistance R_S for contacts with a dimension comparable with the interatomic distance. In figure 2.13 the resistance which is calculated with equation (2.21), normalised with the Sharvin resistance, is plotted as a function of k_Fa for circular contacts with radius a. Note that for large k_Fa the point-contact resistance equals the Sharvin resistance and hence the problem can be treated semiclassically.

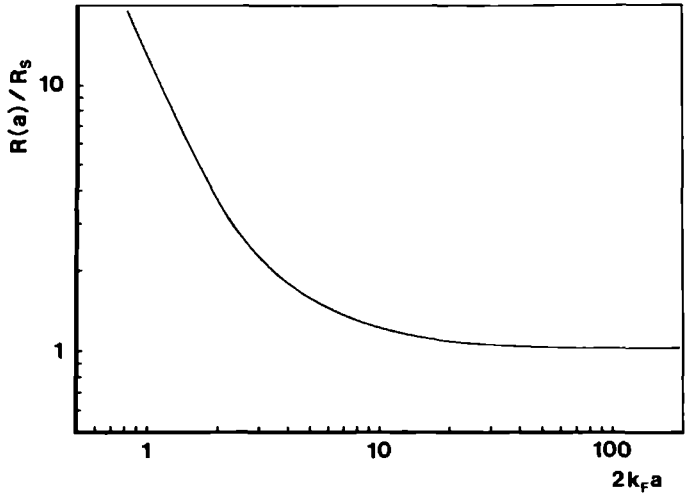

Fig. 2.13. Calculated contact resistance R(a), normalised with the Sharvin resistance R_S, plotted as a function of k_Fa, showing the quantummechanical deviations from this Sharvin resistance for contacts with very small diameters.

When a magnetic field is applied, the summation in the calculation of the

Sharvin resistance now goes over wavefunctions of electrons in a magnetic field, instead of over plane waves, and the index j' now goes over all Landau levels. A calculation (Swartjes et al., 1987) yields two separate oscillations in the point-contact resistance, one with relative amplitude $z^{-3/2}$ and one with $z^{-1/2}$. Including the diffraction at the orifice of an electron wave function in a magnetic field, a considerable enhancement is expected of the oscillatory quantum effects in the magnetoresistance of a point contact ($z^{-1/2}$ dependence compared with $z^{-3/2}$). Figure 2.14 gives an example of these quantummechanical oscillations of a point contact in a magnetic field. The resistance of a Al-Cu point contact shows an oscillatory behaviour, periodic in 1/B, which can be ascribed to Landau tubes in the third zone of the Fermi surface of Al.

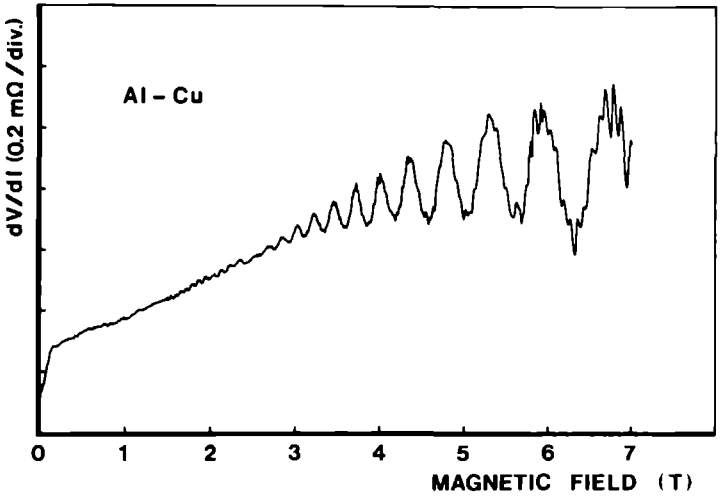

Fig. 2.14. Measured differential resistance dV/dI of a Al-Cu point contact with resistance R_0=1.3 Ω at temperature T=1.85 K, as a function of magnetic field, showing the magneto-oscillations of point contacts in magnetic fields.

2.7.2 Point contacts in high-frequency electromagnetic fields

Already for a long time point contact diodes are used as rectifiers, mixers and harmonic generation elements for high-frequency purposes, i.e. for fre-

quencies up to the near visible. The point contacts which are used for these cases, consist of a whisker, sharpened to a small point and put on a piece of bulk material. The whisker serves as an antenna through which a high-frequency current is induced inside the contact. Because of the nonlinear current-voltage characteristic of such a point contact, the element can be used for purposes as mentioned above.

When a point contact is brought into a high-frequency electromagnetic field, the radiation field acts as a high-frequency current source, because the point-contact resistance is usually smaller than the vacuum impedance. Chopping the radiation at a low frequency, it can easily be shown that the measured voltage at this chopper frequency is proportional to the second derivative d^2V/dI^2 as measured with the traditional techniques, using a low frequency current modulation. Thus with this technique it is for instance also possible to measure the α^2F function, however now using a modulation with a much larger frequency. This effect was first observed by v.d. Heijden et al. (1980), who measured this rectification by a Cu-Cu point contact and found a laser-detected signal which was completely in agreement with the measured second derivative d^2V/dI^2, as measured with a low-frequency modulation.

In order to measure a signal proportional to the second derivative d^2V/dI^2, the processes which determine the current-voltage characteristics have to be fast compared with the applied HF-modulation frequency. In the experiments by van der Heijden et al. the characteristic time τ for these processes is the electron-phonon scattering time $\tau_{el\text{-}ph}$ which is typically 10^{-14}-10^{-13} seconds for Cu at helium temperatures. Therefore the criterion $\omega\tau<1$ for the laser-detected signal to follow the nonlinear DC current-voltage characteristics is fulfilled in these experiments.

The criterion $\omega\tau<1$ will not hold any longer in the situation that heating is the main effect which determines the current-voltage characteristics. Then the characteristic time constant for the nonlinearity is given by the thermal relaxation of the contact. It is given by the quotient of the total heat capacity of the contact and the conduction of heat out of the contact area, i.e. $\tau \sim C/\Lambda \simeq cd^3/(\lambda d^2/d) = cd^2/\lambda$, where d is the contact diameter, c is the specific heat and λ the thermal conductivity of the metal under study. For a contact with a typical dimension of $d \sim 10$ nm one finds $\tau \sim 10^{-9}$ seconds, hence the signals will change in this regime at frequencies in the GHz regime. An example of this is the experiment by Balkashin et al. (1982), who measured the rectification signal of a Ni-Ni point contact at roomtemperature for different HF-modulation frequencies. Figure 2.15 gives their results. Part (a) gives the measured second derivative d^2V/dI^2 obtained with the standard technique at 483 Hz, showing the ferromagnetic transition due to heating of the contact area (see also figure 2.5). Parts (b-f) are the rectification signals measured with increasing frequency. For frequencies below 300 MHz the

observed signal resembles the d^2V/dI^2 spectrum. At higher frequencies deviations occur from this behaviour. One can conclude that the timescale imposed by the 300 MHz radiation is of the same order of magnitude as the

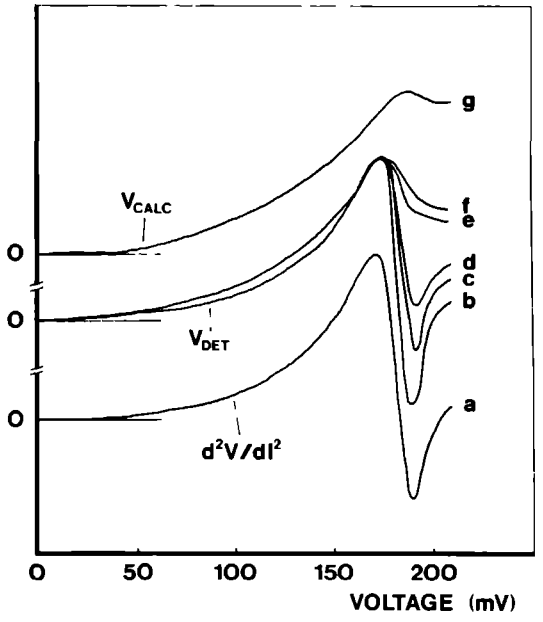

Fig. 2.15. Measured d^2V/dI^2 spectrum (a), rectification signals at five different HF-modulation frequencies (b-f) [after Balkashin et al., 1982] and the calculated rectification signal for the thermal regime (g) as a function of applied voltage for a Ni-Ni point contact with a resistance $R_0 \simeq 3.3\ \Omega$ at room-temperature. The curves have been shifted with respect to each other. The applied radiation frequencies were 0.3 (b), 1.0 (c), 2.0 (d), 12 (d) and 16.6 GHz (e). The theoretical curve was calculated with equation (2.22).

thermal relaxation time of the contact. At higher radiation frequencies the temperature can not follow the modulated current and a constant rise in temperature due to the HF-current modulation will occur. It is easily shown that the in the experiment detected signal is given by (Lysykh et al., 1987b):

$$V_{det.} = \frac{\sqrt{2}i^2}{8} R_s \frac{dR_s}{dV}, \qquad (2.22)$$

where R_s is the static resistance of the point contact and i is the amplitude of the induced HF current. This theoretical rectification signal is also plotted in figure 2.15 (curve g). There is a strong resemblance between this curve and the signal, measured at the highest frequency (166 GHz). A complete agreement is not found since probably the criterion $\omega\tau>>1$ is not yet totally fulfilled at this frequency.

Also for the electron-phonon interaction in clean contacts it is possible that the measured rectification signal does not resemble the second derivative d^2V/dI^2. A considerable broadening of the spectra occurs when the changes in the I-V characteristics take place on a voltage scale comparable with or larger than $\hbar\omega/e$ of the applied radiation. This broadening, only occurring at higher radiation frequencies, can be described with the photon-assisted tunneling (P.A.T.) theory (Tien and Gordon, 1963). The P.A.T. effect can be considered as the quantum mechanical analogue of classical rectification and is mostly observed in tunneling experiments with superconductors. In figure 2.16 the broadening at high radiation frequencies is visualised. The upper curve represents the rectification signal for a Cu point contact measured at a laser frequency of 525 GHz (i.e. 2.2 meV). The shape of the signal resembles the d^2V/dI^2 spectrum of Cu (see e.g. figure 2.2). The lower curve gives the rectification signal of a Cu point contact, measured at a laser frequency of 2523 GHz (i.e. 10.4 meV). Here the broadened signal is fitted with the dashed line which is calculated using the P.A.T. expression for the DC current at voltage V when radiation is applied:

$$I_{DC}(V) = \sum_{n=-\infty}^{n=+\infty} J_n^2(\alpha)\, I(V + n\hbar\omega/e), \qquad (2.23)$$

where I(V) is the DC current in the absence of radiation, J_n is the n^{th} order Bessel function and $\alpha=eV_{AC}/\hbar\omega$ in which V_{AC} is the induced HF-modulation voltage over the contact. Photon-assisted tunneling is mostly seen in experiments on nonlinear elements in which a superconductor is involved. In the experiment by van der Heijden et al. (1984, figure 2.16) it was for the first time observed in a normal-metal element.

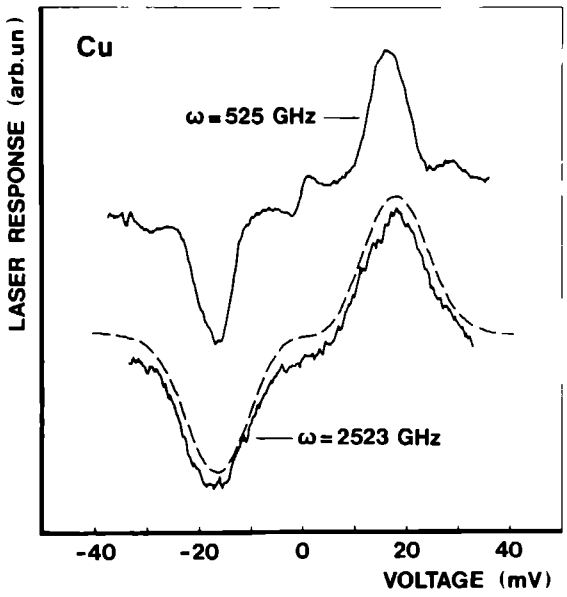

Fig. 2.16. Rectification signals measured with a radiation frequency 525 GHz for a Cu-Cu point contact with resistance R_0=4.9 Ω at temperature T=1.2 K (upper curve) and with radiation frequency 2523 GHz for a Cu-Cu point contact with resistance R_0=42.1 Ω at temperature T=1.2 K (lower curve). In this last curve the photon-assisted tunneling effect gives a considerable broadening of the spectrum. The dashed curve was calculated with equation (2.23).

2.7.3 Transverse electron focussing with double point contacts

By a magnetic field electrons can be focussed in a metal from one point contact to another, revealing details of the trajectories on the Fermi surface. In the experiments the electrons are injected into a single crystal with a point contact (the emitter) and are after focussing detected with a second point contact (the collector). The first experiments of this type were performed by Sharvin and Fisher (1965). They placed emitter and collector at opposite sides of the crystal with the focussing magnetic field parallel to the axis between the two contacts. The method of focussing electrons between two contacts was improved by Tsoi (1974) by using a transverse magnetic field instead of

a longitudinal one. The emitter and collector were now placed on the same side of the crystal (see inset figure 2.17). This opened the possibility to study the Fermi-surface orbits and specular reflections of the conduction electrons with the crystal surface. With this method of transversal electron focussing it turned out to be possible to observe directly the Andreev reflection of electrons on a normal metal-superconductor interface.

Recently the method has been used to study the energy dependence of the electron-phonon interaction. As an advantage compared with the traditional point-contact experiments on this interaction, in the double-point-contact experiments the interaction can be studied on a specific orbit of the Fermi surface.

The technique of transverse electron focussing is easy to understand. As we already mentioned, electrons are injected into the metal by the emitter point contact. A homogeneous magnetic field, parallel to the crystal surface, forces these electrons on paths in real space which are just the orbits in k-space but rotated over 90 degrees and scaled with a factor $\hbar/eB$. The electrons follow paths over the Fermi surface perpendicular to the field direction and return to the surface on a certain distance from the point of injection, depending on the strength of the applied magnetic field. The electrons are injected into all directions, but focussing takes place at a distance $2\hbar k_F/eB$ from the emitter.

For the case of specular reflection on the surface, focussing also occurs at the multiples of this distance from the emitter. Figure 2.17 shows the observed collector voltage on a Ag (001) surface as a function of the magnetic field. For the chosen crystal orientation with respect to the magnetic field, focussing of the electrons on belly orbits (peaks α_1,α_2) and on four-cornered-rosette orbits (peaks β_1,β_2) can be observed. The peak α_1 (β_1) corresponds to the direct focussing and α_2 (β_2) after one reflection. From the relative intensity of successive peaks a study can be made of the internal reflectivity of the Ag surface (Benistant et al., 1986). The electrons on the rosette orbits (β_1,β_2) are seen at negative fields because the effective mass of the electrons on these orbits is negative, resulting in a opposite rotation of the electrons in a magnetic field compared to the belly orbits.

Transverse electron focussing has been applied to investigate the Andreev reflection of electrons at the interface between a normal metal and a superconductor (Bozhko et al., 1982, Benistant et al., 1983). An Andreev reflection describes the process of an electron passing from a normal to a superconducting metal. The traversing electron condenses into the superconducting state by forming a Cooper pair with an other electron, withdrawn from the normal metal. Because of mass, charge, and momentum conservation, a quasi particle with opposite mass, groupvelocity, and charge, i.e. a hole will come back from the interface into the normal metal. A direct observation of the Andreev reflection can be made by evaporating a superconducting film on

the Ag surface opposite to the surface where the emitter and collector are placed. In the inset of figure 2.17 an example of an Andreev reflected quasi particle is given in the presence of a magnetic field. In the same figure the γ-peak detects the focussing of the holes originating from an Andreev reflection. The amplitude of the γ-peak is opposite to the other peaks because of the opposite charge of the quasi particles. Andreev reflection was also observed in an experiment with a single point contact on a thin Ag crystal

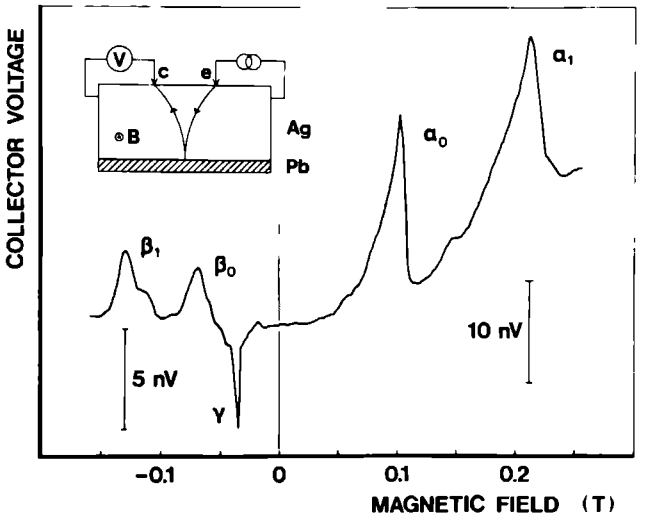

Fig. 2.17. Measured collector voltage on a Ag (001) surface in a TEF experiment as a function of applied magnetic field. The α peaks indicate focussing of electrons on belly orbits, the β peaks of electrons on four-cornered-rosette orbits. The γ peak detects the focussing of holes, originating from Andreev reflections of electrons at the Ag-Pb interface. The inset shows the experimental setup with an example of a trajectory of an Andreev reflected quasi particle from the emitter to the collector in the presence of a magnetic field.

with a Pb-film evaporated at the opposite side (Benistant et al., 1985). This single point contact served both as emitter and as collector in the experiment. Because of the retro-reflection of the quasi particles at the surface between superconductor and normal metal, the Andreev reflected quasi particles return exactly at the place of ballistic injection. The voltage-dependent resistance of the single contact shows a minimum for voltages below the super-

conducting gap, where Andreev reflections are possible. With this experiment the energy dependence of the Andreev reflection has been investigated by measuring the voltage-dependent contact resistance.

A more recent experiment in which TEF between two point contacts was used, is that of van Son et al. (1987) in which the electron-phonon interaction is studied. In this study the magnetic field was tuned at a value B_0 for electron focussing to occur. At this field the decrease of the focussing peak was measured with increasing energy of the emitted electrons. The focussing-peak height P will be a function of the emitter voltage via

$$P(eV) = P(0) \exp [-t/\tau(eV)] , \tag{2.24}$$

in which $\tau(eV)$ is the energy-dependent scattering time of the electrons and $t=\pi m/eB_0$ is the time during which the electrons travel from the emitter to the collector. For T=0 the electron-phonon scattering time is given by (equation (2.5)):

$$\frac{1}{\tau(\epsilon,T=0)} = 2\pi \int_0^{\epsilon/\hbar} d\omega \, \alpha^2F(\omega) \simeq b\epsilon^3 . \tag{2.25}$$

Here $\alpha^2F(\omega)$ is the Eliashberg function which for low energies may be approximated by a quadratic energy dependence. The coefficient b depends on crystal direction. Thus using the effects of TEF it is possible to measure the anisotropy in this coefficient. This is a great advantage of this method compared with the normal point-contact spectroscopy in which an average is made over all possible crystal directions. Figure 2.18 shows the measured TEF signal as a function of applied emitter voltage for an experiment on the (100) surface of Ag with the magnetic field pointing along the [001] direction. Clearly visible is the decrease in signal when the electron energy is increased due to the increasing scattering rate $1/\tau$ of the electrons along their path. At higher voltages a background signal arises with even a second maximum at approximately 12 mV. The background can be ascribed to electrons which scatter close to the emitter into the direction of the focussing orbit. The maximum at about 12 mV coincides approximately with the maximum, observed in traditional point-contact spectra. The dashed curve in figure 2.18 is the calculated voltage dependence of the TEF signal, using equations (2.24) and (2.25) with b as fitting parameter. By measuring the focussing signal at different crystal orientations, v. Son et al. investigated the anisotropy in the electron-phonon scattering.

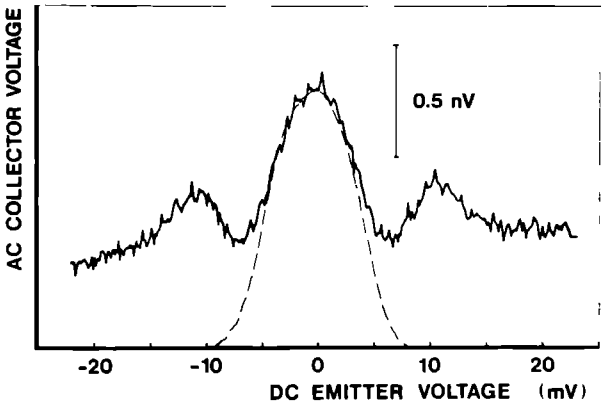

Fig. 2.18. Measured AC collector voltage as a function of applied emitter voltage for a TEF experiment on the (100) surface of Ag with the magnetic field in the [001] direction, showing the decrease of signal at increasing emitter voltage due to an increase of scattering of the electrons along their trajectory. The dashed line is the theoretical TEF signal, calculated with equations (2.24) and (2.25).

2.7.4 Noise in point contacts

Because of the small dimensions of point contacts, $1/f$ noise is the dominant type of noise which is observed for frequencies up to a few kHz. According to Hooge's empirical formula for the powerdensity of this noise, $S_V=\alpha V^2/Nf$ (Hooge and Hoppenbrouwers, 1969), where α is a constant and N is the total number of charge carriers, this $1/f$ noise becomes more important when the number of charge carriers in the fluctuating system is decreased, for instance in semiconducting systems or in systems with very small dimensions, e.g. point contacts. For a contact the total number of charge carriers is given by the product of the electron density n and the contact volume a^3.

Measurements on Na, Cu and Ni indeed show this quadratic voltage dependence for contacts in the dirty limit (Akimenko et al., 1984) for low voltages. For higher voltages deviations occur. Also contacts in the ballistic regime exhibit noise spectra which correspond well with Hooge's formula. However in these spectra an additional structure is observed in the voltage range of the phonon frequencies. The noise spectra reveal features, not

always exactly reproducible, but much sharper and more detailed than in the usual point-contact spectra. A correlation of the maxima and minima in the spectra is found with specific umklapp and normal scattering processes in the electron-phonon interaction.

2.7.5 Generation of phonons with metallic point contacts and their detection

In section 2.3.1 we discussed the background which is often present in the measured phonon spectra. An explanation for this background is the existence of nonequilibrium phonons in the systems and subsequent additional scattering of conduction electrons with these nonequilibrium phonons. Thus in the case of ballistic contacts, we both have electron and phonon systems which are not in equilibrium. So far most experiments on point contacts dealed with the nonequilibrium electron distribution which is reason for most electrical and thermal nonlinearities. Recently some experiments have been performed in which the generated phonon system was studied. Bottleneck in all these experiments is the fact that the phonons which are generated by the point contact have to travel through a metal film and pass the boundary between this metal film and an insulator or semiconductor in which detection takes place. In this transport of phonons from the contact area, extra scattering of these phonons can take place, resulting in a possible thermalisation of the phonon system. Thus both film thickness and boundary have to be controlled very carefully in the experiments.

The non-equilibrium phonon distribution for a ballistic point contact is given by (Jansen et al., 1980):

$$N(\epsilon,eV) = 0.32\ \frac{eV - \epsilon}{\epsilon}\ \frac{a}{\ell_p(\epsilon)} \qquad (\epsilon \leq eV)\ , \tag{2.26a}$$

$$N(\epsilon,eV) = 0 \qquad (\epsilon \geq eV)\ , \tag{2.26b}$$

where $\ell_p(\epsilon)$ is the energy-dependent phonon mean free path and V is the applied bias voltage over the contact. Striking feature of this phonon distribution is the cut off at a phonon energy ϵ=eV. In the case of a normal heater or whenever the phononsystem is thermalised, one has a Bose distribution of phonons which is then given by

$$N(\epsilon,T) = \left[\ \exp\left(\epsilon/(k_B T)\right) - 1\ \right]^{-1}\ . \tag{2.27}$$

This distribution still has a nonzero value for high phonon energies, i.e. up to the Debye energy. In general the temperature T in such a thermal phonon

distribution depends on the applied voltage V. For instance in the case of a point contact in the dirty regime this dependence is just given by equation (2.8).

In an experiment by Goosens et al. (1984) the phonon distribution in a point contact configuration was studied using a fluorescence experiment in ruby. By measuring the R_2 fluorescence, ruby can be used as a detector which is sensitive for phonons with an energy of 3.6 meV. The phonons were generated in a point contact which was made between a Au whisker and a Au film, evaporated on the ruby. The phonon detection was not sensitive enough to detect any signal around an applied voltage of 3.6 mV, where a threshold in the detected signal was expected. For higher applied voltages it was concluded that the point contact acts as a Planck's radiator ($P \propto T_{eff}^4$).

In an other experiment an attempt was made to distinguish between the nonequilibrium distribution (eq. 2.26) and the thermal phonon distribution (eq. 2.27). Here a thin gold film of 40 nm thickness was evaporated on a silicon crystal with thickness 3mm, which was doped with boron impurities. These boron impurities supply a phonon detection mechanism. By illumination with visible light, one creates electron-hole pairs in the silicon. The boron impurities can bind such a hole, forming a B^+ impurity with an ionization energy of 2.0 meV. Phonons with an energy larger than this ionization energy neutralize the acceptors, yielding extra holes in the valence band of the Si and hence increasing its conductivity. A more detailed description of the B-doped Si as a phonon detector can be found in publications by Burger et al. (1984, 1986).

In the evaporated gold film, phonons were generated with a point contact. After travelling through the Au-Si interface and through the Si sample, these phonons were detected with phonon-induced conduction at the opposite side of the Si sample. Figure 2.19 gives an example of the detected signal as a function of bias voltage over the point contact.

Assuming that the observed conduction enhancement is directly proportional to the number of present phonons in the Si, one can write for the measured signal

$$V_{det} \propto \frac{d}{dV} \int_{\epsilon_c}^{\epsilon_D} N(\epsilon)\, F(\epsilon)\, d\epsilon \,. \qquad (2.28)$$

Here ϵ_c is the threshold energy above which the phonons give a contribution, i.e. it is the ionization energy of the B^+ impurities, viz. 2 meV; ϵ_D is the Debye energy; $N(\epsilon)$ is the phonon distribution function and $F(\epsilon)$ is the phonon density of states which in the Debye approximation equals $F(\epsilon) \propto \epsilon^2$.

The voltage derivative in equation (2.28) appears because the measurements were performed with a lock-in technique.

In figure 2.19 this calculated signal is represented by the dashed lines using the phonon distribution of a heater (upper dashed curve) and of a ballistic contact (lower dashed curve). Although the two dashed curves are very similar, the derivative signal dV_{det}/dV which was also measured, is better described with the thermalised phonon distribution of a heater. For this heater model, the heater temperature was related to the applied voltage as for a Planck radiator, i.e. $T^4=T_{bath}{}^4+\alpha^2V^2$, where α is given by the matching for the phonons between the heater (i.e. the hot spot in the Au film) and the Si crystal (Weis, 1969, Rösch and Weis, 1977). In the same figure also the measured signal is drawn for the case where the Au film was used as a uni-

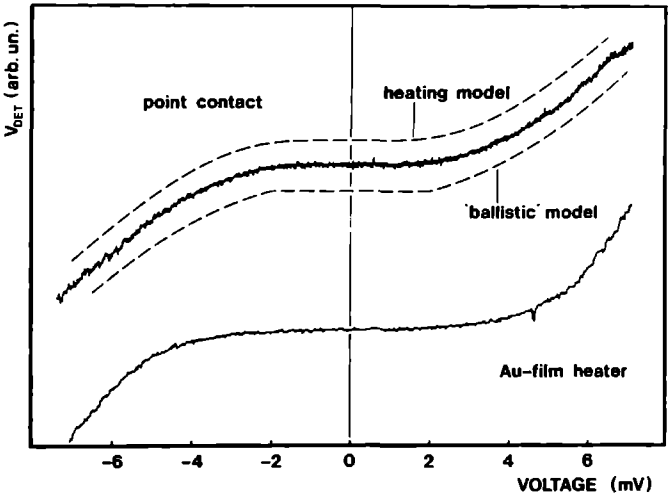

Fig. 2.19. Measured phonon-induced conductivity signal in Si with a Au point contact (upper curves) and a Au film (lower curve) as phonon generator, as a function of applied bias voltage over the generator. The point contact was made between a Au whisker and a Au film, evaporated on the Si crystal. The dashed curves are calculated signals using the heater model (upper dashed curve) and a ballistic-contact model (lower dashed curve).

form heater.

Assuming that the point contact acts as a heater, the factor α which links temperature with voltage, can be obtained from comparing the measured signals with the calculated ones. The theory for the matching between a Au

film and a Si crystal predicts a value of α according to $\alpha^4 AR = 6.3\ 10^{-3}$ K^4m^2s/J, in which A is the area of the hot surface and R the heater resistance. Applying this to the experimental results of the point contact, one finds a hot area of ~200x200 μm^2, much larger than one would expect by a comparison with the contact diameter (~10 nm) or the inelastic electron mean free path (~1 μm).

From the experiments it can be concluded that a threshold at $eV=\epsilon_c$ is not observed. Besides, the measured signals are very well described with a heater model, however this leads to a unexpected large hot area. That a "ballistic" phonon distribution is not observed is probably due to a acoustic mismatch between the gold film and the silicon, preventing most of the phonons to enter the crystal. Therefore most likely a thermalisation of the phonon system takes place, leading to a "normal heater" phonon distribution.

References

Akimenko A.I., Ponomarenko N.M., Yanson I.K., Janos S., and Reiffers M. 1984a Fiz. Tverd. Tela (Leningrad) **26** 2264 [1984a Sov. Phys. Solid State **26** 1374]

Akimenko A.I., Verkin A.B., Ponomarenko N.M., and Yanson I.K. 1982 Fiz. Nizk. Temp. **8** 1084 [1982 Sov. J. Low Temp. Phys. **8** 547]

Akimenko A.I., Verkin A.B., and Yanson I.K. 1984b J. Low Temp. Phys. **54** 247

d'Ambrumenil N. and White R.M. 1982 J. Appl. Phys. **52** 2052

Balkashin O.P., Yanson I.K., Solov'ev V.S., and Krasnogotov A.Yu. 1982 Zh. Tekh. Fiz. **52** 811 [1982 Sov. Tech. Phys. **27** 522]

Benistant P.A.M., van Gelder A.P., van Kempen H., and Wyder P. 1985 Phys. Rev. B **32** 3351

Benistant P.A.M., van Kempen H., and Wyder 1983 Phys. Rev. Lett. **51** 817

Benistant P.A.M., van de Walle G.F.A., van Kempen H., and Wyder P. 1986 Phys. Rev. B **33** 690

Bogachek E.N., Kulik I.O., and Shekhter R.I. 1985 Solid State Commun. **56** 999

Bogachek E.N., Kulik I.O., and Shkorbatov A.G. 1985 Fiz. Nizk. Temp. **11** 1189 [1985 Sov. J. Low Temp. Phys. **11** 656]

Bozhko S.I., Tsoi V.S., and Yakovlev S.E. 1982 Pis'ma Zh. Eksp. Teor. Fiz. **36** 123 [1982 JETP Lett. **36** 152]

Burger W. and Lassmann K. 1984 Phys. Rev. Lett. **53** 2035

Burger W. and Lassmann K. 1986 Phys. Rev. B **33** 5868

Bussian B., Frankowski I., and Wohlleben D. 1982 Phys. Rev. Lett. **49** 1026

Duif A.M., Jansen A.G.M., Wyder P., and d'Ambrumenil 1987 to be published

Frankowski I. and Wachter P. 1982 Solid State Commun. **41** 577

van Gelder 1980 Solid State Commun. **35** 19

van Gelder A.P., Jansen A.G.M., and Wyder P. 1980 Phys. Rev. B **22** 1515

Goossens R.J.G., Dijkhuis J.I., de Wijn H.W., Jansen A.G.M., and Wyder P. 1984 Physica **127B** 422

Harrison W.A. 1961 Phys. Rev. **123** 85

van der Heijden R.W., Jansen A.G.M., Stoelinga J.H.M., Swartjes H.M., and Wyder P. 1980 Appl. Phys. Lett. **37** 245

van der Heijden R.W., Swartjes H.M., and Wyder P. 1984 Phys. Rev. B **30** 3513

Holm R. 1967 Electric Contacts (Berlin: Springer Verlag)

Hooge F.N. and Hoppenbrouwers A.M.H. 1969 Phys. Lett. **29A** 642

Jansen A.G.M., Duif A.M., Lysykh A.A., and Wyder P. 1987 NATO workshop on Narrow Band Phenomena, Staverden, the Netherlands, in press

Jansen A.G.M., van Gelder A.P., and Wyder P. 1980 J. Phys. C **13** 6073

Knudsen M. 1934 Kinetic Theory of Gases (London: Methuen)
Kulik I.O., Omel'yanchuk A.N., and Shekhter R.I. 1977 Fiz. Nizk. Temp. **3** 1543 [1977 Sov. J. Low Temp. Phys. **3** 740]
Kulik I.O. and Shekhter R.I. 1980 Fiz. Nizk. Temp. **6** 184 [1980 Sov. J. Low Temp. Phys. **6** 88]
Kulik I.O. and Yanson I.K. 1978 Fiz. Nizk. Temp. **4** 1267 [1978 Sov. J. Low Temp. Phys. **4** 596]
Kunii S. 1987 J. Magn. Magn. Mater. **63&64** 673
Lifshitz I.M., Azbel' M.Ya., and Kaganov M.I. 1956 Zh. Eksp. Teor. Fiz. **31** 63 [1957 Sov. Phys. JETP **4** 41]
Lysykh A.A., Duif A.M., Jansen A.G.M., Wyder P., and de Visser A. 1987a to be published
Lysykh A.A., Duif A.M., Jansen A.G.M., and Wyder P. 1987b to be published
Lysykh A.A., Yanson I.K., Shklyarevski O.I., and Naydyuk Yu.G. 1980 Solid State Commun. **35** 987
Maxwell J.C. 1904 A Treatise on Electricity and Magnetism (Oxford: Clarendon)
McMillan W.L. and Rowell J.M. 1965 Phys. Rev. Lett. **14** 108
Moser M., Wachter P., and Franse J.J.M. 1986 Solid State Commun **58** 515
Moser M., Wachter P. Hulliger F., and Etourneau J.R. 1985 Solid State Commun. **54** 241
Naidyuk Yu.G., Gribov N.N., Shklyarevskii O.I., Jansen A.G.M., and Yanson I.K. 1985 Fiz. Nizk. Temp. **11** 1053 [1985 Sov. J. Low Temp. Phys. **11** 580]
Neidyuk Yu.G., Grivbov N.N., Lysykh A.A., Yanson I.K., Brandt N.B., and Moshchalkov V.V. 1985 Pis'ma Zh. Eksp. Teor. Fiz. **41** 325 [1985 JETP Lett. **41** 399]
Paulus E. and Voss G. 1985 J. Magn. Magn. Mater. **47&48** 539
Pearson W.B. 1961 Solid State Physics (USSR) **3** 1411
Pepper M. 1980a J ,Phys. C: Solid State Phys. **13** L709
Pepper M. 1980b J ,Phys. C: Solid State Phys. **13** L717
Pepper M. 1980c J ,Phys. C: Solid State Phys. **13** L721
Pong-Fei Lu, Tsui D.C., and Cox H.M. 1985 Phys. Rev. Lett. **54** 1563
Reiffers M., Flachbart K., and Janos S. 1986 Pis'ma Zh. Eksp. Teor. Fiz. **44** 232 [1986 JETP Lett. **44** 298]
Rösch F. and Weis. O. 1977 Z. Physik B 27 33
Sharvin Yu.V. 1965 Zh. Eksp. Teor. Fiz. **48** 984 [1965 Sov. Phys. JETP **21** 655]
Sharvin Yu.V. and Fisher L.M. 1965 Pis'ma Zh. Eksp. Teor. Fiz. **1** 54 [1965 JETP Lett. **1** 152]
Shen L.Y.L. and Rowell J.M. 1968 Phys Rev. **165** 566
Shklyarevskii O.I., Jansen A.G.M., Hermsen J.G.H., and Wyder P. 1986a

Phys. Rev. Lett. **57** 1374
Shklyarevskii O.I., Jansen A.G.M., and Wyder P. 1986b Fiz. Nizk. Temp. **12** 947 [1986b Sov. J. Low Temp. Phys. **12** 536]
van Son P.C., van Kempen H., and Wyder P. 1987a Phys. Rev. Lett. **58** 1567
Swartjes H.M. 1987 Thesis, University of Nijmegen
Swartjes H.M. et al. 1987 to be published
Tien P.K. and Gordon J.P. 1963 Phys. Rev. **129** 647
Trzcinski R., Gmelin E., and Queisser H.J. 1986 Phys. Rev. Lett. **56** 1086
Tsoi V.S. 1974 ZhETF Pis. Red. **19** 114 [1974 JETP Lett. **19** 70]
Verkin B.I., Yanson I.K., Kulik I.O., Shklyarevskii O.I., Lysykh A.A., and Naidyuk Yu.G. 1980 Izv. Akad. Nauk SSSR, Ser. Fiz. **44** 1330
Weis O. 1969 Z. Angew. Phys. **26** 325
Wexler G. 1966 Proc. Phyc. Soc. **89**, 927
Yanson I.K. 1974 Zh. Eksp. Teor. Fiz. **66** 1035 [1974 Sov. Phys. JETP **39** 506]
Yanson I.K. 1983 Fiz. Nizk. Temp. **9** 676 [1983 Sov. J. Low Temp. Phys. **9** 343]
Yanson I.K. and Shklyarevskii O.I. 1986 Fiz. Nizk. Temp. **12** 899 [1986 Sov. J. Low Temp. Phys. **12** 509]

CHAPTER 3

POINT-CONTACT SPECTROSCOPY IN KONDO AND SPIN-GLASS SYSTEMS

3.1. Introduction.

Nonlinearities in the current-voltage characteristics of metallic point contacts have been investigated extensively during the last years. Since the discovery by Yanson[1] point-contact spectroscopy has become a powerful method to study the scattering processes of the conduction electrons with elementary excitations in a metal. The most pronounced example of this is the determination of the energy-dependent Eliashberg function α^2F of the electron-phonon interaction which can be determined directly in a simple way using point contacts[1,2]. This function α^2F is the product of the squared matrix element α^2 of the electron-phonon interaction and the phonon density of states F averaged over the Fermi surface. In the meantime phonon spectra have been measured for a great variety of metals[3], such as the noble metals Cu, Ag, Au, the alkali metals Na, K, Li, the d-metals Fe, Co, Ni, Cr, Mn and numerous others. Other examples of interactions which can be investigated with the point-contact technique are electron-magnon scattering[4], the scattering of electrons with magnetic impurities[5] and with crystal-field levels[6]. Recently also experiments have been performed on valence fluctuation[7] and heavy-fermion systems[8].

In this paper we will discuss point-contact experiments on the dilute magnetic alloys AuMn and CuMn. It is demonstrated that in the regime of lowest concentrations the differential resistance dV/dI of point contacts consisting of these alloys shows a logarithmic voltage dependence which can be explained in terms of the Kondo problem. Applying an external magnetic field of a few tesla, this logarithmic voltage dependence of dV/dI changes into a double-peak structure. The value of the voltage at the splitted maxima in these point-contact spectra is related with the Zeeman energy $\Delta=g\mu_B B$. Measuring this splitting at various magnetic fields, the g-values of the samples are determined. Point contacts consisting of systems with a slightly higher concentration already show a splitting in the differential resistance versus voltage characteristics at zero external field. This behaviour will be explained in terms of the existence of internal fields in these alloys. These internal fields arise from the indirect (RKKY) interaction between the impurities themselves. As such it is possible not only to use point contacts for the study of the interactions between the electrons and the impurities but also for the study of the interaction between the impurities themselves.

3.2. Metals with magnetic impurities.

The interest in systems consisting of magnetic impurities dissolved in non-magnetic metals already started in the early thirties. At that time a min-

imum in the resistance was found in some pure metals at low temperatures. This resistance minimum was ascribed to the presence of magnetic impurities in these pure metals. The term magnetic impurity was introduced because susceptibility measurements showed a Curie-Weiss like behaviour. It turned out that already a very small amount of these impurities will lead to rather drastic anomalies in the resistance.

A simple model was introduced, the so-called s-d model in which the impurity spins S interact with the conduction electrons through an exchange interaction J. Since this s-d interaction is a weak interaction a perturbation treatment of the problem is possible. The s-d Hamiltonian can be written as:

$$H = H_0 + H_1 , \tag{3.1}$$

where

$$H_0 = \sum_{\mathbf{k},\alpha} \epsilon_{\mathbf{k}} \, a_{\mathbf{k}\alpha}^{\dagger} \, a_{\mathbf{k}\alpha} \tag{3.2}$$

and

$$H_1 = \sum_{\substack{\mathbf{k}\alpha \\ \mathbf{k}'\alpha'}} J_{\mathbf{k}\mathbf{k}'} \, \mathbf{S}_i \, (a_{\mathbf{k}'\alpha'}^{\dagger} \, \sigma_{\alpha'\alpha} \, a_{\mathbf{k}\alpha}) . \tag{3.3}$$

Here $\epsilon_{\mathbf{k}}$ is the energy of the conduction electron with spin α and momentum $\mathbf{k}$, $a^{\dagger}$ and a are creation and annihilation operators respectively, $\sigma_{\alpha'\alpha}$ are the Pauli matrices and $\mathbf{S}_i$ is the localized moment. The exchange integral between local moments and electrons is given by $J_{\mathbf{k}\mathbf{k}'}$. Using this s-d model, Kondo explained in a third order calculation the above mentioned resistance minimum[9]. He found in his calculation a logarithmic voltage and temperature dependence of the resistivity. However this term log(kT/D) in which D is the free-electron band width, diverges at T=0. Thus a perturbation treatment is not allowed at very low temperatures. This problem received much attention in the sixties.

So far we only discussed the interaction between the conduction electrons and the magnetic impurities. This interaction gives rise to all sorts of interesting physical effects. These effects can roughly be divided into two groups. The first one is that of the single-impurity effects. When the concentration of impurities is low enough or when the screening is effective enough there is no interaction between the impurity spins so that we are in the "Kondo limit". Criterion for this regime of single-impurity effects is that the charac-

teristic energy $k_B T_K$, where T_K is the Kondo temperature, must be large compared with the characteristic energy nV_0 for the impurity-impurity interaction. Here n is the impurity concentration and V_0 is the strength of this impurity-impurity interaction, which is the so-called RKKY interaction. This interaction, named after Ruderman, Kittel, Kasuya and Yosida is an indirect interaction between the impurity spins, mediated by the conduction electrons. It gives an extra contribution to the Hamiltonian[10]:

$$H_{RKKY} = -\frac{1}{2} \sum_{i,j} J_{ij}\, S_i\, S_j \,. \tag{3.4}$$

Here J_{ij} is the exchange interaction between the impurity spins S_i and S_j and depends only on the spatial distribution between the impurities i and j: $J_{ij}=J(|R_i-R_j|)$. This J(R) is a damped oscillating function:

$$J(R) = V_0 \frac{\cos(2k_F R+\phi)}{(k_F R)^3} \,, \quad (k_F R \gg 1) \,. \tag{3.5}$$

Here V_0 and ϕ are constants and k_F is the Fermi wave number of the host material. Because the sign of the interaction is alternating, the spins will partially prefer a parallel alignment (positive interaction) and partially a antiparallel alignment (negative interaction). When the distance between two impurities becomes very small, the interaction will have a very big positive value. Thus at high concentrations one could expect always to have a parallel alignment of spins and therefore this RKKY interaction always would lead to a ferromagnetic behaviour. However in this concentration regime the RKKY interaction will be overruled by the direct exchange interaction. This will either lead to a ferromagnetic or an anti-ferromagnetic behaviour.

Because the sign of the RKKY interaction alternates (depending on distance) there is no alignment possible which is satisfactory for all spins. Thus this will lead to a "frustration" of some of the bonds and therefore to a number of interesting effects in these systems like the occurrence of the spin-glass transition which is most clearly seen in low-field magnetic susceptibility measurements, Mössbauer splitting and measurements on the anomalous Hall effect.

Systems in which this RKKY interaction plays an important role, i.e. in which $nV_0 > k_B T_K$, are called spin glasses. The RKKY interaction is the basis of a great number of theories which are set up to explain the experimental properties of spin glasses. One of the main properties is the above mentioned existence of a random freezing of impurity moments at a distinct tempera-

ture, the so-called freezing or spin-glass temperature, which shows up in a great number of experiments. We will come back to this later.

When the impurity concentration is increased, short range correlations set in. This already takes place at concentrations of a few thousand ppm. Now clusters are formed which interact with each other via the RKKY interaction. Systems in this concentration regime are called mictomagnets. Although they exhibit interesting experimental properties, they are not the subject of this paper. In the rest of this paper we will restrict to Kondo and spin-glass systems consisting of noble metal hosts with 3d transition metal impurities. Point-contact experiments were carried out on a number of AuMn and CuMn alloys with different concentrations of Mn impurities in the range of 0.03-0.3%. In table 3.1 the alloys which were studied experimentally are enumerated.

alloy	conc (at.%)	sample no.	T_K(K)[11]	T_f(K)[12]
AuMn	0.03	78137		~ 0.3
	0.1	78136	< 0.01	~ 0.8
	0.3	78135		~ 2
CuMn	0.045	8231		~ 0.9
	0.078	8217	~ 0.01	≃ 1.4
	0.10	8230		≲ 2
	0.14	8229		≃ 2.2

Table 3.1. AuMn and CuMn alloys which were studied experimentally, with their estimated Kondo temperature T_K and freezing temperature T_f (after refs 11 and 12).

3.3. Experimental properties.

Although the first experiments on metals with magnetic impurities were performed on systems with a very low impurity concentration, very soon more and more attention was drawn to systems in the somewhat higher concentration regime, the spin-glass systems. The experiments dealed mainly with resistance measurements in which a minimum was found at low temperatures[13], and susceptibility measurements which showed a Curie-Weiss

behaviour[14]. The logarithmic dependence in the resistivity at low temperature was disturbed by applying a magnetic field or by increasing the impurity concentration of the observed alloy. Then the observed resistance maximum even changed into a resistance minimum[13].

The reason why most attention was drawn to spin-glass systems is the occurrence of a transition, the spin-glass transition in these systems. This transition can clearly be seen in susceptibility measurements in which a sharp cusp is seen in the AC-susceptibility $\chi_{AC}(T)$ at a well defined temperature T_f, the spin-glass or freezing temperature[15]. At high temperatures, i.e. above the freezing temperature, the susceptibility behaves Curie-Weiss like with a positive paramagnetic Curie-Weiss constant θ. At low temperatures, i.e. below T_f, the behaviour is dominantly anti-ferromagnetic. The position of the observed sharp cusp at T_f depends slightly on frequency and is rounded off; it is even strongly rounded by weak magnetic fields[16].

The results of measurements on magnetization depend very strongly on the presence of an external magnetic field during the cooling of the samples below the freezing temperature. Magnetization measurements on CuMn show a displacement in the hysteresis loop when the samples are cooled in a magnetic field[17]. The magnetization of CuMn and AgMn shows narrow cycles displaced towards negative fields when the samples are cooled in a positive magnetic field[18]. This remanent magnetization, which is induced by cooling the samples below T_f in a fixed field is called Thermo-Remanent-Magnetization (TRM). However it can also be induced by exposing the sample to a somewhat larger field at constant temperature and is then called Isothermal-Remanent-Magnetization (IRM). Both TRM as IRM decay logarithmically in time[19].

The spin-glass transition can also clearly be observed in Mössbauer experiments where the Mössbauer line splits at a well defined temperature[20]. This temperature however lies well above the freezing temperature, and moreover it is frequency dependent. From this one can conclude that the spins freeze in continuously and that the spin-glass transition is not a sharp phase transition.

The specific heat shows a maximum around the freezing temperature T_f. This is a rather broad maximum and not a sharp transition which would occur in the case of a real phase transition. At low temperatures the excess specific heat Δc_p, i.e. $c_{p\ \text{alloy}} - c_{p\ \text{matrix}}$, is proportional with temperature[21]. At higher temperatures, i.e. well above T_f it is proportional with the inverse temperature $1/T$.

Electron Spin Resonance measurements also show the spin-glass transition. At the freezing temperature a shift in resonance field has been observed in AgMn which can be explained by the onset of an internal field at this spin-glass temperature[22].

Neutron-diffraction experiments show the absence of any long-range

magnetic order in systems in the spin-glass regime[23]. In the more concentrated regime, these type of experiments give information about the size of the spin clusters which then are formed.

So far we only gave a short indication of some experimental properties of metals with magnetic impurities. For more detailed discussions on the experimental and theoretical aspects of these systems, see ref.24.

3.4. Point-contact spectroscopy in Kondo systems.

In very dilute systems point-contact experiments show a logarithmic voltage dependence of the differential resistance. Applying a magnetic field, the maximum at zero bias voltage splits up into a double peak structure. This also occurs in less dilute systems, already without an external magnetic field. The reason for this is the interaction between the impurities themselves which leads to the presence of internal magnetic fields, having the same effect on the differential resistance dV/dI as an externally applied one. We will give an explanation for the appearance of the zero bias anomaly in the point-contact spectra of very dilute systems and the splitting of this anomaly in an external magnetic field. Starting point is the s-d model for the interaction between the conduction electrons and the impurity spins as already described in section 3.2. This model leads to a perturbation of the Hamiltonian:

$$H_{sd} = J \sum_{i} \sum_{\substack{k\alpha \\ k'\alpha'}} c_{k'\alpha'}^{\dagger}\, \sigma_{\alpha'\alpha}\, c_{k\alpha}\, S_i \,, \tag{3.6}$$

where S_i is the localized moment at site i, $\sigma_{\alpha'\alpha}$ are the Pauli matrices and $c^{\dagger}$ and c are creation and annihilation operators respectively. This Hamiltonian we use to calculate the scattering terms Γ in the backflow current $I^{(1)}$ in a point contact[25]:

$$I^{(1)} = ne \sum_{\substack{k\alpha \\ k'\alpha'}} K(\mathbf{k},\mathbf{k}')\{\Gamma(k'\alpha',k\alpha)\, f_{\mathbf{k}'}^{0}(1-f_{\mathbf{k}}^{0}) - \Gamma(k\alpha,k'\alpha')\, f_{\mathbf{k}}^{0}(1-f_{\mathbf{k}'}^{0})\} \,, \tag{3.7}$$

where $K(\mathbf{k},\mathbf{k}')$ is a kinematical factor, $f_{\mathbf{k}}^{0}$ and $f_{\mathbf{k}'}^{0}$ are the normal Fermi distributions:

$$f_k^0 = f^0 (\epsilon_k - \epsilon_F - eV/2) , \tag{3.8}$$
$$f_{k'}^0 = f^0 (\epsilon_{k'} - \epsilon_F + eV/2) \tag{3.9}$$

and $\Gamma(k'\alpha',k\alpha)$ and $\Gamma(k\alpha,k'\alpha')$ are the scattering matrix elements for the scattering from state $|k'\alpha'\rangle$ into state $|k\alpha\rangle$ and for scattering from state $|k\alpha\rangle$ into state $|k'\alpha'\rangle$ respectively. These scattering matrix elements $\Gamma(i,f)$ can be calculated using Fermi's Golden Rule:

$$\Gamma(i,f) = \frac{2\pi}{\hbar} \left| \langle f|T|i\rangle \right|^2 \delta(E_f - E_i) , \tag{3.10}$$

where

$$\langle f|T|i\rangle = \langle f|H_{sd}|i\rangle + \sum_{n\neq i} \frac{\langle f|H_{sd}|n\rangle\langle n|H_{sd}|i\rangle}{E_i - E_n} + ... \tag{3.11}$$

Up to third order in J the scattering matrix elements then become:

$$\Gamma(i,f) = \frac{2\pi}{\hbar} \left\{ \sum_{n\neq i} \left[\frac{H_{in}H_{nf}H_{fi}}{E_i - E_n} + c.c. \right] + \left| H_{if} \right|^2 \right\} \delta(E_f - E_i) . \tag{3.12}$$

Here we used the abbreviation H_{ab} for the matrix element $\langle b|H_{sd}|a\rangle$. If it is possible to calculate these scattering matrix elements, we have an expression for the backflow current $I^{(1)}$ and for the differential resistance dV/dI, since the change in differential resistance due to this backflow current $I^{(1)}$ is directly proportional to $dI^{(1)}/dV$ via:

$$\frac{dV}{dI} = \simeq R_0 \left[1 - R_0 \frac{dI^{(1)}}{dV} \right] . \tag{3.13}$$

Here R_0^{-1} is the voltage-independent derivative $dI^{(0)}/dV$ of the zeroth order current $I^{(0)}$ (i.e. no backflow). This relation holds only when the changes in $I^{(1)}$ are very small compared with those in $I^{(0)}$ upon changing the bias voltage, i.e. when $dI^{(1)}/dV << dI^{(0)}/dV$.

Before giving the final expression for the differential resistance we will first discuss briefly the various terms of the scattering matrix elements $\Gamma(i,f)$. The lowest order contribution to $\Gamma(i,f)$ is the $|H_{if}|^2$ term in equation (3.12).

Since in the expression (3.7) for the backflow current $I^{(1)}$ we find a summation over all conduction electrons and all possible transitions, we have to consider both "normal" transitions and spin-flip transitions. At zero magnetic field all localized spin states are degenerate and therefore equally occupied. Because of this, both normal and spin-flip transitions of the electrons cost no energy and thus are possible. In a magnetic field the spin states split into 2S+1 M-states with an energy difference $\Delta=g\mu_B B$ between these states. At low temperatures all spins will be in the M=-S state. Spin-flip scattering in which an electron with spin up excites a spin from the M=-S into the M=-S+1 state now costs an energy $\Delta=g\mu_B B$. Thus an electron with initial energy ϵ will have a final energy $\epsilon-\Delta$ after such a scattering process. For applied bias voltages $eV<\Delta$ these processes are forbidden by the exclusion principle and for $eV>\Delta$ they are possible again. That means that for low voltages spin-flip scattering is not contributing to the back-flow current and for $eV>\Delta$ it is. In figure 3.1 the first order contribution to the differential resistance dV/dI is represented schematically by $G_0(eV)$[26]. At zero magnetic field this contribution remains constant while varying the applied voltage. In the presence of a magnetic field it exhibits a dip of 2Δ due to the forbidden spin-flip scattering processes in that region. The second order contribution to $\Gamma(i,f)$, i.e. the first term in equation (3.12) is responsible for an anomalous voltage and temperature dependence of the point-contact resistance. In figure 3.1 this second order contribution to dV/dI is represented schematically by $\Delta G(eV)$. At zero magnetic field it has a logarithmic behaviour. As for the

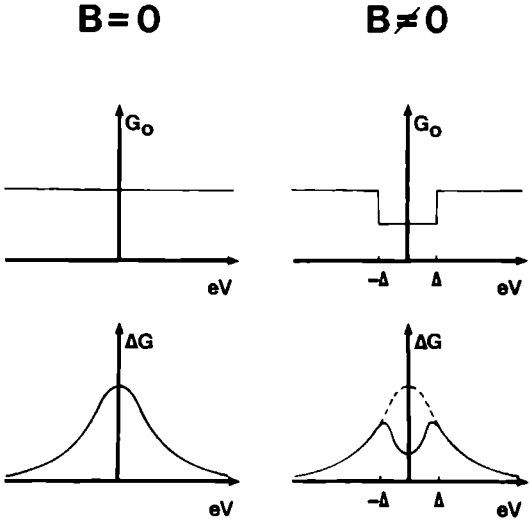

Fig. 3.1. Schematic representation of the first order contribution $G_0(eV)$ and the second order contribution $\Delta G(eV)$ to the differential resistance dV/dI of a point contact with and without an external magnetic field, showing the Zeeman splitting $\Delta=g\mu_B B$.

first order contribution also here spin-flip scattering processes are forbidden when the applied bias voltage is smaller than the Zeeman energy Δ. Therefore $\Delta G(eV)$ splits up in a magnetic field with a splitting $2\Delta=2g\mu_B B$. The schematic representations of $G(eV)$ and $\Delta G(eV)$ in figure 3.1 only give a correct picture at the lowest possible temperatures, i.e. at T=0. At finite temperatures the change in differential resistance ($dI^{(1)}/dV$) can be calculated using the expressions for the backflow current $I^{(1)}$ in equation (3.7) and the scattering matrix elements $\Gamma(i,f)$ in equation (3.12). These equations are completely analogous to the expression for the current and transition probability of metal-oxide-metal tunneljunctions with magnetic impurities in the oxide barrier[27]. Therefore the derivation of the expressions for $dI^{(1)}/dV$ has the result[27]:

$$\frac{dI^{(1)}}{dV} = - << K(\mathbf{k}',\mathbf{k}) >_0>_0 \{ G_0(V,\Delta) + \Delta G(V,\Delta) \} ne^2 . \qquad (3.14)$$

Here n is the density of impurities and $<<...>_0>_0$ means an average of states $\mathbf{k}$ and $\mathbf{k}'$ at the Fermi surface. The complete, rigorous expressions of $G_0(V,\Delta)$ and $\Delta G(V,\Delta)$ are given in appendix A. They are extensions of the expressions for the anomalous conductance G, found by Appelbaum for the case of tunneling through an oxide containing magnetic impurities in a metal-oxide-metal tunneljunction[27]. We will restrict here to the simplified expressions for this change in differential resistance, which is only valid at very low temperatures. Then we can replace the Fermi functions by δ-functions so that then the expressions for G_0 and ΔG are:

$$G_0(V,\Delta) = A \left[1 + \frac{\langle M \rangle}{2S(S+1)} \left\{ \tanh\left(\frac{eV+\Delta}{2k_BT}\right) - \tanh\left(\frac{eV-\Delta}{2k_BT}\right) \right\} \right] , \qquad (3.15)$$

$$\Delta G(V,\Delta) = - A J N(0) [\Delta G_1(V,\Delta) + \Delta G_2(V,\Delta) + \Delta G_3(V,\Delta)] , \qquad (3.16)$$

where $A=\frac{4\pi}{\hbar}S(S+1)J^2N(0)^2$. Here J is the strength of the RKKY interaction and N(0) is the electron density of states. $\langle M \rangle$ is the expectation value of the z-components of the localized spins S_z, i.e. $\langle M \rangle=\Sigma P_M M$. Δ is the Zeeman energy $g\mu_B B$. In equation (3.16) the terms ΔG_i are now given by:

$$\Delta G_1(V,\Delta) = 2\left[1 - \frac{\langle M^2\rangle}{S(S+1)} + \frac{\langle M\rangle}{2S(S+1)}\left\{\tanh\left(\frac{\Delta-eV}{2k_BT}\right) + \tanh\left(\frac{\Delta+eV}{2k_BT}\right)\right\}\right] \cdot \ln\left(\frac{eV+k_BT}{E_0}\right), \quad (3.17a)$$

$$\Delta G_2(V,\Delta) = \left[1 + \frac{\langle M^2\rangle}{S(S+1)} + \frac{\langle M\rangle}{S(S+1)}\tanh\left(\frac{\Delta-eV}{2k_BT}\right)\right]\ln\left(\frac{|eV-\Delta|+k_BT}{E_0}\right), \quad (3.17b)$$

$$\Delta G_3(V,\Delta) = \left[1 + \frac{\langle M^2\rangle}{S(S+1)} + \frac{\langle M\rangle}{S(S+1)}\tanh\left(\frac{\Delta+eV}{2k_BT}\right)\right]\ln\left(\frac{|eV+\Delta|+k_BT}{E_0}\right). \quad (3.17c)$$

In these expressions E_0 is the bandwidth which is normally chosen such to give an optimal resemblance between theory and experiment. From these expressions for G_0 and ΔG we find a logarithmic voltage and temperature dependence at zero magnetic field. G_0 is a constant at zero magnetic field and ΔG reads

$$\Delta G(V,\Delta=0) = -4\,A\,J\,N(0)\ln\left(\frac{|eV| + k_BT}{E_0}\right). \quad (3.18)$$

Figure 3.2 shows the voltage dependence of both a Au-0.03% Mn and a Cu-0.045% Mn point contact. To emphasize a logarithmic voltage dependence the characteristics are also plotted on a logarithmic voltage scale. Only on a limited voltage range such a logarithmic dependence is found in both samples. At low voltages this is probably partially due to thermal smearing, i.e. the k_BT term in equation (3.18). Also magnetic ordering may play a role in this deviation from a logarithmic dependence. Because of the interaction between impurities, internal magnetic fields arise which decrease the differential point-contact resistance at very low voltages. We will come back to this later. At high voltage the deviations from a logarithmic behaviour are due to the interaction of the electrons with phonons which then becomes the dominant scattering mechanism which determines the point-contact spectra. Comparing both the spectra of AuMn and CuMn one can see that the electron-phonon interaction sets in at lower voltages for the AuMn sample than for

bias voltage. Figure 3.3b represents the theoretical curves for the differential resistance of this sample which were derived with equations (3.7-3.14). For the calculation of G_0 and ΔG in equation (3.14) the full expressions as men-

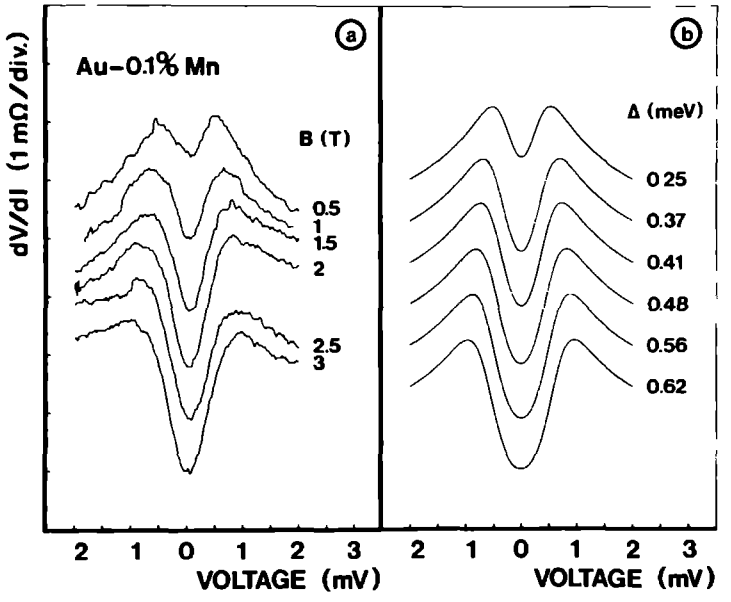

Fig. 3.3. Measured differential resistance dV/dI of a Au-0.1% Mn point contact with R_0=1.1 Ω at temperature T=1.2 K for different applied magnetic fields (part a). Part b represents the calculated spectra for this contact at these magnetic fields. The indicated Zeeman energies Δ have been adjusted in the calculations to obtain an optimum resemblance with the experimental curves. The curves have been shifted with respect to each other.

tioned in appendix A were used and calculated numerically. For the calculations a Zeeman energy $\Delta=g\mu_B B$ had to be assumed. The values of Δ given in figure 3.3b are those which were used in these calculations and which gave an optimal resemblance between theory and experiment. Extrapolating these Zeeman energies Δ to zero external field still leaves some non-zero value. Like the deviation from a logarithmic dependence at low voltages in figure 3.2 this non-zero value can be explained with the interaction between the impurities, leading to internal fields. The determination of the Zeeman energies at different magnetic fields opens a possibility to determine the g-values

of the alloys. The Zeeman energies Δ can be found most easily by measuring the voltage at which the measured derivative dV/dI is maximal, or dI/dV minimal. From equation (3.14) we thus find the equation to calculate the Zeeman energy.

$$\frac{d}{dV}\left[G_0(V,\Delta) + \Delta G(V,\Delta) \right] = 0 \,. \tag{3.19}$$

This equation can be solved numerically.

The point-contact measurements were performed on samples with different impurity concentrations as already mentioned in table 3.1. For the

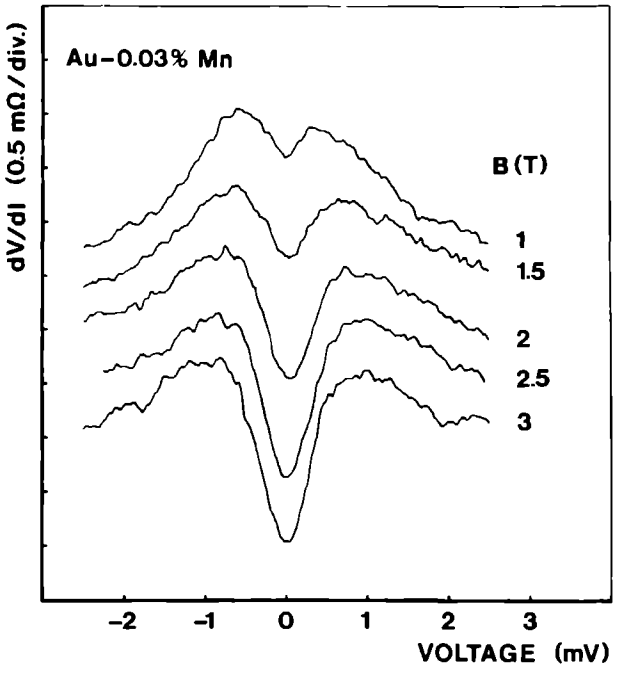

Fig. 3.4. Measured differential resistance dV/dI of a Au-0.03% Mn point contact with resistance R_0=0.63 Ω at temperature T=1.2 K for different applied magnetic fields. The curves have been shifted with respect to each other.

moment we will restrict to the alloys with the lowest Mn concentrations. Figures 3.3-3.5 give the measured voltage dependence of the differential resis-

tance dV/dI at different magnetic fields for some AuMn and CuMn point contacts. From the maxima in the measured spectra the values of the Zeeman energies at the corresponding applied magnetic fields were calculated using equation (3.19). In this equation we used JN(0)=0.08, E_0=300meV and S=5/2 for AuMn. For CuMn a different value for JN(0) was used, viz. JN(0)=0.1. For CuMn one expects also S=5/2, however Smith[29] states S=1.88. Therefore the Zeeman energies were also calculated for Cu-0.078% Mn with S=2. The obtained g-factor is for both cases the same. The calculated Zeeman energies are plotted as a function of magnetic field for the different samples in figure 3.6. The resulting g-values for these samples are summed up in table 3.2.

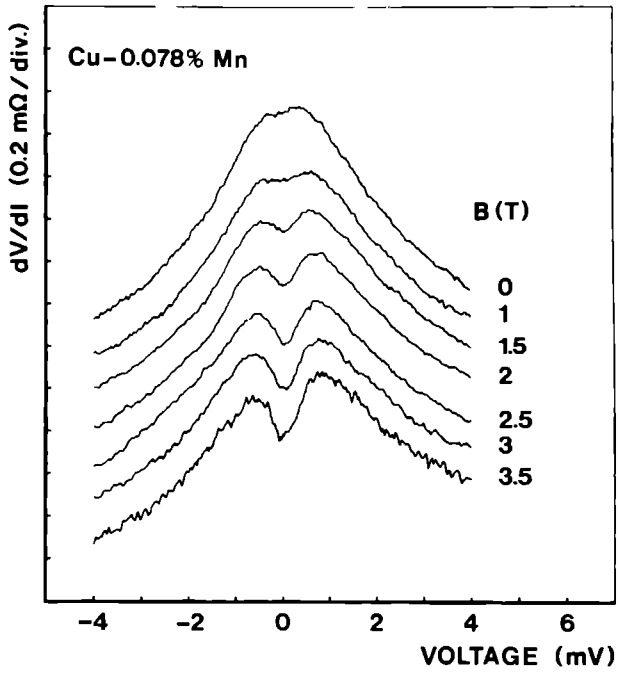

Fig. 3.5. Measured differential resistance dV/dI of a Cu-0.078% Mn point contact with resistance R_0=1.7 Ω at temperature T=1.2 K for different applied magnetic fields. The curves have been shifted with respect to each other.

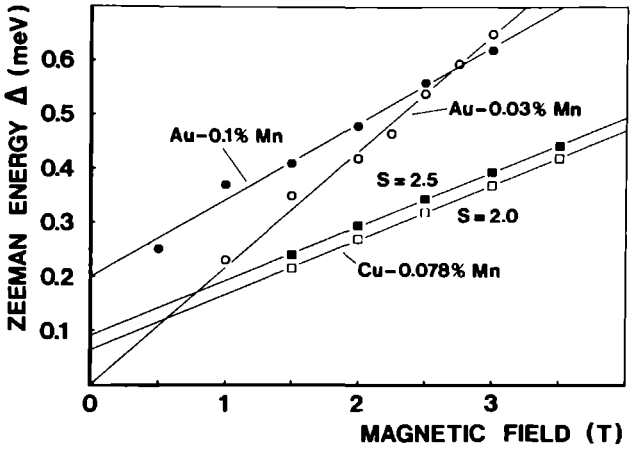

Fig. 3.6. Zeeman energies Δ, calculated from the measured differential resistances of a Au-0.03% Mn, a Au-0.1% Mn and a Cu-0.078% Mn point contact, plotted as a function of the applied magnetic field. For the latter contact the Zeeman energies were calculated using impurity spin S=2.0 and S=2.5. The g-values can be obtained from the slope of the lines, using $\Delta = g\mu_B B$.

alloy	conc (at.%)	obtained g-value
AuMn	0.03	3.7 ± 0.3
	0.1	2.4 ± 0.3
	0.3	9.8 ± 0.9 at T=1.22 K
		3.3 ± 0.9 at T=4.2 K
CuMn	0.045	-
	0.078	1.86 ± 0.05
	0.10	1.1 ± 0.2
	0.14	-

Table 3.2. g-values of the AuMn and CuMn samples obtained from the calculated Zeeman energies Δ as a function of applied magnetic field.

3.5. Point-contact spectroscopy in spin-glass systems.

As we already mentioned in the previous paragraph, the zero bias anomaly observed in the measured point-contact spectra not only splits up into a double-peak structure when an external magnetic field is applied on the very dilute systems, but also occurs in the spectra of the less dilute systems without the presence of an externally applied magnetic field. Figure 3.7 shows this splitting in the point-contact spectra in the more concentrated samples for both some AuMn and CuMn systems. In this figure we can see that the maximum in the contact resistance at zero bias voltage decreases when increasing the concentration resulting in a minimum at zero bias and a maximum at some distinct voltage for the highest concentrations which were examined. This phenomenon is due to the existence of internal fields as are commonly assumed to be present in spin glasses. These internal fields arise from the weak interaction between the impurity spins themselves, the so-called RKKY interaction. As already mentioned in paragraph (3.2) this interaction has the form:

$$H_{RKKY} = - \sum_{\langle i,j \rangle} J(R_{ij})\, \mathbf{S}_i\, \mathbf{S}_j \,, \tag{3.20}$$

where

$$J(R) = V_0\, \frac{\cos(2k_F R)}{R^3} \,. \tag{3.21}$$

Here R_{ij} is the distance between the impurities i and j, $\mathbf{S}_i$ and $\mathbf{S}_j$ are the spins of these impurities and the summation goes over all impurity pairs (i,j). From magnetization measurements the values of V_0 are known to be[29]:

$V_0 = (7.5 \pm 0.9)\ 10^{-50}\ \mathrm{Jm^3}$ for CuMn ,
$V_0 = (2.4 \pm 0.3)\ 10^{-50}\ \mathrm{Jm^3}$ for AuMn .

The internal fields inside the spin glass are now defined by:

$$\mathbf{b}_i = \sum_j J_{ij}\, \mathbf{S}_j \,. \tag{3.22}$$

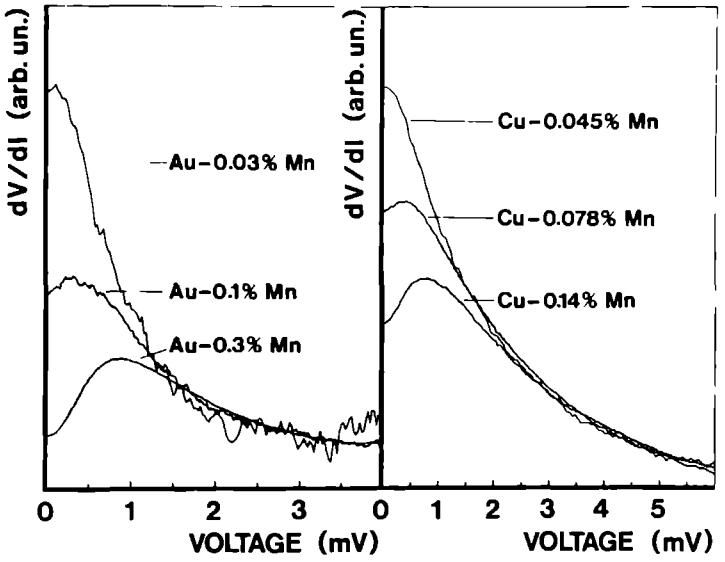

Fig. 3.7. Measured differential resistance dV/dI of three AuMn point contacts and three CuMn point contacts with different Mn concentrations, showing the effects of internal fields in increasing the impurity concentration. The resistances were 0.6 Ω for Au-0.03% Mn, 0.72 Ω for Au-0.1% Mn, 1.46 Ω for Au-0.3% Mn, 1.25 Ω for Cu-0.045% Mn, 1.7 Ω for Cu-0.078% Mn and 2.4 Ω for Cu-0.14% Mn.

This is the internal field at the impurity site i due to all the other impurities j with spin S_j. These internal fields b_i are more or less randomly oriented and distributed statistically with a field distribution given P(b) by[30]:

$$P(b) = \frac{4\,\xi_{T=\infty}}{\pi}\,\frac{b^2}{(b^2+\xi_{T=\infty}{}^2)^2}\,, \tag{3.23}$$

where

$$\xi_{T=\infty} = \frac{8\pi n}{3a^3}\,V_0\,|S|\,. \tag{3.24}$$

Here n is the concentration of magnetic impurities, V_0 is the strength of the

RKKY interaction and a is the lattice constant. This distribution is only valid at sufficiently high temperatures, i.e. when the temperature is large compared to the freezing temperature of the regarded spin-glass system. From this internal-field distribution P(b) thé internal field B_{int} as can be measured in the experiments, can be calculated. The expected value of the internal field is given by

$$B_{int} = \langle b \rangle = \int_0^{b_{max}} b\, P(b)\, db\ . \tag{3.25}$$

Here the integration goes over all possible internal fields up to the maximum field b_{max} which occurs in the spin glass. Using equation (3.23) for the distribution P(b) of internal fields one finds:

$$B_{int} = \frac{2\xi}{\pi} \left[\ln \left((b_{max}/\xi)^2 + 1 \right) + \frac{1}{(b_{max}/\xi)^2+2} - 1 \right]. \tag{3.26}$$

In a computer simulation by Walker and Walstedt[30] of 324 impurity spins in a noble-metal host the largest field which was found was $b_{max} \simeq 10\xi$. Substituting this value in the above obtained expression one finds for the measured internal field:

$$B_{int} \simeq 2.31\ \xi\ . \tag{3.27}$$

Using equations (3.26) and (3.27) we now can determine the expected internal fields in the alloys and from that the Zeeman energies Δ. With this Δ we can calculate the contributions $G_0(V,\Delta)$ and $\Delta G(V,\Delta)$ to the differential resistance as we did in the low-concentration regime, using equations (3.15-3.17). Figure 3.8 shows the results of the calculations on the AuMn samples. Part (a) of this figure gives the measured differential contact resistance dV/dI as a function of bias voltage for the alloys with different concentrations. Part (b) gives the calculated spectra. For these calculations the expressions as given in appendix A were used. As in the calculations on the low-concentration AuMn alloys, also here we used JN(0)=0.08, E_0=300 meV and S=5/2. For the determination of the Zeeman energies Δ due to the internal fields, we used a g-value of 2.

Not only experiments were performed on systems with different impurity concentrations at low temperatures. For the Au-0.1% Mn and the Au-0.3% Mn alloys the point-contact spectra, i.e. differential resistance dV/dI

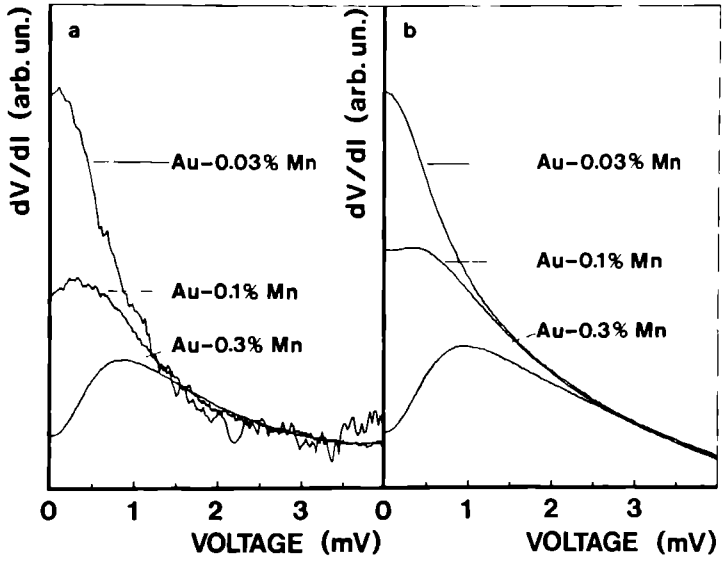

Fig. 3.8. Measured (left curves) and calculated (right curves) differential resistance dV/dI of three AuMn point contacts with impurity concentration as indicated in the figure. Temperature T=1.2 K, contact resistances R_0=0.6 Ω for Au-0.03% Mn, R_0=0.72 Ω for Au-0.1% Mn and R_0=1.46 Ω for Au-0.3% Mn.

versus bias voltage were measured at different temperatures. Figure 3.9 shows both the measured and the calculated spectra of a Au-0.3% Mn point contact at different temperatures. From this figure we can clearly see that the anomalous structure around zero bias voltage decreases when the temperature is increased. However the distance between the maxima, thus the Zeeman energy Δ and thus the internal fields are independent of temperature. In figure 3.10 the measured and calculated spectra of a Au-0.1% Mn point contact are shown at different temperatures. For the calculations of the spectra in figure 3.10b also the internal field is kept constant. In these plots therefore the distance between the maxima is also constant. In the measured plots however, this splitting changes with temperature. An explanation for this can be the following. In the computer simulation by Walker and Walstedt the calculated internal-field distribution P(b) from equation (3.23) is only correct for high enough temperatures, i.e. far above the freezing temperature: $T \gg T_f$. For low enough temperatures, i.e. $T \ll T_f$ they found the same distri-

bution P(b) however with a somewhat higher value of ξ, viz. $\xi_{T=0} \simeq 1.5\ \xi_{T=\infty}$. This implies (equation (3.27)) that the internal field at very low temperatures

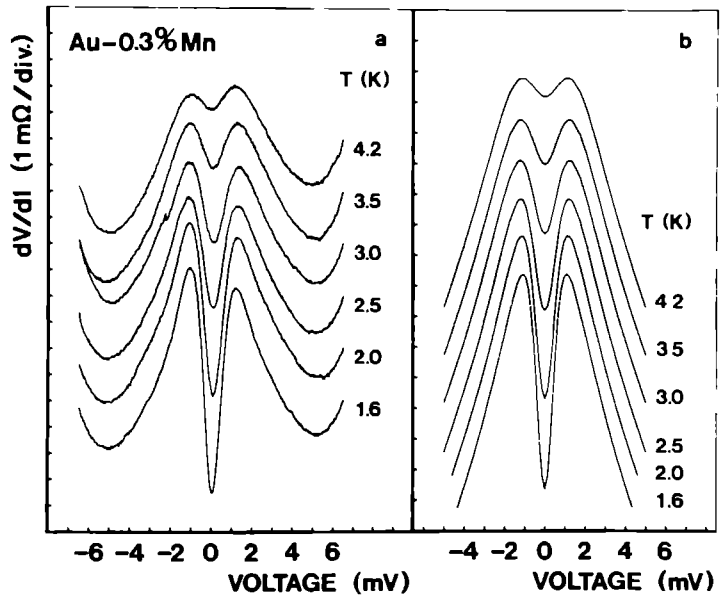

Fig. 3.9. Measured (left curves) and calculated (right curves) differential resistance of a Au-0.3% Mn point contact with resistance R_0=1.5 Ω at different temperatures as indicated in the figure, showing the decrease of the anomalous structure around zero bias in increasing the temperature. The Zeeman splitting however is independent of temperature.

is roughly 1.5 times bigger than at high temperatures. Thus in figure 3.10 it is very well possible that by measuring a change in the splitting of the spectra in increasing the temperature, actually the change in ξ is observed by going through the spin-glass transition. In figure 3.8 this effect of ξ not being constant at all temperatures is taken into account. For the calculations of the Au-0.03% Mn system, a $\xi=\xi_{T=\infty}$ was used because the measuring temperature was below the freezing temperature of this alloy as is known from literature. For the other two systems a $\xi=\xi_{T=0}$ was used.

Measurements at different temperatures were also performed on the CuMn systems. In these alloys however, the effect of the anomalous structure being whiped out by temperature is much stronger. Even in the most concentrated samples already at low temperatures the double-peak structure is

less pronounced than in the AuMn systems. Therefore these measurements were much less interesting than those presented in the figures 3.9 and 3.10.

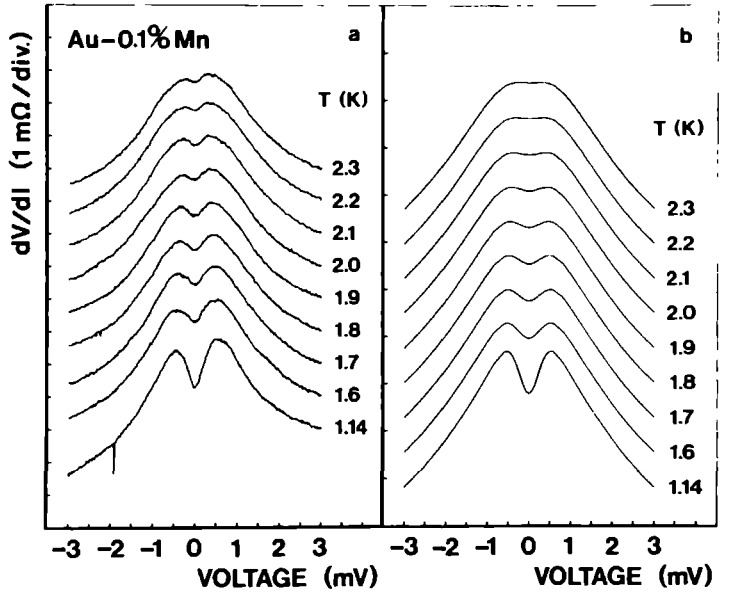

Fig. 3.10. Measured (left curves) and calculated (right curves) differential resistance of a Au-0.1% Mn point contact with resistance R_0=1.04 Ω at different temperatures, as indicated in the figure, showing the decrease of the anomalous structure around zero bias in increasing the temperature. Simultaneous a decrease in Zeeman splitting is observed.

3.6. Discussion.

We will now give a short summary and a discussion of the results which were obtained in the experiments. First we observed a logarithmic voltage dependence of the differential resistance dV/dI on a limited voltage range in the Kondo systems, i.e. in the alloys with the lowest concentration Mn impurities. At low voltages, deviations from this logarithmic voltage dependence occur due to thermal smearing and impurity-impurity interaction. The

latter can be made plausible by looking at the concentration dependence of this effect. Increasing the impurity concentration gives rise to deviations from the logarithmic dependence at considerable higher voltages than in the spectra of alloys in the lowest-concentration regime. At higher voltages deviations from the mentioned logarithmic voltage dependence occur due to electron-phonon interaction which then becomes important.

In a magnetic field the measured zero-bias anomaly splits up into a double-peak structure. This is due to the fact that in a magnetic field, spin-flip scattering of the electrons at low voltages is forbidden by the exclusion principle, which leads to a decrease of the total point-contact resistance. At higher voltage, i.e. above the Zeeman energy $\Delta=g\mu_B B$, these scattering processes can occur again which leads to an increase in point-contact resistance. The magnetic-field dependence of the point-contact spectra can be described nicely by Appelbaum-like formulas. A derivation like the one by Appelbaum for a description of zero-bias anomalies in tunneljunctions, leads to a set of expressions from which plots are very well comparable with the measured spectra. For the fitting of the experimental data with these expressions, the Zeeman energy $\Delta=g\mu_B B$ had to be assumed. From measuring the spectra at different magnetic fields, the g-values of the different alloys were determined. They are summed up in table 3.2. The obtained g-values are not strikingly accurate. This is because the calculated spectra are not very sensitive to small changes in the assumed Zeeman energy, so that from the comparison between theory and experiment the g-values are not obtained very accurately. Moreover the maxima in the measured spectra from which the g-values were calculated (equation (3.19)) where rather broad which also leads to inaccuracies. Finally the impurity concentration may vary considerably between the different point contacts made from the same alloy. This one expects especially for the alloys in the low-concentration regime. Since in AuMn there exist chemical bonds, one expects even in the dilute compounds a certain chemical order. For CuMn this is not expected because there chemical bonds do not exist. Concentration variations on a microscopic scale however can be expected because of statistical fluctuations. Since with point contacts one is sensitive on a microscopic scale, these variations may play a role in the experiments. However this can only be expected in the lowest-concentration alloys. For instance in the Au-0.1% Mn or the Cu-0.078% Mn alloys a volume of $(100\ A)^3$, i.e. a typical point-contact volume, contains about 60 Mn impurities and statistical fluctuations will hardly be noticeable.

Increasing the impurity concentration has the same effect as applying a magnetic field on the low-concentration alloys. The single maximum at zero bias voltage splits up, now due to internal fields which arise from the impurity-impurity interaction. As can be seen by comparing figure 3.8a with figure 3.8b, which is calculated with the Appelbaum-like formulas, this impurity dependence is very well described by the theory. The internal

fields, as can be estimated with equations (3.24-3.27), lead to a splitting which is certainly a good approximation of the structure in the measured spectra. The presented theory also gives a good description of the temperature dependence of the measured spectra of a Au-0.1% Mn and a Au-0.3% Mn point contact. There is however a crucial difference between both spectra. Whereas in the Au-0.3% Mn case the splitting of the double-peak structure stays constant while increasing the temperature, in the Au-0.1% Mn case there is a clear decrease of the distance between the maxima of the point-contact resistance. This decrease could be explained by a decrease in internal field in increasing the temperature. Such a change in internal field occurs when the temperature is passing the spin-glass temperature.

Appendix A.

In this appendix we will give the complete set of expressions for the contributions G_0 and ΔG to the differential resistance as were used for the calculations in paragraphs 4 and 5. The expression for the change in differential resistance, i.e. the voltage derivative of the backflow current $dI^{(1)}/dV$ is:

$$\frac{dI^{(1)}}{dV} = - \langle\langle K(\mathbf{k}',\mathbf{k})\rangle_0\rangle_0 \{ G_0(V,\Delta) + \Delta G(V,\Delta) \} n e^2 , \qquad (3.28)$$

where

$$G_0(V,\Delta) = \frac{4\pi}{\hbar} S(S+1) J^2 \left\{ 1 + \frac{\langle M\rangle}{2S(S+1)} [R(eV+\Delta) - R(eV-\Delta)] \right\}, \qquad (3.29a)$$

and

$$\Delta G(V,\Delta) = - \frac{4\pi}{\hbar} J^3 S(S+1) \left\{ 2 \left[1 - \frac{\langle M^2\rangle}{S(S+1)} \right] F(eV) + \frac{\langle M\rangle}{S(S+1)} S(eV,\Delta) + \right.$$

$$\left. \left[1 + \frac{\langle M^2\rangle}{S(S+1)} \right] [F(eV+\Delta) - F(eV-\Delta)] + \frac{\langle M\rangle}{S(S+1)} [T(\Delta+eV) + T(\Delta-eV)] \right\} \qquad (3.29b)$$

In equation (3.29a) the function R(x) is given by

$$R(x) = \coth(\beta x/2) - (\beta x/2)\,\mathrm{cosech}^2(\beta x/2)\ . \tag{3.30a}$$

In equation (3.29b) the function F(x) is given by

$$F(x) = \int_{-E_0/2}^{E_0/2} - f'_{\epsilon+x}\,[\,g^a(\epsilon) + g^b(\epsilon)\,]\ , \tag{3.30b}$$

S(eV,Δ) by

$$S(eV,\Delta) = \int_{-E_0/2}^{E_0/2} f'_{\epsilon+eV}\,[g^a(\epsilon) + g^b(\epsilon)]\left\{\tanh\left(\frac{\epsilon-\Delta}{2k_BT}\right) - \tanh\left(\frac{\epsilon+\Delta}{2k_BT}\right)\right\} d\epsilon\ , \tag{3.30c}$$

and T(x) by

$$T(x) = \int_{-E_0/2}^{E_0/2} f'_{\epsilon+x}\,(1 - 2\,f_\epsilon\,)\,(\,g^a(\epsilon) + g^b(\epsilon)\,)\,d\epsilon\ . \tag{3.30d}$$

⟨M⟩ and ⟨M²⟩ are the averages of the z component of the spins, given by

$$\langle M\rangle = \sum_{-S}^{+S} P_M M = \tfrac{1}{2}\coth\left[\frac{\Delta}{2k_BT}\right] - (S+1/2)\coth\left[\left(S+\tfrac{1}{2}\right)\frac{\Delta}{k_BT}\right] \tag{3.30e}$$

and

$$\langle M^2\rangle = \sum_{-S}^{+S} P_M M^2 = \langle M\rangle^2 - (S+1/2)^2\,\mathrm{cosech}^2\left[\left(S+\tfrac{1}{2}\right)\frac{\Delta}{k_BT}\right] + \tfrac{1}{4}\,\mathrm{cosech}^2\left[\frac{\Delta}{2k_BT}\right]\ . \tag{3.30f}$$

In these equations is

$$\beta = \frac{1}{k_B T} \; ; \; E_0 = \text{bandwidth} \; , \tag{3.31a}$$

$$f_x = \text{Fermi-Dirac distribution} \; ; \; f_x' = \frac{\partial f}{\partial x} \; , \tag{3.31b}$$

and

$$g^{a(b)}(x) = P \int_{-E_0/2}^{E_0/2} \frac{(f_\epsilon - 1/2)}{\epsilon - x} \rho^{a(b)}(\epsilon) \, d\epsilon \; . \tag{3.31c}$$

References

1. I.K. Yanson, Zh. Eksp. Teor. Fiz. 66, 1035 (1974) [Sov. Phys. JETP 39, 506 (1974)]
2. see e.g. A.G.M. Jansen, F.M. Mueller, and P. Wyder, Phys. Rev. B 16, 1325 (1977)
3. for a review see I.K. Yanson, Fiz. Nizk. Temp. 9, 676 (1983) [Sov. J. Low Temp. Phys. 9, 343 (1983)]
4. A.I. Akimenko and I.K. Yanson, Pis'ma Zh. Eksp. Teor. Fiz. 31, 209 (1980) [JETP Lett. 31, 209 (1980)]
5. A.G.M. Jansen, A.P. van Gelder, P. Wyder, and S. Strässler, J. Phys. F: Metal Phys. 11, L15 (1981)
6. A.I. Akimenko, N.M. Ponomarenko, I.K. Yanson, S. Janos, and M. Reiffers in: Proc. LT-17, eds. U. Eckern, A. Schmid, W. Weber, and H. Wühl (North-Holland, Amsterdam, 1984), p.1085
7. B. Bussian, I. Frankowski, and D. Wohlleben, Phys. Rev. Lett. 49, 1026 (1982)
   E. Paulus and G. Voss, J. Magn. Magn. Mater. 47&48, 539 (1985)
   I. Frankowski and P. Wachter, Solid State Commun. 41, 577 (1982)
   M. Moser, P. Wachter, E. Hulliger, and J.R. Etourneau, Solid State Commun. 54, 24 (1985)
8. E. Paulus and G. Voss, J. Magn. Magn. Mater. 47&48, 539 (1985)
   M. Moser, P. Wachter, E. Hulliger, and J.R. Etourneau, Solid State Commun. 54, 24 (1985)
   M. Moser, P. Wachter and, J.J.M. Franse, Solid State Commun. 58, 515 (1986)
9. J. Kondo, Progr. Theor. Phys. (Kyoto) 32, 37 (1964)
10. M.A. Ruderman and C. Kittel, Phys. Rev. 96, 99 (1954)
    T. Kasuya, Progr. Theor. Phys. 16, 45 (1956)
    K. Yosida, Phys. Rev. 106, 893 (1957)
11. H. Suhl, Magnetism vol.5 (Academic, New York, 1973), p.32
12. V. Cannella and J.A. Mydosh, A.I.P. Conf. Proc. 18, 651 (1974) and Proc. Int. Conf. on Magn. 2, 74 (Publ. House Nauka, Moscow, 1974)
    C.L. Foiles, Phys. Lett. 67A, 214 (1987)
    D.L. Martin, Phys. Rev. B 21, 1902 (1980)
13. see e.g. P. Monod, Phys. Rev. Lett. 19, 1113 (1967)
    J.W. Loram, T.E. Whall, and P.J. Ford, Phys. Rev. B 3, 9953 (1971)
14. see e.g. J. Owen, M. Brown, W.D. Knight, and C. Kittel, Phys. Rev. 102, 160 (1956)
    J. Owen, M. Brown, V. Arp, and A.F. Kip, J. Phys. Chem. Solids 2, 85 (1957)
15. V. Cannella, J.A. Mydosh, and J.I. Budnick, J. Appl. Phys. 42, 1689 (1971)

V. Cannella and J.A. Mydosh, Phys. Rev. B 6, 4220 (1972); A.I.P. Conf. Proc. 10, 785 (1973); 18, 651 (1974) and Proc. Int. Conf. on Magn. 2, 74 (Publ. House Nauka, Moscow, 1974)
16. C.A.M. Mulder, A.J. van Duyneveldt, and J.A. Mydosh, Phys. Rev. B 23, 1394 (1981)
C.A.M. Mulder and A.J. van Duyneveldt, Physica (Utrecht) 113B, 123 (1982)
C.A.M. Mulder, A.J. van Duyneveldt, H.W.M. van der Linden, B.H. Verbeek, J.C.M. van Dongen, G.J. Nieuwenhuys, and J.A. Mydosh, Phys. Lett. A 88, 74 (1981)
17. R.W. Schmitt and I.S. Jacobs, Canad. J. Phys. 34, 2385 (1956)
I.S. Jacobs and R.W. Schmitt, Phys. Rev. 113, 459 (1959)
J.S. Kouvel, C.D. Graham, and J.J. Becker, J. Appl. Phys. 29, 518 (1958)
J.S. Kouvel, J. Phys. Chem. Solids 16, 107 (1960); 21,57 (1961); J. Appl. Phys. 31, 1425; 3105 (1960)
R. Street, J. Appl. Phys. 31, 310S (1960)
18. J.S. Kouvel, J. Phys. Chem. Sol. 21, 57 (1961)
19. J.L. Tholence, Thesis, Université de Grenoble, 1973
J. Souletie, J. Physique 39, C2-2 (1978)
20. C. Violet and R.J. Borg, Phys. Rev. 149, 540 (1966; 162, 608 (1967)
21. J.E. Zimmerman and F.E. Hoarse, J. Phys. Chem. Solids 17, 52 (1960)
J. de Nobel and J.J. du Chantenier, Physica (Utrecht) 25, 969 (1959)
22. E.D. Dahlberg, M. Hardiman, R. Orbach, and J. Souletie, Phys. Rev. Lett. 42, 401 (1979)
23. A. Arrott, J. Appl. Phys. 36, 1093 (1965)
24. K.H. Fischer, Phys. Stat. Sol.(b) 116, 357 (1983)
K.H. Fischer, Phys. Stat. Sol.(b) 130, 13 (1985)
K. Binder, Rev. Mod. Phys. 58, 801 (1986)
J.A. Mydosh, Lecture Notes on Physics, vol. 149, p.87 (Berlin: Springer Verlag, 1981)
25. A.G.M. Jansen, A.P. van Gelder, and P. Wyder, J. Phys. C: Solid State Phys. 13, 6073 (1980)
26. after L.Y.L. Shen and J.M. Rowell, Phys. Rev. 165, 566 (1968)
27. J.A. Appelbaum, Phys. Rev. Lett. 17, 91 (1966)
J.A. Appelbaum, Phys. Rev. 154, 633 (1967)
28. see e.g. A.G.M. Jansen, A.P. van Gelder, and P. Wyder: J. Phys. C: Solid State Phys. 13, 6073 (1980)
29. F.W Smith, Phys. Rev. B 14, 241 (1976)
30. C. Held and M.W. Klein, Phys. Rev. Lett. 35, 1783 (1975)
31. L.R. Walker and R.E. Walstedt, Phys. Rev. B 22, 3816 (1980)

CHAPTER 4

SUPERCONDUCTIVITY IN Bi OBSERVED WITH POINT CONTACTS

The resistance of metallic point contacts depends on the applied voltage because of the voltage-dependent scattering of the conduction electrons in the contact area. Therefore, point contacts are used as a spectroscopic tool to study the energy dependence of the interaction of the electrons with other excitations in the metal, especially with phonons[1,2]. In an attempt to do point-contact spectroscopy in the semimetal bismuth we observed a different type of nonlinear structure in the current-voltage characteristics at liquid-helium temperatures. We relate this anomalous structure to the quenching of small superconducting clusters (≃100 nm) near the contact area. Recently, superconducting inclusions have been observed in point-contact experiments with Ga[3].

Most of the metallic contacts were prepared by pressing a sharply etched Au needle against an electrolytically cleaned Bi sample (99.999% pure). The discussed effect was also observed in symmetric contacts of two pieces of Bi pressed against each other. We used both undeformed and deformed polycrystalline Bi. The Bi was plastically deformed by squeezing the sample at room temperature. We also studied point contacts consisting of a Au needle pressed on evaporated thin Bi films with thicknesses of 100 and 300 nm. The point contacts were adjusted by a differential screw mechanism at liquid-helium temperature. The obtained contact resistances ranged from 5 to 50 Ω. A magnetic field up to 3.5 T could be applied.

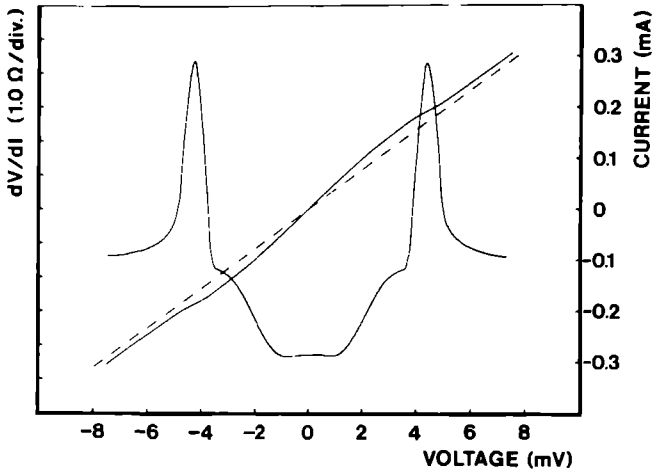

Fig. 4.1. Current and differential resistance as a function of the applied voltage for a Bi-Au point contact. Contact resistance R=20 Ω, temperature T=1.25 K. The dashed curve is an extrapolated linear I-V curve showing an excess current at high bias voltages.

In figure 4.1 we have plotted the current-voltage characteristic of a Bi-Au point contact at 1.2 K together with the differential resistance. Instead of the usual behaviour for the semimetal Bi, a continuous decrease in resistance with increasing bias voltage, we observed for several contacts maxima in the differential resistance followed by a higher resistance than the resistance at zero bias. The positions of the maxima vary from contact to contact between 1.5 and 8 mV. We interpret this phenomenon in terms of the quenching of superconducting inclusions close to the contact at a certain critical current. Sometimes we observe more than one maximum in the differential resistance, which can be the result of the presence of a few superconducting clusters or of the complex structure of the cluster. At the superconducting-normal transition the change in the dynamical resistance does not exceed 30-35%.

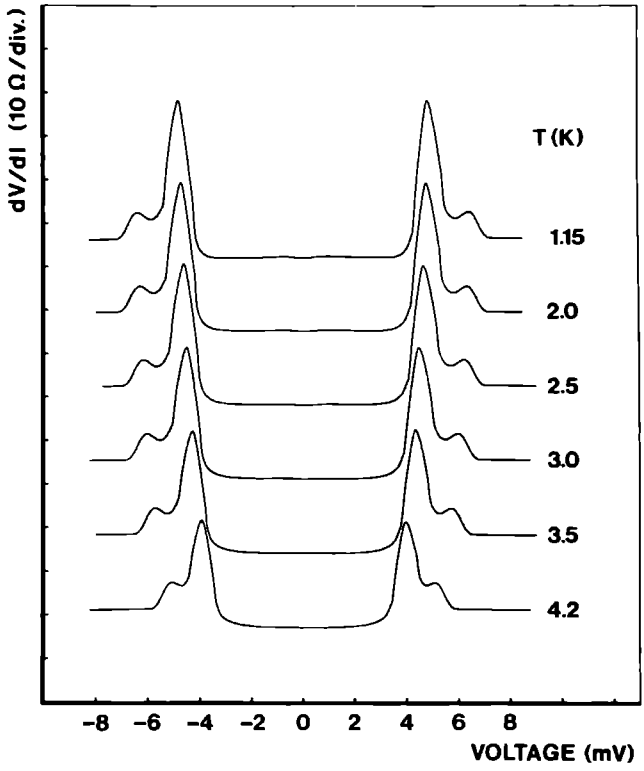

Fig. 4.2. Differential resistance as a function of the applied voltage showing the anomaly for point contacts with Bi at different temperatures. Au-Bi point contact; R=23 Ω.

Only 1-2% of the contacts with undeformed Bi show such anomalous maxima in the differential resistance. Figure 4.2 shows the contact resistance for a contact with undeformed Bi at different temperatures. There is only a small dependence of the position of the maxima on temperature below 4.2 K. For point contacts with deformed Bi the anomaly occurs more often (roughly 10% of the contacts) and the maxima disappear around 4 K (figure 4.3).

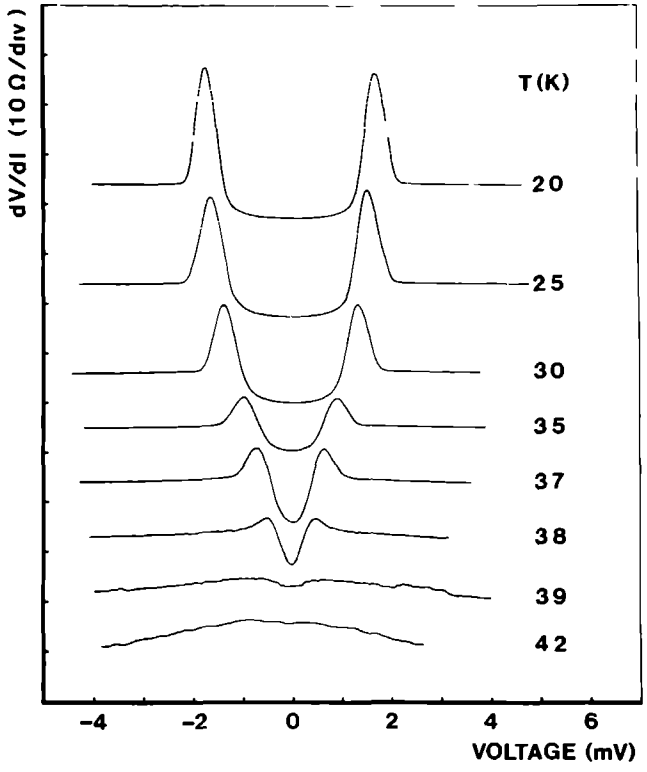

Fig. 4.3. Differential resistance as a function of applied voltage showing the anomaly for point contacts with Bi at different temperatures. Bi_{def}-Bi point contact; R=11 Ω.

In figure 4.4 we have plotted the critical voltage V_c normalized to the critical voltage V_c^0 at the lowest measuring temperature (1.2 K) as a function of the reduced temperature T/T_c for several contacts. The critical voltage was defined by the voltage at the measured maximum in the resistance. Because of the small change in resistance a similar result would be obtained by plotting the critical current of the anomaly. The data are in good agree-

ment with the BCS dependence of the reduced order parameter $\Delta/\Delta_0(T/T_c)$, if the critical temperature T_c for the observed superconductivity is 5.9 K for the undeformed samples and 3.9 K for the deformed ones. Also the experiments with metallic contacts on thin Bi films reveal the superconducting phase with a critical temperature of 5.9 K, but now the phenomenon occurs, however, in nearly every contact.

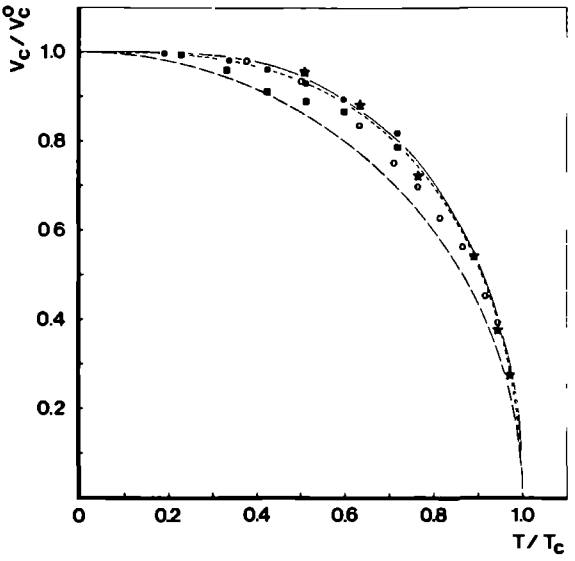

Fig. 4.4. Normalized voltage V_c/V_c^0 of the anomaly in the resistance as a function of the reduced temperature T/T_c. The symbols ● and ■ for undeformed Bi (●Bi-Au, R=23 Ω; ■ Bi-Au, R=5.3 Ω) with a critical temperature T_c=5.9 K. The symbols ✱ and ○ for deformed Bi (✱ Bi_{def}-Au, R=8.6 Ω; ○ Bi_{def}-Bi, R=11 Ω) with T_c=3.9 K. The full curve shows the BCS dependence for the order parameter. The long and short dashed curves represent, respectively, the functions $(1-T^2/T_c^2)^{1/2}$ and $(1-T^3/T_c^3)^{1/2}$.

It is well known that there exist superconducting phases of Bi under pressure, so-called Bi II (T_c=3.95 K) and Bi III (T_c=7.25 K) phases[4]. In addition, Bi has an amorphous phase[5] with a critical temperature $T_c \simeq 6$ K. According to the data in figure 4.3 we observe the amorphous phase in point contacts with polycrystalline Bi and the Bi II phase in contacts with deformed Bi. In contrast to Ga, magnetic susceptibility measurements in polycrystalline Bi do not reveal any trace of superconductivity in Bi[6]. From the sensitivity of these

susceptibility measurements it can be concluded that, if present, such clusters have a total volume less than 10^{-7} of the volume of the Bi crystal. Therefore, our observed effect is mainly a surface phenomenon. It is known that by deformation at low temperatures, bulk Bi shows superconducting traces in the conductivity below 4 K, which are removed by annealing at 77 K[7]. We probe this phase at the surface of our sample, which was, however, deformed at room temperature. Of coarse we may introduce the superconducting phase by the distortion of the lattice with the adjustment of the contact, but the fact that we do not observe the Bi II phase in point-contact experiments with pure Bi, makes it improbable that the applied pressure in the contact area is the cause of the observed effect in deformed Bi. For the observed amorphous phase we cannot totally rule out the influence of distortion at the contact. The amorphous phase in pure Bi is either rarely produced near the contact or appears in a diluted distribution over the surface.

In a magnetic field the behaviour of the point-contact anomalies confirms the observation of two different phases. In the point contacts with pure Bi the superconductivity is not suppressed in fields up to 3.5 T, which is in agreement with the observed high critical fields of the amorphous phase of Bi. For the squeezed Bi samples we observe critical fields between 1 and 2 T.

With point contacts between a normal metal and a superconductor similar curves as in figure 4.1 were observed[8] and in these experiments the critical voltage was equal to the superconducting order parameter. Because of the spreading in the measured critical voltage for different contacts and the high values of the voltages [compared with Δ=1.2 meV for amorphous Bi (ref.5)] it is not probable in our case that we are directly probing the energy gap. In point contacts fabricated by evaporating a metal in a pinhole in the oxide layer on a crystal of Bi, Sb or BiSb, Esaki and Stiles observed a similar change in the dynamical resistance at a critical current[9]. They suggested that the superconductivity could arise from a dipole layer at the contact interface induced by the difference in the contact potentials. However, Nanney[10] explained the nonlinearities by a thermal instability based on the specific temperature dependence of the electrical and thermal conductivity of the material under study. In a view of the model by Nanney we have to consider thermal effects in the point-contact measurements.

For a point contact in the dirty limit (mean free path l smaller than the contact radius a) the maximum temperature T_m at the center of the contact is given by the Kohlrausch relation[11]

$$T_m^2 = T^2 + (L_0/4)\, V^2 \,, \tag{4.1}$$

where T is the bath temperature and L_0 the Lorenz number. With a few millivolts the critical temperature can be reached in the contact. Assuming that

the anomaly will occur at $T_m=T_c$ we expect a dependence like $V_c \sim (1-T^2/T_c^2)^{1/2}$. This functional dependence does not describe the data in figure 4.3 very well. Using the Sharvin[12] formula ($R_{Sh} \simeq \rho l/a^2$) for the resistance of a clean contact ($l>a$) we obtain diameters from 100 to 300 nm for the investigated contacts. These values are smaller than the electronic mean free path in pure Bi. In this case there is no equilibrium between electrons and phonons and equation (4.1) will not hold any more. The electron mean free path becomes of the order of the contact dimension at voltages corresponding to the bulk phonon frequencies (Debye energy 10.3 meV). Monotonically increasing the voltage could then yield temperature changes at the phonon voltages. Also the superconducting-normal transition alters the thermal properties near the contact. It is difficult to give a detailed picture of the observed quenching phenomenon in this nonequilibrium situation. In figure 4.3 we have also plotted the dependence $V_c \sim (1-T^3/T_c^3)^{1/2}$. Such a relation was used to show the resemblance between bulk resistivity measurements as a function of temperature and resistivity measurements as a function of voltage for Bi point contacts[7], which did not show the superconducting anomaly. On the basis of the experimental data it is not possible to discriminate between the last mentioned function and the BCS curve for the order parameter.

The thermal instability in Nanney's model explains the observed phenomenon with the use of the electrical and thermal conductivity of Bi in the normal state. However the observation of two different phases in Bi, the temperature dependence which yields appropriate values for the critical temperatures and the magnetic field dependence require a model with superconductivity at the surface of the samples. Another confirmation for the presence of superconductivity in Bi point contacts is the observed excess current[13] even at voltages above the maximum in the resistance (see figure 4.1). The dashed curve in figure 4.1 shows the extrapolated normal-state resistance R_N. Only for a few contacts does the excess current δI_{exc} exceed 10-15% of the theoretical value given by $\delta I_{exc}=8\Delta/3eR_N$. At the anomaly the relative change $\delta R/R$ in the contact resistance will be 100% for a contact between a superconductor and a normal metal. For the case that only part of the contact is occupied by the superconducting inclusion the value for $\delta R/R$ will be reduced by the quotient of the superconducting area and the total contact area. For a contact with R=20 Ω and $\delta R/R$=30% we find a contact diameter of 160 nm and a cluster diameter of 90 nm.

In conclusion, we have observed the superconducting phases of amorphous Bi and Bi II at the surfaces, respectively, of pure Bi and plastically deformed Bi using point contacts on these samples. Point contacts are very suitable to probe the existence of superconducting phases within roughly 100 nm of the surface of the sample.

References

1. I.K. Yanson, Fizk. Nizk. Temp. 9, 676 (1983) [Sov. J. Low Temp Phys. 9, 343 (1983)]
2. A.G.M. Jansen, A.P. van Gelder, and P. Wyder, J. Phys. C 13, 6073 (1980)
3. O.I. Shklyarevskii, N.N. Gribov, and Yu.G. Naidyuk, Fiz. Nizk. Temp 9, 1068 (1983) [Sov. J. Low Temp. Phys. 9, 553 (1983)]
4. M.A. Il'ina and E.S. Itskevich, Fiz. Tverd. Tela (Leningrad) 14, 395 (1972) [Sov. Phys. Solid State 14, 328 (1972)]
5. T.T. Chen, J.T. Chen, J.D. Leslie, and H.J.T. Smith, Phys. Rev. Lett 22, 526 (1969)
6. A.G. Klimenko, E.V. Matizen, and M.A. Starikov, Fiz. Nizk. Temp. 5, 352 (1979) [Sov. J. Low Temp. Phys. 5, 167 (1979)]; and (private communication)
7. I.L. Broneva and Yu. V. Sharvin, Pis'ma Zh. Eksp. Teor. Fiz. 28, 127 (1978) [JETP Lett. 28, 117 (1978)]
8. D.B. Sullivan and C.E. Roos, Phys. Rev. Lett. 18, 212 (1967)
9. L. Esaki and P.J. Stiles, Phys. Rev. Lett. 15, 152 (1965)
10. C.A. Nanney, Phys. Rev. Lett. 16, 313 (1966)
11. R. Holm, Electric Contacts (Springer-Verlag, Berlin, 1967)
12. Yu.V. Sharvin, Zh. Eksp. Teor. Fiz. 48, 984 (1965) [Sov. Phys. JETP 21, 655 (1965)]
13. G.E. Blonder, M. Tinkham, and T.M. Klapwijk, Phys. Rev. B 25, 4515 (1982)

CHAPTER 5

THERMAL POINT-CONTACT SPECTROSCOPY IN UPt_3

5.1. Introduction.

Point-contact spectroscopy is used to study the energy dependence of the interaction of the electrons with elementary excitations in a metal[1,2]. Mainly this technique has been applied for a direct determination of the Eliashberg function for the electron-phonon coupling from the measured non-linearity in the current-voltage characteristic of a metallic point contact. For a long list of materials[1], point-contact spectroscopy has been applied successfully to the study of the electron-phonon interaction. Recently, point contacts have been used for the study of less common compounds with rare earths and actinides[3-6]. Valence fluctuations and heavy fermions are very interesting phenomena in these systems. Structure in the current-voltage characteristics of point contacts with these systems has been analysed in terms of electron-scattering with valence fluctuations[3] and density of states effects[4-6]. However, alternative explanations have been raised in a description of local heating of the contact area[7,8]. In an introduction we will sketch the problem by mentioning the relevant dimensional parameters, i.e. contact dimension with respect to the mean free path of the electrons, and their influence in a point-contact experiment. We will discuss the effect of an energy-dependent density of states on the non-linearity of a current-voltage characteristic for a point contact. Experimentally, we investigated point contacts of the heavy-fermion system UPt_3 as a function of temperature between 4 and 100 K. Others reported point-contact experiments on UPt_3 with the interpretation in a simple model for the spectroscopy of the density of states[9]. We will apply the model with local heating of the contact area to analyse the results.

5.2. Dimensional criteria.

Important parameters in the evaluation of point-contact experiments are the contact dimension and the mean free path of the electrons. The contact dimension can be defined by the radius a of a circular contact between two semi-infinite metallic parts. For the mean free path of the electrons we consider the inelastic scattering of the electrons, given by the inelastic scattering length ℓ_ϵ or the inelastic diffusion length $\Lambda_\epsilon = (\ell_\epsilon \ell_i)^{1/2}$ for the case of strong elastic scattering (mean free path ℓ_i). The inelastic mean free path depends on the electron energy ϵ with respect to the Fermi level.

In the regime where $\ell_\epsilon, \ell_i >> a$, electrons are injected ballistically through the contact in the presence of an applied voltage V. The relevant electron mean-free-path ℓ_ϵ is then determined by the energy ϵ=eV. In this so-called ballistic regime we can obtain in an optimum way spectroscopic information of the scattering of the electrons. The non-equilibrium distribution of the

ballistically injected electrons relaxes via spontaneous emission of phonons, yielding voltage-dependent corrections to the current. The spectroscopic information is measured directly in the second derivative d^2I/dV^2 of the current I with respect to the voltage V via the expression[1,2]

$$d^2I/dV^2 \propto a^3\, \alpha^2F(eV)\ . \tag{5.1}$$

The voltage-dependent d^2I/dV^2 signal is proportional to the Eliashberg function α^2F for the electron-phonon interaction. The above described inelastic scattering of the electrons contributes to the signal most efficiently for processes occurring in the contact region, yielding the contact volume a^3 in the proportionality of equation (5.1).

In the diffusive regime where $\Lambda_\epsilon > a > \ell_i$, the non-equilibrium distribution of the electrons is similar in energy space as for the ballistic regime. Only the momenta are randomised due to elastic scattering. The spectroscopic information again is given by equation (5.1). The factor a^3 in equation (5.1) has to be multiplied by a factor ℓ_i/a which results in a smaller efficiency volume equal to $a^2\ell_i$[10]. Thus with small elastic mean free paths as in metallic alloys, it is still possible to do phonon spectroscopy; however with a decreased intensity of the measured signals[11]. Note, that in the ballistic and diffusive regime the Joule heat is released in a volume (defined by ℓ_ϵ or Λ_ϵ) greater than the contact area. In first order heating effects can be neglected in the interpretation of the non-ohmic behavior in these clean contacts.

In the thermal regime where $a \gg \ell_\epsilon, \ell_i$, it is no longer possible to do energy-resolved spectroscopy in a point-contact experiment. Due to the strong scattering, the electron and phonon systems are in equilibrium. Joule heating of the contact area can't be ignored. Already in 1900 Kohlrausch solved this problem for an arbitrary contact geometry[12]. Assuming equal flow lines for electrical and thermal conduction, the following relation exists between the applied voltage V and the maximum temperature T_{max} at the center of a contact at a temperature T_{bath}

$$V^2 = 8 \int_{T_{bath}}^{T_{max}} \rho\lambda \, dT\ , \tag{5.2}$$

where ρ and λ are respectively the electrical resistivity and thermal conductivity of the bulk material. Because the equipotential surfaces coincide with the surfaces of constant temperature, this relation contains no factor depending on the specific geometry of the contact. If the Wiedemann-Franz law $\rho\lambda = LT$ holds and $T_{max} \gg T_{bath}$, then equation (5.2) gives that the maximum

temperature in the contact is proportional to the applied voltage. For the Sommerfeld value of the Lorenz number L ($2.45\ 10^{-8}\ V^2/K^2$) this yields a hot spot in the contact with an increase in the temperature of 3.2 K per mV across the contact. In the thermal regime the resistance R_M of a contact is obtained from a solution of the Maxwell equations with appropriate boundary conditions yielding

$$R_M = \rho/2a\ , \tag{5.3}$$

for a circular contact of radius a. For a dirty contact the voltage-dependent contact resistance resembles the temperature-dependent bulk resistivity using equation (5.2) to map the applied voltage to the contact temperature. Equation (5.2) gives only the maximum temperature in the contact region. For a temperature dependent resistivity an integral of the resistivity over the temperature profile near the contact has to be taken to calculate the voltage-dependent contact resistance. As such the geometry enters the problem[13]. Because the dominant contribution of the contact resistance is given by the resistivity in the middle of a contact, a good approximation will be given by taking the resistivity at the maximum temperature instead of the detailed temperature profile. To account for the local resistivity in the contact area it is better to compare the voltage dependence of the dynamical contact resistance dV/dI(V) at low temperatures with the temperature dependence of the contact resistance R(T) at zero bias voltage instead of with the temperature-dependent bulk resistivity[7].

5.3. Influence of the density of states.

The heavy-fermion character at low temperatures is ascribed to the occurrence of a many-particle resonance in the density of states around the Fermi level. In an explanation of point-contact data of mixed-valence and heavy-fermion systems it has been argued that one observes the energy dependence of the electron density of states $N(\epsilon)$ in these systems[5,6]. Analogously to the tunneling formula one writes the current through a contact as the following integral

$$I \propto \int_0^{eV} N(\epsilon)\, d\epsilon\ . \tag{5.4}$$

Then, the differential conductance dI/dV is proportional to N(eV). In an

exact description of the point-contact problem in the ballistic limit, the density of states does not enter the problem as given in the last equation. To clarify this, we derive the resistance of a contact in the clean limit considering specific band-structure effects. In zeroth order without collisions the current I_0 through a contact can be written as[1,2]

$$I_0 = 2e \int d^2r \int d^3k \; v_{kn} \; f_k^0(r) \; , \tag{5.5}$$

where v_{kn} is the velocity component normal to the contact area. The surface integral $\int d^2r$ runs over the contact area and equals πa^2 for a circular contact. The electronic distribution function $f_k^0(r)$ describes a filled Fermi sphere with differences in the electro-chemical potential depending on the velocity direction of the electrons. At the orifice the distorted Fermi sphere consists of two filled half-spheres with energy radii $(E_F+eV/2)$ and $(E_F-eV/2)$. Evaluating equation (5.5) in the limit of low temperatures we get

$$I_0 = \frac{e}{4\hbar\pi^3} \pi a^2 \int_{E_F-eV/2}^{E_F+eV/2} d\epsilon \int_{\epsilon=\epsilon_k} dS_k \; |n_k \cdot s| \; . \tag{5.6}$$

dS_k is an infinitesimal area on the Fermi surface with constant energy ϵ (the integration is only over half the Fermi sphere). n_k and s are unit vectors, respectivily parallel to v_k and perpendicular to the contact surface. The current is proportional to a projection of the Fermi surface on the plane of the contact. For an average over all orientations of the crystal with respect to the contact we take $|n_k \cdot s| = 1/2$, which is exact for the isotropic case. As a result for the differential conductance dI_0/dV we get

$$dI_0/dV = \frac{e^2}{32\hbar\pi^3} \pi a^2 \left[S(E_F + eV/2) + S(E_F - eV/2)\right] , \tag{5.7}$$

where S(E) is the energy-dependent area of the Fermi surface. In equation (5.7) we have added a factor 1/2 for the area S(E) to be related to the total Fermi sphere. For a quadratic dispersion relation ($S(E) \propto E$), the contact resistance is independent of the applied voltage and equals the Sharvin[14] formula $R_{Sh} = 4\rho\ell/3\pi a^2$ for the resistance of a clean contact; here, we have used $\rho\ell = mv_F/n_0e^2$ with the electron concentration $n_0 = k_F^3/3\pi^2$. For a non-quadratic dispersion relation the voltage derivative of the conductance of the contact may depend on the applied voltage via the asymmetry in the effective mass ($m(E) \propto dS/dE$) around the Fermi level. In the point-contact problem the density of states does not show up in the simple description given by

equation (5.4). In terms of the Fermi-surface area S(E) the density of states can be written as $N(E) \propto S^{1/2}\, dS/dE$. Non-quadratic dispersion and anisotropy are important to include band-structure and mass-renormalization effects in the description of a point-contact.

5.4. Experimental details.

Point-contact experiments were performed on poly-crystalline UPt_3 between 4 and 100 K using a flow-cryostat. To make the contact, two pieces of bulk material were pressed against each other. The current-voltage characteristics and its derivatives of the voltage with respect to the current were measured using a phase-sensitive detection technique at 500 Hz. Due to differences in thermal expansion of the various parts in the sample holder, the metallic contacts were not stable and changed continuously at a temperature above roughly 80 K. In a first attempt to do temperature-dependent experiments these disturbing effects occurred at still lower temperatures. Therefore, we mounted a spring bended from copper wire in the contact set-up to reduce the induced changes in the force on the contact area upon varying the temperature.

The obtained contact resistances ranged from 0.1 to 10 Ω. Using the value for the bulk resistivity $\rho(4\ K) = 3\ 10^{-7}\ \Omega m$ in the a/b plane of a single crystal[15], we obtain with equation (5.3) contact radii from 1500 to 15 nm. For 6 f-electrons in the unit cell (volume $140.9\ 10^{-30}\ m^3$) of UPt_3 we get the free-electron value $\rho\ell = \hbar k_F / n_0 e^2 = 1.04\ 10^{-15}\ \Omega m^2$. Using this value for the product $\rho\ell$ we obtain a mean free path of 3 nm at 4 K. Hence, the studied contacts will be in the thermal limit ($\ell < a$). For the temperature-dependent measurements the resistances below 1 Ω turned out to be the most stable.

5.5. Experimental results and discussion.

In figure 5.1 we have plotted the differential resistance $dV/dI(V,T_{bath})$ for a UPt_3 point contact as a function of the applied voltage V for different temperatures T_{bath} up to 100 K. The characteristics were symmetric around V=0. With increasing temperature the drop in resistance at bias voltages below 20 mV gradually disappears and is not visible above 25 K. For the lowest measuring temperature the differential resistance as a function of the voltage resembles the bulk resistivity as a function of the temperature[15]. The bulk resistivity of UPt_3 shows a sharp rise at low temperatures (< 20 K) followed by a less strong increase at higher temperatures with a tendency to

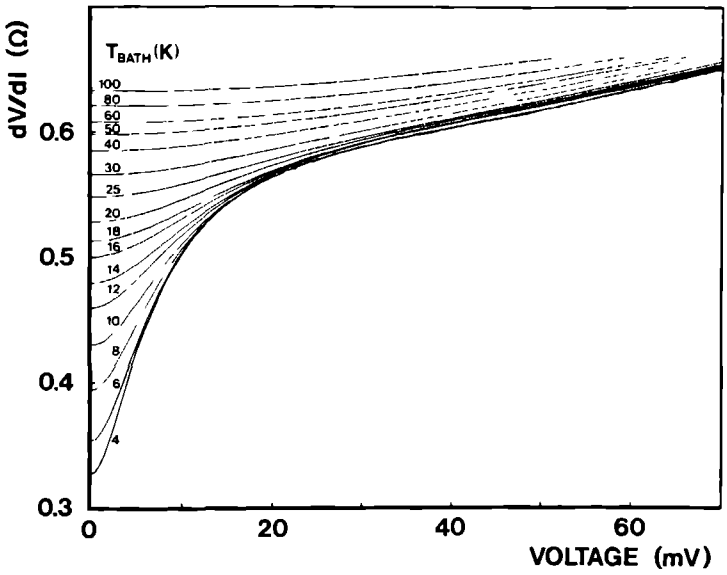

Fig. 5.1. Measured differential resistance dV/dI as a function of applied voltage of a UPt_3 point contact at different bath temperatures T_{bath} as indicated in the figure, showing the drop in resistance at low bias voltages and low temperatures which disappears at high temperatures (T_{bath}>25 K).

saturation in the room-temperature region.
Spin-fluctuation scattering ($\rho(T) \propto T^2$) and a Kondo lattice behavior with screening of the scattering centers play a role in the drop of the resistivity at low temperatures. Regarding the temperature dependence between 4 and 100 K, the relative change in bulk resistivity is roughly a factor 5 larger than the relative change in point-contact resistance at zero voltage for the data of figure 5.1. As a consequence, a determination of the contact dimension from the temperature dependence of the contact resistance yields a discrepancy with the same factor as compared to the obtained contact radius from the low temperature resistance value. This discrepancy is often encountered in an analysis of point-contact data in the thermal limit[4,7,8]. For pure metals (i.e. Cu) the two determinations show a good agreement[16]. A reason for this could be that on the local scale of the point-contact the temperature-dependent resistivity deviates from the bulk value. Because of the relatively small effects of the pressure on the bulk resistivity for UPt_3 [15], it is improbable that a distortion in the contact region fully explains this local deviation from the bulk resistivity. Although the temperature dependence of the contact res-

istance itself is not in detail understood from the temperature-dependent resistivity, we will analyse the voltage-dependent contact resistance quantitatively by the use of the temperature-dependence of the contact resistance instead of that of the bulk resistivity.

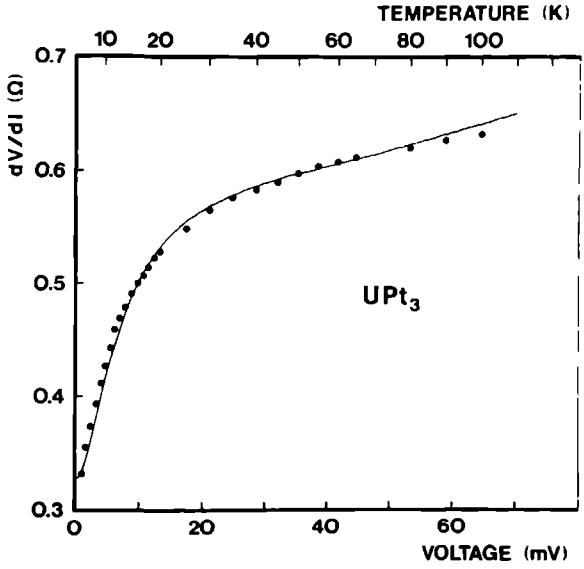

Fig. 5.2. Comparison between the voltage-dependent differential resistance $dV/dI(V,T_{bath}=4\ K)$ of a UPt_3 point contact (solid line) and its temperature-dependent differential resistance $dV/dI(V=0,T_{bath})$ (dots). The heating model has been used for the scaling between temperature and voltage.

In figure 5.2 the dynamical resistance $dV/dI(V,T_{bath}=4\ K)$ has been plotted together with the data points of $dV/dI(V=0,T_{bath})$. For the scaling of the temperature with respect to the voltage scale we used equation (5.2). Due to the strong electron-electron scattering in UPt_3 the thermal conductivity of the phonons has a significant contribution and this results in a Lorenz number with a value higher than the Sommerfeld value. From the measured temperature dependence of the specific resistivity and the thermal conductivity of bulk UPt_3 the temperature-dependent Lorenz number has been determined[17]. With these experimental data we calculated with equation (5.2) the relation between the maximal temperature in the contact and the applied voltage. Using this scaling between voltage and temperature (roughly 1.5 K increase in temperature for each mV), we see in figure 5.2 a good agreement

between the curve of $dV/dI(V,T_{bath}=4\ K)$ and the data points of $dV/dI(V=0,T_{bath})$. The data above 80 K are less reliable because of the afore mentioned difficulties in preserving the same contact.

A comparison of $dV/dI(V,T_{bath}=const.)$ and $dV/dI(V=0,T_{bath})$ can be done for all measured bath temperatures by the corresponding scaling between voltage and temperature in equation (5.2). Graphically this comparison has been realized for all temperatures in figure 5.3. Using equation (5.2) with the temperature-dependent transport data, we have drawn in the V-T_{bath} plane of figure 5.3 the curves with the same temperature T_{max} in the center of the contact. For the data in figure 5.1 a set of data-points V-T_{bath} can be obtained for each T_{max} by equalizing $dV/dI(V=0,T_{max})$ to $dV/dI(V,T_{bath})$. Again we see that the data show a good agreement for temperatures up to 60 K.

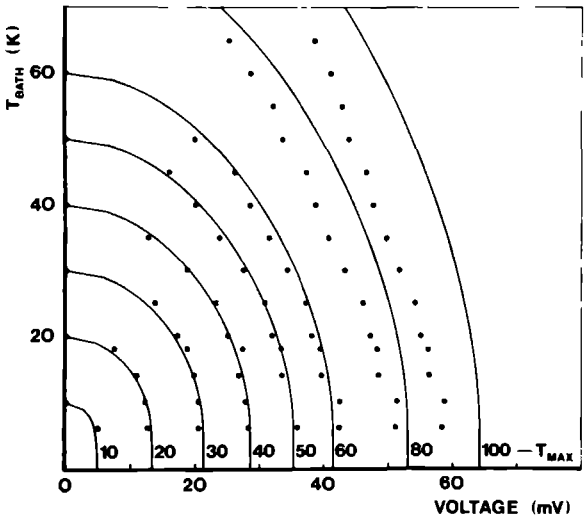

Fig. 5.3. Calculated curves in the V-T_{bath} plane with the indicated temperature T_{max} at the center of a UPt_3 point contact according to the heating model, using equation (5.2). The dots represent the values of the voltage and bath temperature belonging to a point on the curves of figure 5.1, where the resistance is equal to the resistance at zero voltage (for the various bath temperatures).

To look at the reproducibility we plotted in figure 5.4 the voltage derivative $d(dV/dI)/dV$ of the dynamical resistance as a function of the voltage for different point-contacts at low temperatures ($\simeq$4 K). For comparison we also

have drawn the temperature derivative of the bulk resistivity in the a/b plane of UPt_3 as a function of the temperature[15]. The amplitudes of d(dV/dI)/dV were adjusted to coincide with the temperature-dependent data in the region between 10 and 20 mV. Again we used mapping between voltage and temperature as discussed before. As can be seen in figure 5.4, there is a difference in the observed non-linearity from contact to contact. We believe that the local pressure and deformation in the contact area plays a role for the understanding of this effect. A realistic force of 10^{-3} kgf on a area of 10 $(\mu m)^2$ gives already a pressure of 10 kbar on the contact. In the same way, the $d\rho/dT$ curve of the resistivity shows a shift of the maximum (0.35 K/kbar) with increasing pressure[15].

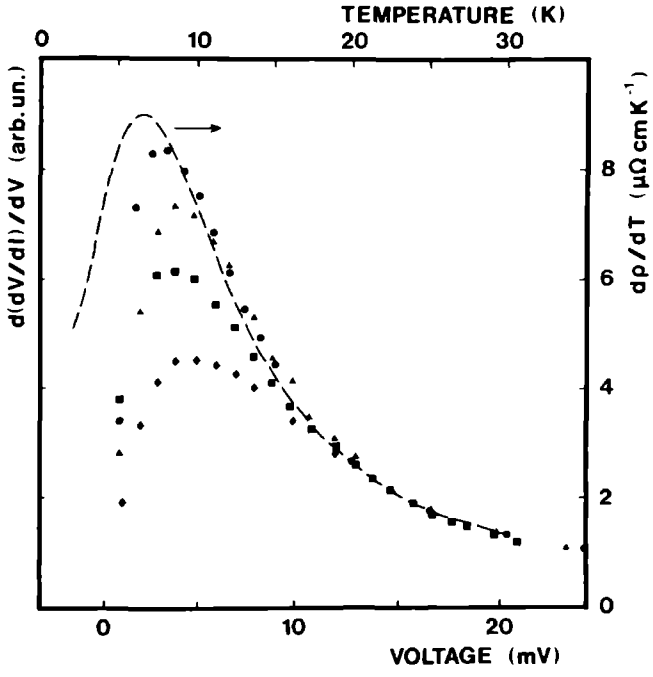

Fig. 5.4. Comparison of the voltage derivative of the differential resistance d(dV/dI)/dV as a function of applied voltage for different UPt_3 point contacts at T=4.2 K (dots) with the temperature derivative of the bulk resistivity dρ/dT in the a/b plane of UPt_3 as a function of temperature (dashed line, after ref.15). The heating model has been used for the scaling between temperature and voltage.

5.6. Conclusions.

Due to the strong scattering of electrons in UPt_3 the point contacts with this heavy-fermion system are in the dirty limit ($\ell < a$). For UPt_3, the measured nonlinear point-contact characteristics can be described in a model of Joule heating in the contact area by a comparison with the temperature-dependent contact resistance. As should be for the thermal limit, the relative change of contact resistance with temperature cannot be explained quantitatively from the temperature-dependent resistivity. However, the functional temperature-dependences are similar for the contact resistance and the bulk resistivity. Local heating of the point contact can be neglected in pure contacts ($\ell > a$). For contacts in this limit, the voltage dependence of the resistance is quite different from the temperature dependence[18].

Also for other metals with narrow-band phenomena (heavy fermions, mixed valancies) heating of the contact has to be considered in the interpretation of the point-contact data. It will depend on the specific system under study to what extend the heating model influences the experimental data.

The energy dependence of the density of states cancels against the electron velocity in a simple free-electron description of the voltage dependence of the resistance of a clean contact. In order to see any influence of the electronic band-structure in the point-contact spectra, a detailed theory should include non-parabolicity and anisotropy of the electronic bands.

References:

1. I. K. Yanson, Fiz. Nizk. Temp. 9, 676 (1983) [Sov. J. Low Temp. Phys. 9, 343 (1983)].
2. A. G. M. Jansen, A. P. van Gelder, and P. Wyder, J. Phys. C 13, 6073 (1980).
3. B. Bussian, I. Frankowski, and D. Wohlleben, Phys. Rev. Lett. 49, 1026 (1982).
4. E. Paulus and G. Voss, J. Magn. Magn. Mat. 47&48, 539 (1985).
5. I. Frankowski and P. Wachter, Solid State Commun. 41, 577 (1985).
6. M. Moser, P. Wachter, F. Hulliger, and J. R. Etourneau, Solid State Commun. 54, 241 (1985).
7. Yu. G. Neidyuk, N. N. Grivbov, A. A. Lysykh, I. K. Yanson, N. B. Brandt, and V. V. Moshchalkov, Pis'ma Zh. Eksp. Teor. Fiz. 41, 325 (1985) [JETP Lett. 41, 399 (1985)].
8. A. G. M. Jansen, A. de Visser, A. M. Duif, J. J. M. Franse, and J. A. A. J. Perenboom, J. Magn. Magn. Mat. 63&64, 670 (1987).
9. M. Moser, P. Wachter, and J. J. M. Franse, Solid State Commun. 58, 515 (1986).
10. I.O. Kulik and I. K. Yanson, Fiz. Nizk. Temp. 4, 1267 (1978) [Sov. J. Low Temp. Phys. 4, 596 (1978)].
11. A. Lysykh, I. K. Yanson, O. I. Shklyarevski, and Yu. G. Naydyuk, Solid State Commun. 35, 987 (1980).
12. R. Holm, Electric contacts (Springer Verlag Berlin) 1967.
13. J. A. Greenwood and J. B. P. Williamson, Proc. Roy. Soc. A 246, 13 (1958).
14. Yu. V. Sharvin, Zh. Eksp. Teor. Fiz. 48, 984 (1965) [Sov. Phys. - JETP 21, 655 (1965)].
15. A. de Visser, J. J. M. Franse, and A. Menovsky, J. Magn. Magn. Mat. 43, 43 (1984).
16. A. P. van Gelder, A. G. M. Jansen, and P. Wyder, Phys. Rev. B 22, 1515 (1980).
17. J. J. M. Franse, A. Menovsky, A. de Visser, C. D. Bredl, U. Gottwick, W. Lieke, H. M. Mayer, U. Rauchschwalbe, G. Sparn, and F. Steglich, Z. Phys. B 59, 15 (1985).
18. A. G. M. Jansen, A. M. Duif, A. A. Lysykh, and P. Wyder, in press, NATO workshop on Narrow Band Phenomena, Staverden, The Netherlands (1987).

CHAPTER 6

HIGH-FREQUENCY RECTIFICATION IN UPt_3 POINT CONTACTS

6.1. Introduction.

During the last few years point-contact spectroscopy has been used in the study of various valence fluctuation and heavy fermion compounds. In most of these experiments large nonlinearities are observed in the current-voltage characteristics and their derivatives[1-4]. Explanations of these effects are given in terms of the scattering of the conduction electrons with the intermediate valence configurations[1], with the existence of a hybridisation gap in the electron-density of states[2], and in terms of density of states effects[3,4]. For these spectroscopic explanations the point contact under study has to be in the ballistic regime, i.e. the electron mean free path has to be larger than the contact dimension. An other explanation is given in terms of local heating in the contact area, which takes place in point contacts in the so-called dirty regime[5-7]. Here the electron mean free path has to be small compared with the contact dimension.

In an experiment we investigated the high-frequency rectification of UPt_3 point contacts. From the utilized optical frequency in these measurements an estimation can be made about the timescale of the processes which determine the shape of the current-voltage characteristics and its derivatives. For a ballistic and a dirty contact the relaxation times are expected to be quite different. For the ballistic model the relevant time scale is given by the scattering of the electrons, for the heating model by the thermal relaxation of the contact area.

6.2. Point-contact experiments on UPt_3.

Point-contact spectroscopy in metals can be performed in three different regimes. In the ballistic regime, the inelastic mean free path ℓ_i and the elastic mean free path ℓ_e of the electrons is larger than the contact radius a, i.e. $\ell_i, \ell_e >> a$. In this regime spectroscopic information is obtained about the energy dependence of the scattering of the conduction electrons with elementary excitations in the metal. This information is directly determined with a metallic point contact at low temperatures by measuring the second derivative d^2V/dI^2 of the current I with respect to the voltage V via

$$\frac{d^2I}{dV^2}(eV) \propto a^3\, S(eV)\,, \tag{6.1}$$

where S(eV) is the spectral function for the concerned interaction. For instance in the case of the electron-phonon interaction this spectral function

S(eV) equals the Eliashberg function $\alpha^2F(eV)$ for the electron-phonon interaction[8,9].

Analogously to a tunnel experiment it is often stated that with point-contact experiments one can also observe the energy dependence of the electron density of states using the integral $I(eV) \propto \int_0^{eV} N(\epsilon)\, d\epsilon$ for the current.

Hence the differential conductance dI/dV is proportional to the density of states. However for a point contact in the ballistic regime this proportionality does not hold. The ballistic electron current through a constriction, i.e. the current in zeroth order without any collisions is for a spherical Fermi distribution given by[9]

$$I^{(0)} \propto \int k^2\, v_k\, dk = \int_{E_F-eV/2}^{E_F+eV/2} k^2\, v_k \left(\frac{\partial k}{\partial E}\right) dE\,, \tag{6.2}$$

where v_k is the velocity of an electron with wave vector k. Writing $v_k=\partial E/\partial k$ we can see that the electron density of states $N(eV)\propto\partial k/\partial E$ drops out so that only remains:

$$I^{(0)} \propto \int k^2\, dE\,. \tag{6.3}$$

Hence the density of states can not be observed directly by measuring the differential conductance dI/dV. Only non-parabolicity and anisotropy can make the electronic bandstructure enter the problem.

The second point-contact regime is the diffusive regime where the elastic scattering is strong, i.e. where $\ell_e \ll a$, but where the inelastic diffusion length $\Lambda_i=(\ell_i\ell_e)^{1/2}$ is large compared with the contact diameter, i.e. $\Lambda_i > a$. In this regime still spectroscopic information is obtained, however the intensities of the spectra are reduced since in equation (6.1) an extra factor ℓ_e/a has to be added[10]. This factor is due to the reduced efficiency volume $a^2\ell_e$ where the crucial scattering processes take place.

The thermal point-contact regime in which $\ell_i,\ell_e \ll a$, does not allow energy-resolved spectroscopy any longer. Due to the small electron mean free path, the electrons are not injected ballistically and the Joule heat is released in the contact area itself. The electron and phonon systems are in equilibrium

and a complete thermalisation takes place. With the assumption that the electrical and the thermal current follows equal paths, one can calculate the maximum temperature at the center of the contact at a certain applied voltage. This maximum temperature is independent of the specific contact geometry and given by[11]

$$T_{max}^2 = T_{bath}^2 + V^2/4L \ . \tag{6.4}$$

Here T_{bath} is the bath temperature and L is the Lorenz number.

In this thermal regime the resistance of the point contact is given by the so-called Maxwell value

$$R_M = \rho/2a \ , \tag{6.5}$$

where a circular contact is assumed with contact radius a. In this equation ρ is the bulk resistivity of the metal under study. A combination of the expressions (6.4) and (6.5) indicates that in this regime a measurement of the point-contact resistance as a function of bias voltage should correspond to a measurement of the bulk resistivity ρ as a function of temperature.

In point-contact measurements on the heavy-fermion system UPt_3 large nonlinearities were observed in the current-voltage characteristics and its derivatives. In an explanation in terms of the heating model a difference in the relative resistance change was found in the comparison of the measured differential point-contact resistance as a function of bias voltage and the bulk resistivity as a function of temperature[7]. However a quantitative comparison of this dV/dI(V) with the measured point-contact resistance as a function of temperature was satisfying. It was suggested that probably the local temperature-dependent resistivity in the point-contact case deviates from the bulk value. The reason for this is not understood.

6.3. Point-contacts in high-frequency electromagnetic fields.

6.3.1 Ballistic regime

Because of the nonlinear current-voltage characteristics of metallic point contacts, these can be used as rectifiers for high-frequency electromagnetic radiation. Since the contact resistance is in most cases much smaller than the vacuum impedance, such a HF-radiation field is then used as a HF-current source. The whisker from which the point contact is made serves as an antenna to couple in the radiation.

When with HF-EM radiation an AC current $i_0 \cos \omega t$ is induced in a point contact and if this radiation is chopped, it is easily shown that the measured AC voltage at this chopper frequency equals:

$$V_{sig.} = \frac{i_0^2}{4} \left. \frac{d^2V}{dI^2} \right|_{I_0} = \frac{i_0^2}{4} R_D \left. \frac{dR_D}{dV} \right|_{I_0} \tag{6.6}$$

Here I_0 is the applied DC current through the contact and $R_D = dV/dI$ is the dynamical resistance of the point contact. Thus this technique enables an other method for measuring the second derivative d^2V/dI^2. For instance at FIR frequencies, rectification measurements on Cu point contacts reveal the phonon structure as can also be measured with a traditional low-frequency modulation technique[12]. In order to measure with this rectification technique the second derivative d^2V/dI^2 according to equation (6.6), it is necessary that the characteristic time τ for the processes of the observed nonlinearities is short compared with the timescale imposed by the radiation. In other words, the voltage over the point contact must follow the induced AC current modulation. For the mentioned rectification experiments on Cu this characteristic time τ is the electron-phonon scattering time $\tau_{el\text{-}ph}$ which is typically 10^{-14}-10^{-13} seconds for Cu at electron energies corresponding to the Debye phonon frequencies. With a FIR-radiation of approximately 500 GHz one finds $\omega_{FIR}\tau_{el\text{-}ph} \simeq 10^{-2} << 1$. This explains why the electron-phonon spectra are observed in the rectification experiments on Cu.

6.3.2 Thermal regime

For the case that a point contact is not in the ballistic, but in the thermal regime, one has to derive an other expression for the detected signal. Since the heating in the contact area is a slow process compared to the FIR frequency, the AC current modulation will not follow the nonlinear DC current-voltage characteristics, and no rectification will be observed. However the induced HF current can increase the local temperature in the contact area, causing a detectable change in the voltage across the constriction. The voltage over the contact will be $V(I_0)|_{no\ rad.} = V(I_0)|_T = I_0 R_S(I_0)|_T$ in absence of radiation, and $V(I_0)|_{with\ rad.} = V(I_0)|_{T+\Delta T} = I_0 R_S(I_0)|_{T+\Delta T}$ in the presence of radiation. Here $R_S = V(I)/I$ is the static resistance, depending on the temperature T. In a rectification experiment the detected voltage then will be:

$$V_{det.} = V(I_0)|_{with} - V(I_0)|_{no} \simeq I_0 \frac{dR_S}{dT} \Delta T \,, \tag{6.7}$$

when the temperature difference ΔT is small. In the presence of a HF current $i_0 \cos\omega t$ across the contact, we have to take the effective value $\langle V+i_0 R_s \cos\omega t\rangle_{eff}$ for the voltage V in equation (6.4). Using this expression for the effective voltage in equation (6.4), the detected voltage in equation (6.7) yields

$$V_{det.} = \frac{\sqrt{2} i_0^2}{8} R_S \frac{dR_S}{dV} . \qquad (6.8)$$

Note that the specific voltage-dependence of the contact temperature can deviate from equation (6.4), but still the result of the last expression is found. Comparing the equations (6.6) and (6.8) for the measured signals in both regimes, the difference is the replacement of the dynamical resistance in equation (6.6) by the static resistance in equation (6.8). In the traditional way of measuring point-contact spectra, i.e. with a low-frequency current modulation and detection of the second derivative at the double frequency, the same signal is measured as equation (6.6). The difference between the expected signals for the ballistic and the thermal regime enables one to distinguish between both regimes in an experiment.

The expression for the detected voltage in the thermal regime is derived with the assumption that $\omega\tau > 1$, where ω is the applied radiation frequency and τ the characteristic time for the thermal relaxation. When a radiation frequency is used which is low enough, i.e. $\omega\tau < 1$ again, one detects a signal conform equation (6.6). For Ni-Ni point contacts which are in the thermal regime at high bias voltages, this effect has been observed by Balkashin et al[13]. They measured the signal at a few frequencies where $\omega\tau \sim 1$. A considerable change in the shape of the signal was observed which can be described to the effects mentioned above.

6.4. Experimental details.

Rectification experiments were performed on UPt_3-UPt_3 and on Cu-UPt_3 point contacts. In the latter case a Cu whisker was pressed on a piece of bulk poly-crystalline UPt_3. The UPt_3-UPt_3 point contacts were formed by pressing two small pieces of bulk poly-crystalline UPt_3 together. However the sample from which the whisker was made had a rather small diameter (~0.2 mm) in order to facilitate the coupling of the radiation to the point contact. The point contacts were made at helium temperatures by means of a differential screw mechanism. The obtained contact resistances varied from 0.3 to 8.5 Ω. The radiation was focussed onto the contact by means of a light cone

which was mounted at the end of an oversized waveguide. Most of the measurements were performed at a radiation frequency of 562 GHz (i.e. 533.7 μm). However also some measurements were performed at laser frequencies 2523 GHz (i.e. 118.8 μm) and 639 GHz (i.e. 469 μm). The measurements were performed at temperatures between 1.5 and 4.2 K.

6.5. Experimental results and discussion.

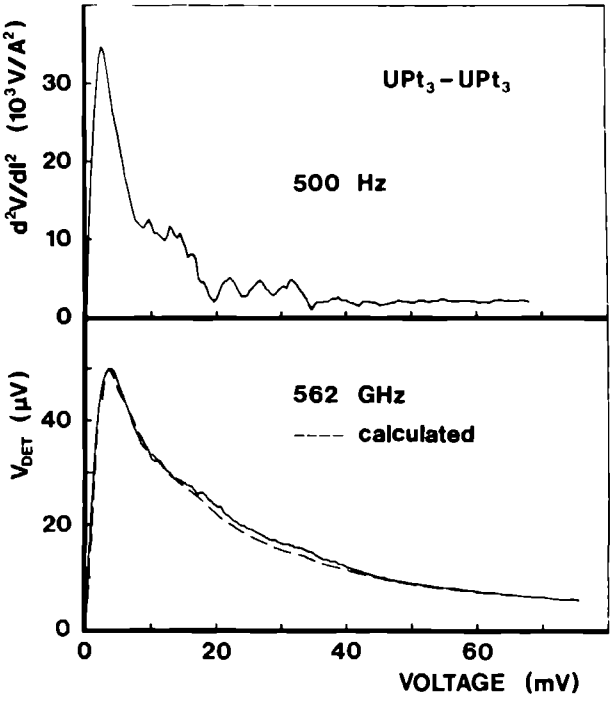

Fig. 6.1. Measured d^2V/dI^2 spectrum (upper curve) and the detected rectification signal V_{det} (lower curve) for a UPt_3-UPt_3 point contact with resistance $R(V=0)=1.3\ \Omega$ at bath temperature $T_{bath}=2$ K. The applied radiation frequency was 562 GHz. The dashed curve represents the expected rectification signal in the model of local heating, calculated with expression (6.8).

Figure 6.1 shows both the measured second derivative d^2V/dI^2 (upper curve) and the laser-detected signal (lower curve) for a UPt_3-UPt_3 point contact as a function of applied voltage V. The second derivative d^2V/dI^2 was measured with a standard low-frequency modulation technique. From this figure it is clear that the signal measured with the rectification method is broader than the measured second derivative. One can conclude that the rectified signal is not the expected signal for a point contact in the ballistic regime with a sufficiently fast response ($\omega\tau<1$, equation 6.6). The expected signal for the thermal regime with a slow response was also calculated using the measured dynamic resistance dV/dI of the contact in equation (6.8). The calculated curve is represented by the dashed line in figure 6.1. There is a

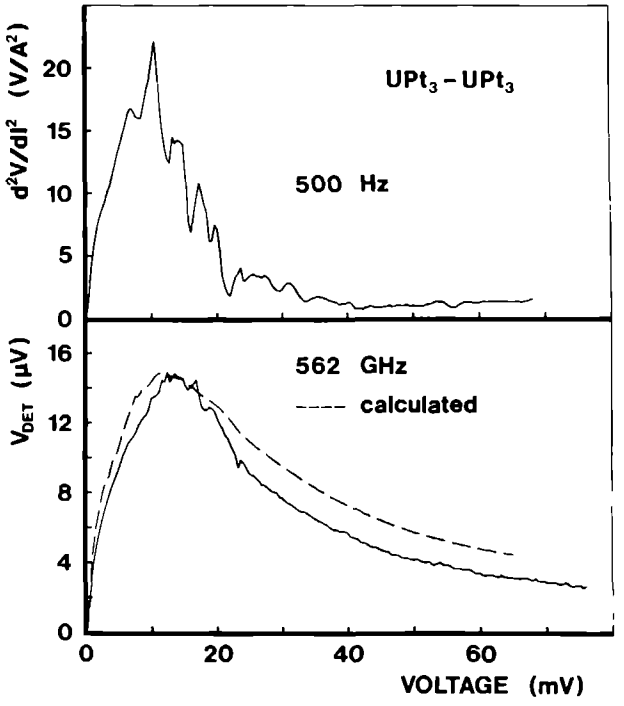

Fig. 6.2. Measured d^2V/dI^2 spectrum (upper curve) and the detected rectification signal V_{det} (lower curve) for a UPt_3-UPt_3 point contact with resistance $R(V=0)=0.44\ \Omega$ at bath temperature $T_{bath}=2$ K. The applied radiation frequency was 562 GHz. The dashed curve represents the expected rectification signal in the model of local heating, calculated with expression (6.8).

good agreement between the measured and the calculated curves. For an other contact (figure 6.2) the measured second derivative d^2V/dI^2 already is much broader than the one in figure 6.1. The observed difference between point contact spectra with UPt_3 is probably due to local pressure effects in the contact area[7]. For the experimental data in figure 6.2 the rectification signal also differs from the measured d^2V/dI^2 signal. The dashed curve again represents the with equation (6.8) calculated signal. In order to optimise the coupling of the electro-magnetic radiation with the point contact, we measured also contacts between a Cu whisker (antenna) and UPt_3 with an experimental result shown in figure 6.3. Also here there is a good agreement between the rectification signal and the calculation in the thermal model with a slow response.

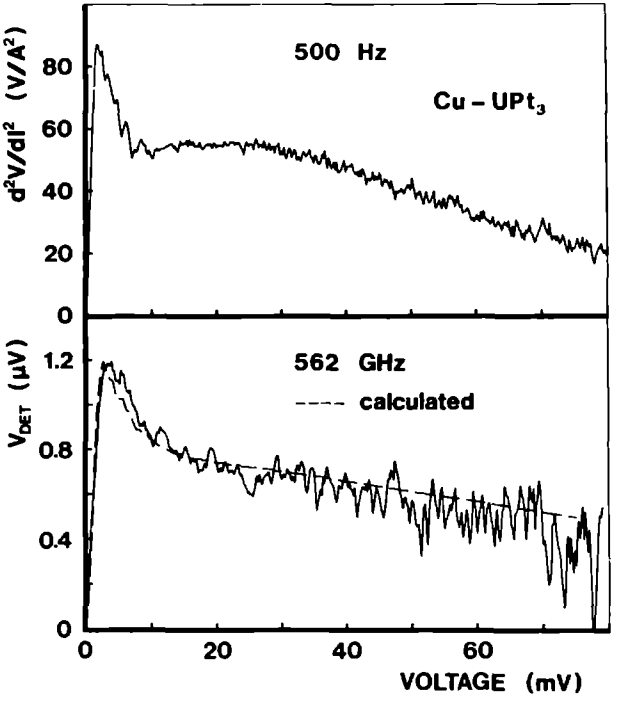

Fig. 6.3. Measured d^2V/dI^2 spectrum (upper curve) and the detected rectification signal V_{det} (lower curve) for a Cu-UPt_3 point contact with resistance $R(V=0)=1.3\ \Omega$ at bath temperature $T_{bath}=4.2$ K. The applied radiation frequency was 562 GHz. The dashed curve represents the expected rectification signal in the model of local heating, calculated with expression (6.8).

Measurements on UPt_3-UPt_3 point contacts were also performed at radiation frequencies 639 GHz and 2523 GHz. In all measurements the same results were found as at 562 GHz. Also the intensity of the radiation was changed during some measurements. The shape of the signal turned out to be independent of the applied intensity.

From the agreement between the measured and the calculated signals one may conclude that the point contacts are in a regime where $\omega\tau>1$. For UPt_3 we can make an estimation for the scattering time τ of the conduction electrons. At 4 K the value of $\tau=\ell/v_F^*$ will be $1.5\ 10^{-12}$ seconds. Here we used the value of the specific resistivity at low temperatures ($\rho=3\ \mu\Omega$cm) together with the renormalised Fermi velocity ($v_F^*=7\ 10^3$ m/s) for this heavy fermion system[14]. Thus $\omega\tau\sim1$ in this case. Therefore it is not clear what kind of rectification signal will be measured at low temperatures and zero voltage. At higher temperatures and at higher voltages, the electron mean free path will decrease strongly and the Fermi velocity may obtain a normal higher value. The scattering time τ of the electrons will also decrease, i.e. $\tau<1.5\ 10^{-12}$ in this case. Therefore $\omega\tau<1$ for a higher temperature or higher voltage. Thus in this case, a rectification signal according to equation (6.6) can be expected. We want to emphasize that this is only the case when electronic processes determine the current-voltage characteristics of the point contact. From the experiments ($\omega\tau>1$), we can conclude that electronic processes do not determine the nonlinear characteristics, but simply heating effects have to be considered.

One could imagine that the heating which is observed is not local heating by an induced high-frequency AC current but simply by absorption of radiation in the bulk sample, and therefore heating of the whole sample. It is therefore useful to estimate the essential timescales for both processes. For the case of local heating in the contact area one expects a timeconstant τ given by the quotient of total heat capacity C of the contact and conduction of heat Λ out of the contact area, i.e. $\tau \sim C/\Lambda \simeq cd^2/(\lambda d^2/d) = cd^2/\lambda$, where d is the diameter of the contact, c the specific heat and λ the thermal conductivity of UPt_3. Using a typical value for the contact diameter $d\sim100$ nm and experimental values for c and λ[15], one finds $\tau\sim10^{-9}$ seconds. Thus the condition $\omega\tau<1$ is fulfilled for the applied radiation frequencies. When the whole sample is heated by the radiation, the thermal conduction is determined by the Kapiza resistance to the bath. A very rough estimate gives $\tau\sim10^{-3}$ seconds for this case. However a prominent effect of the chopper frequency is not observed. If heating of the whole sample would take place with a constant temperature change independent of the applied voltage, equation (6.7) yields a signal approximately linear in bias voltage at sufficiently large voltages. These effects are not observed either.

6.6. Conclusions.

The measurements reported in this paper demonstrate that the measured large nonlinearities in the current-voltage characteristics and its derivatives of UPt_3 point contacts are not due to electronic scattering processes, but can be described with a heating model. Because of the small electron mean free path, local heating in the contact area takes place. This local heating involves a thermal time constant which is much slower than the timescale imposed by the applied radiation, hence leading to rectification signals which differ from the measured second derivative d^2V/dI^2.

References:

1. B. Bussian, I. Frankowski, and D. Wohlleben, Phys. Rev. Lett. 49, 1026 (1982).
2. I. Frankowski and P. Wachter, Solid State Commun. 41, 577 (1985).
3. E. Paulus and G. Voss, J. Magn. Magn. Mat. 47&48, 539 (1985).
4. M. Moser, P. Wachter, F. Hulliger, and J. R. Etourneau, Solid State Commun. 54, 241 (1985).
5. A. G. M. Jansen, A. de Visser, A. M. Duif, J. J. M. Franse, and J. A. A. J. Perenboom, J. Magn. Magn. Mat. 63&64, 670 (1987).
6. Yu. G. Neidyuk, N. N. Grivbov, A. A. Lysykh, I. K. Yanson, N. B. Brandt, and V. V. Moshchalkov, Pis'ma Zh. Eksp. Teor. Fiz. 41, 325 (1985) [JETP Lett. 41, 399 (1985)].
7. A.A. Lysykh, A.M. Duif, A.G.M. Jansen, P. Wyder, and A. de Visser, to be published (1987)
8. I. K. Yanson, Fiz. Nizk. Temp. 9, 676 (1983) [Sov. J. Low Temp. Phys. 9, 343 (1983)].
9. A. G. M. Jansen, A. P. van Gelder, and P. Wyder, J. Phys. C 13, 6073 (1980).
10. I.O. Kulik and I. K. Yanson, Fiz. Nizk. Temp. 4, 1267 (1978) [Sov. J. Low Temp. Phys. 4, 596 (1978)].
11. R. Holm, Electric contacts (Springer Verlag Berlin) 1967.
12. R.W. van der Heijden, A.G.M. Jansen, J.H.M. Stoelinga, H.M. Swartjes, and P. Wyder, Appl. Phys. Lett. 37, 245 (1980).
13. O.P. Balkashin, I.K. Yanson, V.S. Solov'ev, and A.Yu. Krasnogorov, Zh. Tekh. Fiz. 52, 811 (1982) [Sov. Phys. Tech. Phys. 27, 522 (1982)].
14. A. de Visser, J.J.M. Franse, A. Menovsky, and T.T.M. Palstra, Physica 127B, 442 (1984)
15. J.J.M. Franse, A. Menovsky, A. de Visser, C.D. Bredl, U. Gottwick, W. Lieke, H.M. Mayer, U. Rauchschwalbe, G. Sparn, and F. Steglich, Z. Phys. B59, 15 (1985).

CHAPTER 7

PHONON GENERATION BY METALLIC POINT CONTACTS AND DETECTION WITH PHONON-INDUCED CONDUCTIVITY IN Si

7.1. Introduction.

Metallic point contacts exhibit current-voltage characteristics which do not obey Ohm's law. The deviations which are found give information about the energy-dependent scattering of electrons with elementary excitations in the metal. Most clearly these nonlinearities in the current-voltage characteristics are observed for the study of the electron-phonon interaction[1,2]. At low temperatures the second derivative d^2V/dI^2 of the voltage V with respect to the current I exhibit structures which coincide with the structures in the Eliashberg function α^2F for the electron-phonon interaction. These structures are observed for point contacts in the ballistic regime, i.e. in which the mean free path of the electrons is large compared with the contact dimension. The observed nonlinearities have been explained in terms of ballistic injection of electrons from one side into the other side of the contact and subsequent energy-dependent interaction with phonons, followed by a possible backflow through the contact. In this way the spontaneous emission of phonons results in a change of the contact resistance related to the energy-dependent electron-phonon interaction. In the case of a small electron mean free path compared with the contact diameter (thermal regime), the measured I-V characteristics and its derivatives do not contain the spectral information about the electron scattering any more. In this regime the Joule heat is released close to the contact area. This leads to a hot spot at the center of the contact. In contrast with the ballistic regime, where the electron and phonon systems are not in equilibrium, in this thermal regime there is an equilibrium between the two systems.

For the generation of high-frequency phonons (50-1000 GHz) incoherent sources are available with either a broadband or a narrow-band phonon frequency spectrum. By electrical or optical heating of an evaporated metal film, phonons in a broad frequency band can be generated in an insulating crystal. The frequency distribution of these heaters can be described by a Planck formula. For a frequency-selective analysis the phonon emission spectrum of a superconducting tunneljunction has a narrow band around the energy gap 2Δ due to the recombination of quasi particles[3]. The scheme of crystal field levels in an insulator diluted with impurities (e.g. Cr^{3+} in Al_2O_3), offers the opportunity for monochromatic spectroscopy with phonons, using optical techniques for the excitation and detection of the relevant energy levels[4].

The generation of high-frequency phonons with point contact gives a possible method for frequency-selective phonon injection into insulating and semiconducting crystals. When the contact is made between a metal whisker and a metal film evaporated on the crystal, phonons can be generated in the metal film by applying a voltage over the contact and travel into the crystal. The point contact could be used as a tunable phonon source because the

applied voltage defines the maximum phonon frequency to be generated. First experiments in which the R_2 fluorescence in ruby was used to detect the phonons with an energy of 3.6 meV, were not sensitive enough to detect any signal at the corresponding point-contact bias voltage (3.6 mV). For higher applied voltages the detected signal could be described with a thermalised phonon system[5].

In this paper we will describe another experiment in which the distribution of phonons emitted by a point contact was studied. The phonons were generated with a point contact in a Au film which was evaporated on a silicon crystal, doped with boron impurities. By measuring the phonon-induced conduction of the silicon, the phonons could be detected frequency selective.

7.2. Phonon generation by point contacts.

In order to determine the nonequilibrium phonon distribution which is generated by a point contact we must solve the transport equation for phonons in the point-contact case, which reads[2]

$$c_{\mathbf{q}} \frac{\partial N_{\mathbf{q}}(\mathbf{r})}{\partial \mathbf{r}} = \left.\frac{\partial N_{\mathbf{q}}}{\partial t}\right|_{\text{coll}} = \frac{c_{\mathbf{q}}}{\epsilon\, l_p(\epsilon)} \{\, \gamma(\mathbf{r})\,[1 - \gamma(\mathbf{r})]\,(eV-\epsilon) - \epsilon\, N_{\mathbf{q}}(\mathbf{r})\,\} \,. \quad (7.1)$$

Here $\mathbf{q}$ is the phonon wavevector, $c_{\mathbf{q}}$ is the phonon velocity and $\epsilon=\hbar\omega_{\mathbf{q}}$ is the phonon energy. The function $\gamma(\mathbf{r})$ is the solid angle under which the orifice is seen at position $\mathbf{r}$. The first term in the expression of the collision term in equation (7.1) contains the gain of phonons due to the spontaneous emission of phonons by the accelerated electrons. The second term describes the loss of phonons by the creation of electron-hole pairs in a relaxation time approximation. When we, analogously to the solution of the transport equation for electrons, assume that the phonon mean free path $\ell_p(\epsilon)$ is large compared with the diameter of the contact, then the solution of this transport equation at the orifice ($\mathbf{r}=0$) is given by[2]

$$N(\epsilon,eV) = \langle N_{\mathbf{q}}(0)\rangle_{\text{av.}} = 0.32\, \frac{eV-\epsilon}{\epsilon}\, \frac{a}{\ell_p(\epsilon)} \qquad (\epsilon \le eV)\,, \quad (7.2a)$$

$$N(\epsilon,eV) = 0 \qquad (\epsilon \ge eV)\,. \quad (7.2b)$$

Here an average is made over all $\mathbf{q}$ directions. Striking feature of this phonon distribution function $N(\epsilon,eV)$ is the cutoff at a phonon energy $\epsilon=eV$: phonons

with $\epsilon > eV$ can not be generated with a point contact. In the case of a normal heater one would expect to have a Planck radiation of phonons, i.e. to have an effective temperature $T_{eff.}$ which is given by the proportionality $P \propto T_{eff.}^4$, where P is the dissipated power. Hence this relation yields $T_{eff.}^4 \propto V^2$. The distribution of phonons with this effective temperature is now given by the well-known Bose distribution

$$N(\epsilon, eV) = N(\epsilon, T_{eff.}) = \left[\exp\left(\epsilon/(k_B T_{eff.})\right) - 1 \right]^{-1} . \qquad (7.3)$$

This thermal phonon distribution function still has a tail at high energies, i.e. it still has a nonzero value for energies higher than eV, up to the Debye energy. This is the main difference between both distribution functions of contacts in the ballistic and in the thermal regime. The aim of the experiment described in this article was to distinguish between these two distributions.

7.3. Phonon detection by phonon-induced conductivity.

A very sensitive method to detect high-frequency phonons, generated by point contacts, is the method of phonon-induced conductivity. In this method the conduction of a semiconductor is measured which is enhanced by phonon-ionisation of D^- or A^+ centers in this semiconductor. These D^- and A^+ centers can be created by illumination of the sample, for instance with visible light. The created electron-hole pairs can be trapped by donors and acceptors to form D^- and A^+ centers close to the conduction and valence band. In the described measurements we used a silicon crystal doped with boron impurities. The B^+ centers in the Si which are present during illumination have an ionisation energy of 2.0 meV. Phonons with an energy higher than the ionization energy neutralize the acceptor yielding extra holes in the valence band of the semiconductor. This phonon detection mechanism in the conductivity of a semiconductor already has been used to do energy-resolved phonon detection using a superconducting Al tunnel junction as a tunable phonon generator[6,7].

In the experiment described here this threshold energy of 2meV for phonon detection was used to distinguish between the two discussed phonon distributions. The "ballistic" phonon distribution should not lead to ionisation of the B^+ centers at applied voltages below the threshold. The "thermal" distribution however, does not have the cutoff and hence should already at lower voltages lead to an enhanced conduction of the Si.

7.4. Experiment.

The experiments were performed with a gold point contact as phonon generator and a Si:B (5 10^{13} cm^{-3}) crystal as detector. A thin gold film of 40 nm thickness was evaporated on the silicon crystal with thickness 3 mm. With a differential screw mechanism a sharply etched Au whisker was pressed on this film. This was done at helium temperatures. At the opposite side of the crystal two Al strips were evaporated on a distance of about 1 mm from each other. With help of an optical fiber the sample was illuminated between these two strips during the measurement. Between the strips the conduction was measured. The total experimental setup is given in figure 7.1. The point-contact characteristics were recorded with a standard modula-

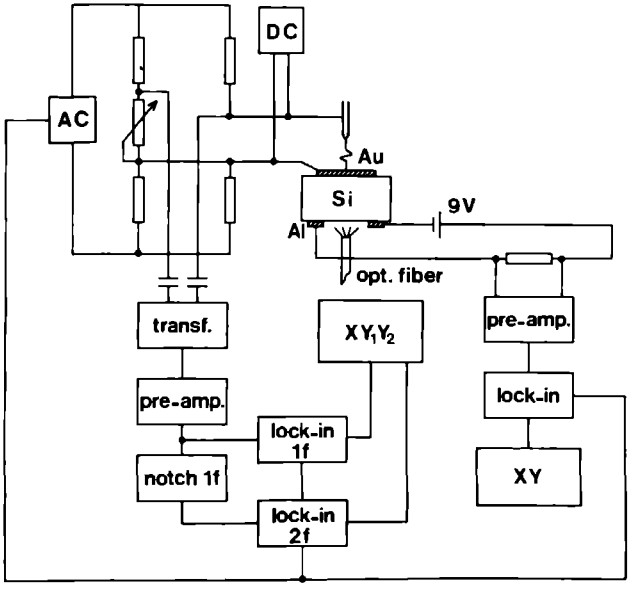

Fig. 7.1. Experimental setup. The point contact is made between a Au whisker and a Au film, evaporated on the Si crystal. Its characteristics are measured with a standard technique. The phonon-induced conduction was measured over a 2MΩ series resistor at the opposite side of the crystal.

tion technique. Here a bridge circuit was used to compensate for the point-

contact resistance at zero bias. The phonon-induced conduction was measured by measuring the AC current through a 2 MΩ series-resistor, using a battery-fed bias voltage of 9 V. The signal was measured with a lock-in technique.

Figure 7.2 gives the measured signal as a function of point-contact voltage both for low and for high illumination of the detector. A clear difference is observed at high bias voltages. A similar dependence on the intensity of the applied illumination was found in the experiments of Burger and Lassmann with the Al tunnel junction as generator[6]. An explanation for this effect is still missing. At low applied voltages the shape of the spectra is insensitive for the illumination intensity.

Since we are mainly interested in the behaviour around the threshold energy of 2 meV, most of the signals were measured for low bias voltages. Figure 7.3 gives the measured signal as a function of point-contact voltage for this low-energy regime.

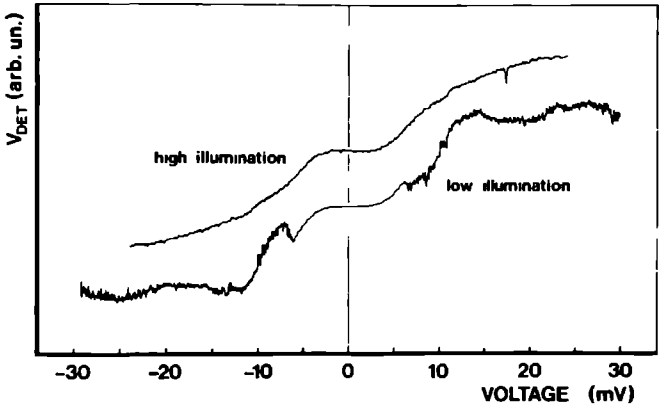

Fig. 7.2. Measured phonon-induced conduction signal V_{det} as a function of applied voltage over the point contact for low (lower curve) and high illumination (upper curve) of the detector. Contact resistance 1.0 Ω; temperature 1.35 K.

7.5. Discussion.

In order to draw a conclusion from the measured spectra concerning the two models for the phonon distributions we must make a model for the signal to be expected in both cases. If we assume that the enhancement of

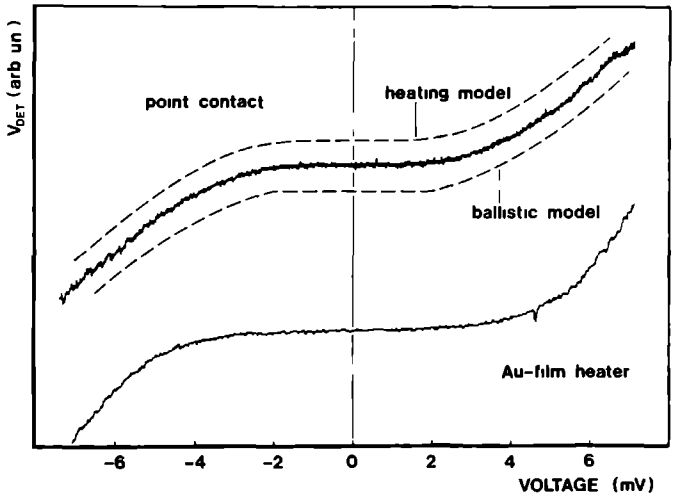

Fig. 7.3. Measured phonon-induced conduction signal in Si with a Au point contact (upper curves) and a Au film (lower curve) as phonon generator. Contact resistance 1.3 Ω; film-heater resistance ~0.1 Ω; temperature 1.3 K. The dashed curves are the calculated signals using the ballistic-contact model (lower dashed curve) and the heater model (upper dashed curve).

the measured conduction is proportional to the total number of phonons with an energy larger than the threshold energy, we can write the following expression for the expected signal:

$$V_{det} \propto \frac{d}{dV} \int_{\epsilon_c}^{\epsilon_D} N(\epsilon)\, F(\epsilon)\, d\epsilon \,. \tag{7.4}$$

Here ϵ_c and ϵ_D are the threshold energy, i.e. the ionization energy of the A^+ centers and the Debye energy respectively. The phonon occupation number is the product of the phonon distribution function $N(\epsilon)$ and phonon density of states $F(\epsilon)$. The voltage derivative enters equation (7.4) because the measurements are performed with a lock-in technique. Substituting the expressions for the phonon-distribution functions $N(\epsilon)$ from equations (7.2) and (7.3) into

this expression yields expressions for the expected signals.

If in the ballistic regime the energy-dependent phonon mean free path is assumed to be energy independent and if furthermore the Debye approximation $F(\epsilon) \propto \epsilon^2$ is used, the expected signal can be calculated, yielding

$$V_{det.} \propto (eV)^2 - \epsilon_0^2 \qquad (eV > \epsilon_0) , \tag{7.5a}$$

$$V_{det.} = 0 \qquad (eV < \epsilon_0) . \tag{7.5b}$$

Hence in this regime the signal is expected to be zero up to the threshold energy and to increase quadratically for voltages above this critical voltage.

In the thermal regime the expected signal is given by the integral

$$V_{det.} \propto \frac{V}{(T_0^4 + \alpha^4 V^2)^{1/4}} \int_{\frac{\epsilon_0}{k_B}(T_0^4+\alpha^4V^2)^{-1/4}}^{\infty} \frac{x^3 \exp(x)}{(\exp(x) - 1)^2} \, dx . \tag{7.6}$$

Here a Bose distribution as in equation (7.3) is used with an effective temperature $T_{eff.}$ which is according to Weis[8] given by

$$T_{eff.}^4 = T_0^4 + \alpha^4 V^2 . \tag{7.7}$$

Here T_0 is the bath temperature and the coefficient α is determined by the phonon flow out of the hot area. According to the acoustic mismatch model, this α is given by[8]

$$\alpha^4 = \frac{1}{AR} \frac{120\hbar^3}{\pi^2 k_B^4} \left(e_l/c_l^2 + 2\, e_t/c_t^2 \right)^{-1} , \tag{7.8}$$

where A is the hot area, c_l and c_t are the sound velocities for longitudinal and transversal phonons respectively and e_l and e_t are transmission coefficients depending on the heater-substrate interface. Equation (7.6) can be calculated numerically.

In figure 7.3 the calculated signals are represented for the ballistic regime and the thermal regime respectively. A comparison between calculated and measured curves does not give a decisive answer. Figure 7.4 gives the signal measured at the double frequency, i.e. the derivative of the signal in figure 7.3. Also the derivatives of the calculated signals (eqs. 7.5 and 7.6) are represented in this figure. Here a smearing of the spectra due to the bath temperature is taken into account. From a comparison between measured and calculated plots, one may conclude that a heating model gives a better description

of the measurements than a ballistic model. However the saturation of the measured derivative at voltages above 4 mV is not described very well by theory.

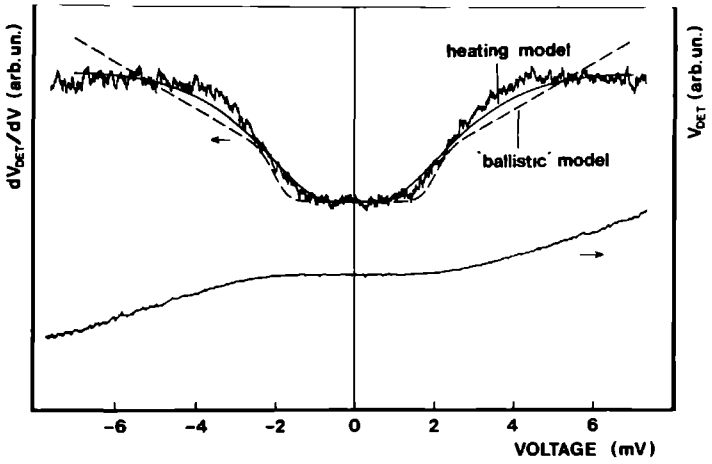

Fig. 7.4. Measured phonon-induced conduction signal $V_{det.}$ (lower curve) and its voltage derivative $dV_{det.}/dV$ (upper curve) as a function of applied voltage over the contact. Contact resistance 2.7 Ω; temperature 1.3 K. The solid and the dashed line in this figure represent the calculated voltage derivatives of the signal, using the heater model and the ballistic-contact model respectively.

We will now discuss the obtained results in view of the heating model, described above. From fitting the measured spectra with the theoretical dependence of equation (7.6) it is possible to estimate the coefficient α which relates the effective heater temperature with the applied voltage (equation 7.7). With this value of α the area of the hot spot can then be calculated, using equation (7.8)[9]. One could expect in the point-contact case a hot spot with a diameter of the same order of magnitude as the film thickness. For such a hot area of 40x40 nm^2 and a typical point-contact resistance of 1 Ω, equation (7.8) yields α=33.4 K/(mV)$^{1/2}$. The from the experimental results estimated values however, are much lower, viz. α=1.8±0.2 K/(mV)$^{1/2}$. To investigate this discrepancy we also used the whole Au film as a heater.

In figure 7.3 the measured signal is given as a function of the applied voltage over the heater film (lower curve). A clear difference is observed between the signals of a point contact and the film. The value of α which is

found in the latter case is α=0.6±0.1 K/(mV)$^{1/2}$. Equation (7.8) predicts for this heater film α=0.21 K/(mV)$^{1/2}$. One can conclude from this that the Au film is considerably warmer than one would expect. Reason for this can be a non-ideal match between film and crystal, decreasing the phonon transport through the interface and thus leading to an increase in temperature of the heater film.

In figure 7.5 the measured and expected temperatures for the point contact and the Au film are plotted as a function of bias voltage. Here the lowest curve corresponds with an α=0.21 which is predicted for the Au film. The middle curve indicates the regime in which the temperature of the Au film lies, as determined from the measured signals. The highest curve corresponds with the obtained temperatures of the point contact.

From the obtained values of α, the hot area in the point-contact case can be calculated. Using equation (7.8) and the experimental values for α for the point-contact case, a hot area of about 200x200 μm^2 is found.

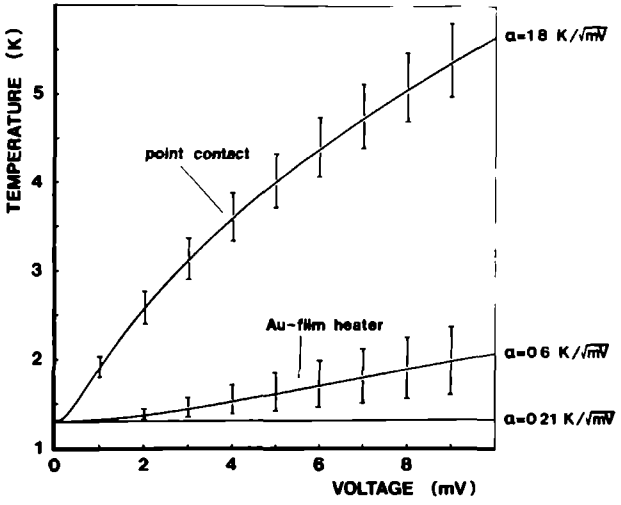

Fig. 7.5. Measured and expected temperatures for the point contact and the Au film as a function of the applied voltage, in view of the heater model. The lowest curve represents the predicted temperature-voltage dependence for the Au-film heater, the middle curve indicates the regime in which the temperature of the Au film in the experiments lies, and the upper curve corresponds with the obtained point-contact temperatures.

7.6. Conclusion.

In the measured phonon-induced conductivity signals a threshold at $eV=\epsilon_c$, which is expected for a point contact in the ballistic regime, is not observed. Probably due to a large mismatch between Au and Si, the phonons do not enter the Si within a mean free path length, but are reflected at the interface. This leads to a thermalisation of the phonon system in the metal film. A description with such a thermalised phonon system is possible and leads to a heater area of about 200x200 μm^2. The obtained heater area is very large compared to the contact dimension (~10 nm) and even larger than the inelastic scattering length of the electrons (~1 μm).

References.

1. I.K. Yanson, Fiz. Nizk. Temp. 9, 676 (1983) [Sov. J. Low Temp. Phys. 9, 343 (1983)]
2. A.G.M. Jansen, A.P. van Gelder, and P. Wyder, J. Phys. C 13, 6073 (1980)
3. K.F. Renk in Phonon Scattering in Condensed Matter, ed. W. Eisenmenger, K. Lassmann and S. Döttinger, p.10 (1984, Berlin: Springer-Verlag)
4. W. Eisenmenger in Physical Acoustics, Vol. XII, ed. W.P. Mason (1976, Academic Press)
5. R.J.G. Goossens, J.I. Dijkhuis, H.W. de Wijn, A.G.M. Jansen, and P. Wyder, Physica 127B, 422 (1984)
6. W. Burger and K. Lassmann, Phys. Rev. Lett. 53, 2035 (1984)
7. W. Burger and K. Lassmann, Phys. Rev. B 33, 5868 (1986)
8. O. Weis, Z. Angew. Phys. 26, 325 (1969)
9. for calculations of e_l and e_t see F. Rösch and O. Weis, Z. Phys. B 27, 33 (1977)

SUMMARY

The scattering of conduction electrons with excitations in a material can be examined with point contacts when the diameter of the contact is small compared with the inelastic mean free path of these electrons. In that case, applying a bias voltage over the contact, "hot" electrons are injected ballistically from one side into the other side of the contact where they relaxate due to the interaction with these excitations. Since this relaxation is strongly energy dependent, the current-voltage characteristics reveal nonlinearities due to this interaction. In the past the electron-phonon interaction has been studied thoroughly with this method. However it is also possible to study other types of interactions of the electrons, e.g. with magnons, paramagnetic impurities and crystal-field levels. In this thesis a number of experiments on point contacts are described in which the main subject was not the determination of phonon spectra but a study of other scattering mechanisms and the investigation of some aspects and applications of point contacts.

After a general introduction a review is given about point-contact spectroscopy. In this review a short summary is given of the most important theoretical and experimental results of point-contact spectroscopy. Then a number of interesting experiments, performed during the last few years are discussed. With these experiments the point-contact technique as a spectroscopic tool is illustrated and the important criteria for a point-contact experiment will be explained. Also a number of experiments is discussed in which point contacts are used not for spectroscopic purposes but in which the small contact dimension is exploited.

In the next part point-contact experiments are described on the dilute magnetic alloys AuMn and CuMn, both in the Kondo as well as in the spin-glass state. A model is presented, based on the existing theories for the scattering of the conduction electrons with the impurity spins and this is compared with the experimental data. This comparison works satisfying and supplies information about the alloys themselves. For instance the g-values of the dilute samples are determined using this method. For the more concentrated samples in the spin-glass state the method gives the possibility to study the weak interaction between the impurity spins themselves.

The following subject deals with point-contact experiments on bismuth. The current-voltage characteristics of point contacts on this semimetal show an anomalous structure which is because of its temperature and voltage dependence ascribed to the presence of superconducting clusters at the surface. The experiments were performed on both deformed and undeformed bismuth. In each of these two cases a different superconducting phase was found, namely the amorphous Bi phase in experiments on undeformed and the Bi-II phase in experiments on deformed bismuth. From the relative change in point-contact resistance the diameter of the superconducting clus-

ters can be estimated. In most cases a diameter of about 100 nm was found.

The next chapter reports about the point-contact experiments on the heavy-fermion system UPt_3. Point contacts of these materials are believed not to be in the ballistic regime but in the thermal regime where the electron mean free path is small compared with the contact dimensions, thus leading to heating in the contact area. In that case the experiments do not supply energy-resolved information. The temperature-dependent experiments show that the voltage-dependent contact resistance at low temperatures resemble the temperature-dependent contact resistance at zero voltage.

Then an other type of experiments on UPt_3 is described, dealing with the high-frequency rectification of point contacts in this system. Point contacts placed in a far-infrared electromagnetic field exhibit a DC response which is proportional to the second derivative d^2V/dI^2 as measured with a normal low-frequency modulation technique. However this is only the case when the processes which determine the current-voltage characteristics are fast compared with the applied modulation frequency. The signals obtained in the rectification experiments on UPt_3 do not reproduce the d^2V/dI^2 dependence exactly but one which can be explained with the assumption that the processes in this material are slow compared with the applied HF modulation (~1 THz). One could imagine that heating of the contact area is such a slow process.

The last part of the thesis deals not with the electric properties of point contacts but describes experiments in which the main subject was to examine the phonons emitted by metallic point contacts. In the experiments the point contacts were made between a metallic whisker and a metal film which was evaporated on a lightly doped silicon crystal. This crystal, doped with boron impurities was used as a phonon detector. At the opposite side of the crystal the conductivity was measured. Because of the presence of phonons this conductivity was enhanced due to the ionization of B^+ impurity levels in the Si. With this method information was obtained about the phonons generated by the point contacts and their behaviour in the metal film.

SAMENVATTING

De verstrooiing van geleidingselektronen aan exitaties in een materiaal kan onderzocht worden met behulp van puntkontakten wanneer de diameter van het kontakt klein is vergeleken met de inelastische vrije weglengte van deze elektronen. In dat geval worden, wanneer een spanning aangelegd wordt over het kontakt, "hete" elektronon ballistisch geinjecteerd in de andere kant van het kontakt alwaar ze relaxeren ten gevolge van de interactie met deze exitaties. Aangezien de relaxatie sterk energie-afhankelijk is, vertonen de stroom-spanningskarakteristieken niet-lineariteiten ten gevolge van deze interaktie. Met behulp van deze methode is in het verleden de elektron-fonon wisselwerking uitvoerig bestudeerd. Het is echter eveneens mogelijk om andere soorten van interakties van de elektronon te bestuderen, zoals die met magnonen, paramagnetische verontreinigingen en kristalveld-niveaus. In dit proefschrift zijn een aantal experimenten beschreven waarin niet het voornaamste doel was het bepalen van fonon-spektra, maar het bestuderen van andere verstrooiingsmechanismen en de waarneming van enkele andere aspekten en toepassingen van puntkontakten.

Na een algemene inleiding wordt een overzicht gegeven over puntkontaktspektroskopie. In dit overzicht wordt een korte samenvatting gegeven van de belangrijkste theoretische en experimentele resultaten van puntkontaktspektroskopie. Vervolgens wordt een aantal experimenten besproken die de laatste jaren verricht zijn. Met deze experimenten wordt de puntkontakttechniek toegelicht en worden de belangrijke kriteria voor een puntkontaktexperiment uiteengezet. Tevens wordt een aantal experimenten besproken waarin puntkontakten niet gebruikt zijn voor spektroskopische doeleinden, maar waarin gebruik gemaakt wordt van de kleine kontaktafmetingen.

In het volgende deel is een beschrijving van puntkontaktexperimenten aan de verdunde magnetische legeringen AuMn en CuMn, beide zowel in de Kondo als ook in de spin-glas toestand. Er wordt een theorie gepresenteerd, gebaseerd op bestaande modellen voor de verstrooiing van de geleidingselektronen aan de spins van de onzuiverheden, en deze theorie wordt vergeleken met de experimentele resultaten. Deze vergelijking werkt bevredigend en geeft bovendien additionele informatie over de legeringen zelf. Bijvoorbeeld werden met behulp van deze methode de g-waarden van de verdunde preparaten bepaald. In de wat meer gekoncentreerde preparaten bestaat de mogelijkheid om met behulp van deze methode de zwakke wisselwerking tussen de spins zelf te bestuderen.

Het volgende onderwerp handelt over puntkontaktexperimenten aan bismuth. De stroom-spanningskarakteristieken van puntkontakten aan dit halfmetaal vertonen een anomale struktuur die, vanwege zijn temperatuur- en spanningsafhankelijkheid toegeschreven wordt aan de aanwezigheid van supergeleidende klusters aan het oppervlak. De experimenten werden verricht

aan zowel gedeformeerd als ook aan niet-gedeformeerd bismuth. In elk van beide gevallen werd een andere supergeleidende fase gevonden, namelijk de amorfe-Bi fase in experimenten aan niet-gedeformeerd en de Bi-II fase in experimenten aan gedeformeerd bismuth. De afmetingen van de klusters kan worden afgeschat uit de relatieve verandering van de puntkontaktweerstand. In de meeste gevallen werd een diameter gevonden van ongeveer 100 nm.

In het volgende hoofdstuk wordt bericht over punt-kontakt experimenten aan het zware-fermion systeem UPt_3. Verondersteld wordt dat puntkontakten van deze materialen niet in de ballistische limiet verkeren, echter in de thermische gebied waar de vrije weglengte van elektronen klein is vergeleken met de kontaktafmetingen, daarom leidend tot opwarming in het kontaktgebied. In dat geval leveren de experimenten geen energie-opgeloste informatie. De temperatuur-afhankelijke metingen laten zien dat de spannings-afhankelijke kontaktweestand bij lage temperaturen lijkt op met de temperatuur-afhankelijke kontaktweerstand zonder aangelegde spanning.

Vervolgens wordt een ander type van experimenten aan UPt_3 beschreven, waarin het gaat om hoogfrekwent-gelijkrichting van puntkontakten van dit systeem. Puntkontakten, geplaatst in een ver-infrarood elektromagnetisch veld, vertonen een DC-response dat evenredig is met de tweede-afgeleide d^2V/dI^2, zoals die gemeten wordt met een laagfrekwente modulatie-techniek. Dit is echter alleen het geval wanneer de processen die de stroom-spanning karakteristiek bepalen, snel zijn vergeleken met de modulatie-frekwentie. De signalen verkregen met de gelijkrichtings-experimenten aan UPt_3, vertonen deze d^2V/dI^2-afhankelijkheid niet, maar een die verklaard kan worden met de aanname dat de bovengenoemde processen in dit materiaal langzaam zijn ten opzichte van de aangelegde HF-modulatie (~1 THz). Men zou zich kunnen voorstellen dat opwarming van het kontaktgebied zo'n langzaam proces is.

Het laatste gedeelte van het proefschrift handelt niet over de elektrische eigenschappen van puntkontakten maar beschrijft een aantal experimenten waarin het ging om de fononen te onderzoeken die door een puntkontakt uitgezonden worden. De puntkontakten in het experiment werden vervaardigd tussen een metalen naald en een metaalfilm, opgedampt op een lichtgedoopt silicium kristal. Dit kristal, gedoopt met boor-verontreinigingen werd gebruikt als fonon-detektor. Aan de andere zijde van het kristal werd de geleiding gemeten. Deze geleiding werd vergroot door de ionisatie van B^+-verontreinigingen in het Si door fononen. Met behulp van deze methode werd informatie ingewonnen betreffende de fononen, gegenereerd door puntkontakten en hun gedrag in de metaalfilm.

CURRICULUM VITAE

A.M. Duif

3 juni 1958	Geboren te Venlo.
1964-1970	Lagere school, Nijmegen.
1970-1975	HAVO, Scholengemeenschap Nijmegen-West, Nijmegen.
1975-1977	VWO (Atheneum-B), Dominicus College, Nijmegen.
1977-1983	Studie Natuurkunde, Katholieke Universiteit, Nijmegen.
december 1983	Doktoraal Examen Experimentele Natuurkunde, specialisatie Vaste Stof Fysika.
1984-1985	Promotie-onderzoek in dienst van de Stichting voor Fundamenteel Onderzoek der Materie aan de afdeling Experimentele Natuurkunde 4, Fakulteit der Wiskunde en Natuurwetenschappen, Katholieke Universiteit, Nijmegen, o.l.v. prof. dr. P. Wyder.
1985-1987	Detachering in het kader van het promotie-onderzoek aan het Hochfeld-Magnetlabor van het Max-Planck-Institut für Festkörperforschung, Grenoble, Frankrijk.

STELLINGEN

behorende bij het proefschrift

"Applications of Point-Contact Spectroscopy"

van A.M. Duif

I

De standaard beschrijving van quantum-oscillaties in een elektronengas, zoals gegeven door Lifschitz en Kosevich, gaat in het algemeen niet op voor een elektronengas met sterk twee-dimensionale eigenschappen.
I.M. Lifschitz en A.M. Kosevich, Sov. Phys. JETP 2, 636 (1956).

II

Het gebruik van de vrije-elektron-waarde voor de parameter $\rho\ell$ in gallium, zoals gedaan door Shklyarevskii en anderen, is niet terecht. De door genoemde auteurs gevonden waarde voor de renormalisatie-parameter λ van de elektron-fonon wisselwerking moet derhalve als onbetrouwbaar worden beschouwd.
O.I. Schklyarevskii, N.N. Gribov en Yu.G. Naidyuk, Sov. J. Low Temp. Phys. 9, 553 (1983).

III

De voortplanting van licht in inkommensurabele kristallen wordt merkbaar beinvloed door langgolvige strukturele eigenschappen van de modulatie. De relevante Fourierkomponenten en de korresponderende symmetrie-eigenschappen van de diëlektrische tensor volgen direkt uit de superruimte-symmetrie.

IV

Een alternatieve verklaring van de Raman-piek bij 3678.2 cm^{-1} Stokes shift, waargenomen door Knippers en anderen bij metingen aan ethyleen, is een fundamentele Raman-overgang in water.
W. Knippers, K. van Helvoort, S. Stolte en J. Reuss, Chem. Phys. 98, 1 (1985).

V

Voor de omrekening van de gemeten weerstand van een preparaat naar de soortelijke weerstand van het in het preparaat verwerkte materiaal, zijn aannames over de homogeniteit van het preparaat onvermijdelijk. Het verdient daarom aanbeveling soortelijke weerstandsmetingen te doen op een manier die toetsing van deze aannames mogelijk maakt. Extra, onafhankelijke weerstandsmetingen, gedaan aan hetzelfde preparaat, zijn daarvoor zeer geschikt. Een dergelijke methode is reeds ontwikkeld voor geleiders in een magneetveld*. Echter, een soortelijke weerstandsmeting, die geen gebruik maakt van een aangelegd magneetveld, is zowel vanuit praktisch als fundamenteel oogpunt interessant.

*A.P. van Gelder, niet gepubliceerd.

VI

Het berekenen van de carrier-temperatuur voor elektronen in silicium als funktie van het longitudinale elektrische veld met behulp van de Einstein-relatie door uit te gaan van de empirische relatie voor de beweeglijkheid (Caughy en Thomas) en de metingen van de diffusiecoëfficiënt (Canali), levert onfysische resultaten.

D.M. Caughy en R.E. Thomas, proc. IEEE55 (1967).

C. Canali in Hot Electron Transport in Semiconductors, ed. L. Reggiani (Springer Verlag, 1985).

VII

Door de warmtebehandeling die Debowska en anderen aan NaY zeolite preparaten geven, zijn deze preparaten slecht gekarakteriseerd aangezien rond de gekozen uitstooktemperatuur één van de positronannihilatielevensduurkomponenten sterk varieert ten gevolge van dehydratatie.

M. Debowska, A. Baranowski, K. Jerie en W. Swiatkowski, Phys. Stat. Sol. (a) 97, K35 (1986).

H. Nakanishi en Y. Ujihira, J. Phys. Chem. 86, 4446 (1982).

VIII

De in neutronenstrooiingsexperimenten door Goldman en anderen gevonden ferromagnetische korrelaties in het basisvlak van het heavy-fermion systeem UPt_3 zijn moeilijk te rijmen met het optreden van antiferromagnetische ordening in datzelfde vlak voor $U(Pt_{0.95}Pd_{.05})_3$.

A.I. Goldman, G. Shirane, G. Aeppli, E. Bucher en J. Hufnagl, preprint 1987.

P. Frings, B. Renker en C. Vettier, J. Magn. Magn. Mat. 63&64, 202 (1987).

IX

Het is niet mogelijk om in het regime van sterke lokalisatie van licht te komen met bestaande diëlektrische strooiers.

X

De limiet van sterke lokalisatie zou bereikt moeten kunnen worden met resonante strooiing van geluidsgolven aan bellen in "Weissbier".

XI

Gezien de belangrijke bijdrage van hoge-T_c supergeleiding aan LT-18, is het te overwegen over drie jaar HT-19 te organiseren.

XII

Bij het ontwerp van een natuurkundig laboratorium verdient het aanbeveling dat de architekt terdege ingelicht wordt over de lengte van hevels en de hoogte van heliumvaten.

lab 100-107 van het Max-Planck-Institut in Grenoble.

lab NK005 van de Fakulteit der Wisk. en Natuurwetensch. te Nijmegen.